Lawrence Berkeley National Laboratory
Recent Work

Title

THE GROWTH AND CHARACTERIZATION OF SINGLE CRYSTAL (Cd, Zn)S THIN FILMS RELEVANT TO THE STUDY OF THE (Cd, Zn)S/CuxS PHOTOVOLTAIC CELL

Permalink

https://escholarship.org/uc/item/7b58m4qj

Author

Chin, B.L.

Publication Date

1983-08-01

eScholarship.org Powered by the California Digital Library
University of California

LBL-16117
c.2

Lawrence Berkeley Laboratory

UNIVERSITY OF CALIFORNIA

RECEIVED
LAWRENCE
BERKELEY LABORATORY
JAN 17 1984
LIBRARY AND
DOCUMENTS SECTION

Materials & Molecular Research Division

THE GROWTH AND CHARACTERIZATION OF SINGLE CRYSTAL (Cd,Zn)S THIN FILMS RELEVANT TO THE STUDY OF THE (Cd,Zn)S/Cu_xS PHOTOVOLTAIC CELL

B.L. Chin
(Ph.D. Thesis)

August 1983

TWO-WEEK LOAN COPY

This is a Library Circulating Copy which may be borrowed for two weeks. For a personal retention copy, call Tech. Info. Division, Ext. 6782.



Prepared for the U.S. Department of Energy under Contract DE-AC03-76SF00098

LBL-16117
c.2

DISCLAIMER

This document was prepared as an account of work sponsored by the United States Government. While this document is believed to contain correct information, neither the United States Government nor any agency thereof, nor the Regents of the University of California, nor any of their employees, makes any warranty, express or implied, or assumes any legal responsibility for the accuracy, completeness, or usefulness of any information, apparatus, product, or process disclosed, or represents that its use would not infringe privately owned rights. Reference herein to any specific commercial product, process, or service by its trade name, trademark, manufacturer, or otherwise, does not necessarily constitute or imply its endorsement, recommendation, or favoring by the United States Government or any agency thereof, or the Regents of the University of California. The views and opinions of authors expressed herein do not necessarily state or reflect those of the United States Government or any agency thereof or the Regents of the University of California.

LBL-16117

THE GROWTH AND CHARACTERIZATION OF SINGLE CRYSTAL (Cd,Zn)S THIN FILMS RELEVANT TO THE STUDY OF THE (CD,Zn)S/Cu_xS PHOTOVOLTAIC CELL

Barry Lee Chin
(Ph.D. Thesis)

Materials and Molecular Research Division
Lawrence Berkeley Laboratory
University of California
Berkeley, California 94720

August 1983

This work was supported by the U.S. Energy Research and Development Administration and the Division of Solar, Geothermal, Electric and Storage Systems, U.S. Department of Energy under Contract No. DE-AC03-76SF00098.

The Growth and Characterization of Single Crystal (Cd,Zn)S Thin Films Relevant to the Study of the (Cd,Zn)S/Cu_xS Photovoltaic Cell

CONTENTS

ABSTRACT v

I. INTRODUCTION 1

1.1 Nature of the Problem and Approach 1

1.2 Theory 4

a. General Aspects of Heterojunctions 4

b. Conduction Mechanisms in the Cu_xS/CdS Heterojunction. 7

1.3 Previous Related Research. 9

a. The Copper-Sulfur System and Formation 9

b. Properties of (Cd,Zn)S 11

c. Crystal Growth Techniques for (Cd,Zn)S 12

II. EXPERIMENTAL PROCEDURE. 13

2.1 Thin Film Growth and Characterization Methods. 13

2.2 Electrical and Optical Measurement Apparatus 15

2.3 Auger Electron Spectroscopy System 20

III. FILM GROWTH AND CHARACTERIZATION RESULTS. 22

3.1 Initial Growth Experiments 22

3.2 Growth on (111) Ga-face GaAs Substrates. 25

3.3 Effect of GaAs Substrate Preparation and Orientation 28

3.4 Films Grown in Van der Pauw Geometry 33

3.5 Films Grown on (111) Ge Substrates 34

IV. ELECTRICAL AND OPTICAL MEASUREMENTS 36

4.1 Hall Effect Results. 36

4.2 Current-Voltage Measurements 37

4.3 Spectral Response Measurements 39

V. AUGER ELECTRON SPECTROSCOPY STUDIES 40

5.1 Introduction 40

5.2 Experimental Results 42

VI. DISCUSSION. 51

6.1 Thin Film Growth 51

6.2 Electrical and Optical Characteristics 52

6.3 Auger Studies. 53

6.4 Suggestions for Future Work. 55

REFERENCES 57

TABLES 65

ACKNOWLEDGEMENTS 78

FIGURE CAPTIONS. 79

FIGURES. 85

The Growth and Characterization of Single Crystal (Cd,Zn)S Thin Films Relevant to the Study of the (Cd,Zn)S/Cu_xS Photovoltaic Cell

by

Barry Lee Chin

Material and Molecular Research Division
Lawrence Berkeley Laboratory
Materials Science and Mineral Engineering
University of California
Berkeley, California 94720

ABSTRACT

Single crystal thin films of (Cd,Zn)S were deposited and characterized to study the factors affecting the operation of the (Cd,Zn)S/Cu_xS photovoltaic heterojunction. To obtain higher conversion efficiency, the n-type side of the CdS/Cu_xS heterojunction has been replaced by (Cd,Zn)S. Previous studies have shown an increase in open-circuit voltage with the mixed crystal cell; however, a decrease in short-circuit current with increasing Zn content has also been measured.

Single crystal (Cd,Zn)S thin films of varying compositions were deposited by a hot-wall vacuum deposition technique to eliminate the effects of grain boundaries and to provide a planar interface. The heteroepitaxial films were grown on both (111) and off-(111) GaAs and

(111)Ge substrates. The deposited films were characterized using X-ray diffraction, SEM-EDAX and Hall mobility measurements. It was found that the composition and growth rate of the single crystal (Cd,Zn)S thin films depended very strongly upon the ratio of ZnS to CdS evaporated and the substrate surface. Heterojunctions with Cu_xS were formed by both a solid-state ion exchange reaction and reactive sputtering. Current-voltage characteristics and spectral response data were measured on completed devices.

Compositional Auger electron spectroscopy depth profiling was performed on heterojunctions using both processes for forming the Cu_xS layer. A sharp interface was found for the reactively sputtered Cu_xS/II-VI heterojunction whereas a diffuse interface existed for the ion-exchange formed Cu_xS. Relative sensitivity factors were calculated using fixed compositions and sulfur as the standard. For the heterojunction formed by the ion-exchange reaction on (Cd,Zn)S, an excess of Zn and Cd in the form of a second phase at the interface was determined. A model to explain this effect on heterojunction operation is discussed.

I. INTRODUCTION

1.1 Nature of the Problem and Approach

The energy situation of the 1970's has focused attention upon this society's dependence upon fossil fuels as an inexpensive available energy source. Two possible energy alternatives with potential time time scales to exhaustion in billions of years are nuclear fusion and solar energy. Two of the major problems associated with nuclear fusion are the confinement of the fuel and the radioactive wastes which are a product of the process; neither of which has any near-term solutions. The other renewable alternative energy source is that of the sun from which the earth receives 1.7×10^{14} kWh of energy each hour. The use of solar energy in thermal conversion has become more widely implemented for the heating and cooling of homes because of its cost competitiveness with other methods.

Another solar energy conversion process uses the photovoltaic effect in which solar cells convert sunlight "directly" into electricity. The main limitations presently are its high cost and low conversion efficiencies. Many different semiconductors and structures have been studied for large scale terrestial use.[1] Single crystal Si cells were initially employed for spacecraft missions and much research has been directed towards reducing cell cost. Alternative approaches to single crystal Si have included production of Si cells on single crystal sheets or polycrystalline material and depositing Si in the amorphous state. Highly efficient GaAs single crystal cells are also being examined for use in tandem cell structures under sun-

light concentration but require complex processing and suffer from the high cost of the starting material and tracking concentrators. Thin film Cu_xS/CdS cells are attractive because of their low cost of fabrication by either vacuum evaporation or spray pyrolysis techniques. Conversion efficiencies of greater than 9 percent have been reported,[2] but the cell output has been known to degrade with time.

This work deals with a perturbation of the Cu_xS/CdS cell in which the n-type side of the heterojunction is replaced by (Cd,Zn)S in order to increase the cell efficiency and also improve the stability of these devices. These benefits are expected because of (1) better electron affinity matching resulting in higher open-circuit voltage (V_{oc}), (2) decreased copper diffusivity in the mixed crystal (Cd,Zn)S leading to better stability and (3) higher short-circuit current (I_{sc}) due to better lattice matching at the interface. One of the initial studies was performed by Palz et al.[3] in which they reported higher V_{oc} with $(Cd_{0.9}Zn_{0.1})S$ than for an equivalent CdS cell. Peterson[4] examined single crystal $(Cd_{0.75}Zn_{0.25})S$ cells and also observed an increase in V_{oc}. Studies of (Cd,Zn)S prepared by evaporation and spray pyrolysis and their heterojunctions with Cu_xS have also been performed.[5] Researchers at the University of Delaware Institute of Energy Conversion have been studying polycrystalline (Cd,Zn)S/Cu_2S cells and have reported efficiencies of 10 percent.[6] In all of these investigations an increase in V_{oc} was measured with increasing Zn content but a decrease in I_{sc} was also found. The

development of the (Cd,Zn)S thin film solar cell has been reviewed by Burton.[7]

In forming the Cu_xS layer by a conversion process the presence of grain boundaries in polycrystalline CdS or (Cd,Zn)S results in a very complex interface. This poses a very difficult problem in attempting to analyze the electrical, chemical and structural nature of the heterojunction. This work involves the formation of a more simple planar interface by studying single crystal (Cd,Zn)S thin films and their heterojunction formation with Cu_xS.

The major objective of this work was to deposit single crystal (Cd,Zn)S thin films with varying compositions from pure CdS to pure ZnS and characterize their properties relevant for photovoltaic application. A hot-wall vacuum deposition technique was used and the films characterized using X-ray diffraction and scanning electron microscopy (SEM) with energy-dispersive analysis of X-rays (EDAX). The X-ray diffraction data was used to determine crystallinity and composition and the SEM-EDAX for surface morphology and compositional uniformity. Hall effect experiments were used for measuring electron mobility of the deposited films to correlate with growth conditions and to compare with other published data to verify suitability for hetero-junction formation. The characterization data was used in a feed-back process to determine the deposition parameters for subsequent growth experiments.

Information concerning the decrease in I_{sc} with increasing Zn content in the base material could be obtained without the complicating

effects of grain boundaries by forming heterojunctions with single crystal films with different compositions. Heterojunctions with Cu_xS have been mostly formed by a conversion process which because of the ion-exchange mechanism involved, is dependent upon the Zn content of the base film. Two methods for Cu_xS formation were examined in this study: (1) the solid-state "dry" conversion process and (2) reactive sputtering of Cu_xS which is not dependent upon the base material composition. After the heterojunction was formed and heat-treated, contacts were made to both sides of the device. Current-voltage characteristics and spectral response measurements were taken to verify that the fabrication procedure would produce functional cells and to indicate processing steps requiring improvement. To further analyze the chemical nature of these cells and to correlate with the previous data acquired at each of the fabrication steps, Auger electron spectroscopy measurements were also performed. A flow chart of this experimental approach is shown in Fig. 1.1.

1.2 Theory

a. General Aspects of Heterojunctions.

A brief summary of the important aspects of heterojunctions with respect to their operation as photovoltaic cells is presented here. A heterojunction is formed when two semiconductors with different bandgap E_g, electron affinity χ, work function ϕ, and crystal structure are brought into intimate contact. Figure 1.2a shows the energy band diagrams of a small band gap E_{g1} p-type semiconductor and a larger band gap E_{g2} n-type semiconductor. When the two semiconductors are

joined (assuming no interfacial states) the equalization of the Fermi levels results in the equilibrium band diagram shown in Figure 1.2b. The abrupt junction model developed by Anderson[8,9] is a direct modification of the homojunction diffusion model developed by Shockley.[10] Anderson's work was concerned with the Ge-GaAs heterojunction in which the lattice constants and coefficients of linear expansion are almost identical so that the effects of interface states could be reasonably neglected. The effects of interface states were studied by Oldham and Milnes.[11] They found that with a lattice mismatch of a few percent the heterojunction behavior could be totally dominated by the interface states. They suggested a metal-like layer of interface states between the two semiconductors in which recombination was dominant. Riben and Feucht[12] proposed a model involving stepwise tunneling and subsequent recombination through individual interface states in the depletion region. A detailed explanation of the various models of heterojunction transport have been reviewed in articles by Van Ruyven,[13] Tansley,[14] Fahrenbruch and Aranovich,[15] and the book by Milnes and Feucht.[16]

From Figure 1.2b it can be seen that there is a discontinuity in the bottom of the conduction band and top of the valence band edges. The conduction band step is given by

$$\Delta E_c = \chi_1 - \chi_2 \qquad (1.1)$$

and may be positive, as shown, or negative. The energy step in the valence band is given by

$$\Delta E_v = (E_{g2}-E_{g1})-(\chi_1-\chi_2) \tag{1-2}$$

so that

$$\Delta E_c + \Delta E_v = E_{g2}-E_{g1} \tag{1-3}$$

Because of the many heterojunction structures possible, several different energy band configurations may result. The portion of the barrier voltage, $V_b = V_{b1} + V_{b2}$, appearing on either side of the heterojunction is given by

$$\frac{V_{b1}}{V_{b2}} = \frac{N_2\epsilon_2}{N_1\epsilon_1} \tag{1-4}$$

where N_i and ϵ_i are net dopant concentration and dielectric constant of either semiconductor, respectively. The space charge regions on either side of the junction is given by

$$X_1 = \left(\frac{N_2}{N_1}\right)^{1/2} X_0 \qquad X_2 = \left(\frac{N_1}{N_2}\right)^{1/2} X_0$$

$$X_o = \left(\frac{2\epsilon_1\epsilon_2 V_b}{q(\epsilon_1 N_1+\epsilon_2 N_2)}\right)^{1/2} \tag{1-5}$$

where q is the magnitude of the electronic charge. Note that the model shown in Figure 1.2 assumes no interfacial states so that band bending due to trapped charge is neglected.

The general features of heterojunctions are now applied for the case of the Cu_xS/CdS heterojunction. Cu_2S is a degenerate p-type semiconductor with a carrier concentration of $\sim 10^{19}$ cm^{-3} with an orthorhombic crystal structure. CdS is n-type with $N_d \sim 10^{16}$-10^{17} cm^{-3} and a wurtzite crystal structure. From Equation 1-5 it can be seen that the space charge penetration into the p-type Cu_xS side of the junction is very small. For front wall cells in which the light is incident on the Cu_xS, the major portion of the current is due to electron injection from Cu_xS to CdS.

b. Conduction Mechanisms in the Cu_xS/CdS Heterojunction

Since the discovery of the photovoltaic effect in CdS with Cu, Ag or Au contacts by Reynolds et al.[17] in 1954, various models have been proposed to explain the current-voltage characteristics of these cells in the dark and under illumination. The first models of junctions formed between electroplated Cu and CdS included the photoemission across a metal-semiconductor barrier[18] and also the formation of a diffused p-n junction in the CdS.[19] Cusano[20] in 1963 proposed that a heterojunction with p-type Cu_xS was formed and created the necessary potential barrier. There is general agreement now that light absorption occurs in the Cu_xS and the various models have been reviewed by van Aerschodt et al.[21] and Stanley.[22] Some of these proposed models are briefly summarized.

Gill[23] proposed that there is a conduction band spike at the Cu_xS/CdS interface ($\Delta E_c > 0$ as shown in Fig. 1.2) in which the forward bias current is dominated by tunneling through the barrier and recombination via interface states. Peterson's[4] results found the existence of a conduction band spike to be untenable. His model also indicated that a positive step of greater than ~kT would be extremely detrimental to the transmission of electrons from the Cu_xS layer. Martinuzzi and Mallem[24] have used the model of multistep tunnel conduction via interface states proposed by Riben and Feucht[12] to explain their experimental results. Partain et al.[25] has invoked a space-charge-limited current model to quantitatively model the electrical properties of the Cu_xS/CdS heterojunction. Rothwarf[26] has developed a model in which the recombination of electrons with holes at the CdS conduction band edge via interface states dominates the I-V characteristics. The equation for the open-circuit voltage is given by:

$$qV_{oc} = E_{g1} - \Delta\chi + kT \ln [j_L A_\perp / qN_{c2} S_I A_j] \qquad (1\text{-}6)$$

where E_{g1} is the band gap of Cu_2S, $\Delta\chi$ is the electron affinity difference between Cu_2S and CdS and A_j is the total junction area (this may exceed the normal planar area of the cell $A_\perp$, due to the formation of Cu_xS along grain boundaries in polycrystalline CdS). These various proposed models indicate the difficulties in analyzing the Cu_xS/CdS cell in which important parameters are not well known

(e.g., electron affinity, carrier mobility, lifetime and diffusion lengths of minority carriers, interface structure), and which are certain to vary with the different processing methods used. The problems associated with the Cu_2S/CdS cell have been reviewed by Savelli and Bougnot.[27]

1.3 Previous Related Research

a. The Copper-Sulfur System and Formation

Cu_2S is a degenerate p-type semiconductor with an indirect bandgap of approximately 1.2 eV and a direct bandgap of approximately 1.8 eV as given by the rigid band model proposed by Mulder.[28] At room temperature, however, several copper sulfide phases exist very close to the stoichiometric chalcocite phase, Cu_2S. Cook[29] has completed a review of the literature along with his results dealing with the reactions of copper with sulfur. The following is a summary of stable and metastable Cu_xS compounds and phases at room temperature according to Cook.

Chalcocite: Cu_2S is a common sulfide ore with limited solid solubility. The compound has been described as orthorhombic with a = 11.84, b = 27.33, and c = 13.49. The structure of the low temperature orthorhombic form consists of ordered copper atoms in a slightly distorted hexagonal close-packed sulfur matrix.

Djurleite: $Cu_{1.96}S$ named for the discoverer of the compound[30] is orthorhombic with a = 31.42, b = 13.56 and c = 26.84. It was established by Cook that the true composition of djurleite is

$Cu_{1.93}S$ with the sulfur atoms in the same packing arrangement as for chalcocite.

Digenite: $\sim Cu_{1.8}S$ is pseudocubic with a composition range which is still a subject of discussion. The cubic close-packed sulfur arrangement was found for this phase.

Covellite: CuS has a hexagonal structure with a = 3.79 and c = 16.33. It deviates from stoichiometry by $< \pm 0.001$.

Different methods for forming Cu_xS have been examined. Cu_xS has been formed by conversion of CdS by dipping in a hot (90-100°C) cuprous chloride solution for several seconds. This dipping or "wet" process developed by Shiozawa et al.[31] involves a topotaxial reaction in which one cadmium ion is replaced by two copper ions and the sulfur sublattice remains fixed. This method suffers from several limitations: (1) the rapid diffusion of highly mobile copper ions along grain boundaries resulting in vertical junctions; (2) an inhomogeneous growth pattern due to the sudden interruption of the reaction upon reaching the desired thickness (typically only 3000Å thick due to its high absorption[28]); (3) the presence of Cu and Cd gradients in the Cu_xS. In order to obtain Cu_2S, which is the optimum composition for obtaining high efficiency cells, various other methods for formation have been examined. One method involves the vacuum evaporation of CuCl onto the II-VI compound and subsequent heat treatment[32] referred to as the solid-state "dry" process. The standard free energies of reaction for CdS and ZnS in the ion exchange

$$MS + 2CuCl \longrightarrow Cu_2S + MCl_2$$

where M = Cd or Zn are -12.48 and -4.94 kcal/mole, respectively.[33] Hence, (Cd,Zn)S up to 100 percent Zn would be expected to react to completion (exhuastion of available CuCl) although more slowly as the zinc content is increased. Reactive sputtering has also been used to form Cu_xS films[34] to avoid the necessity for converting part of the II-VI film.

b. Properties of (Cd,Zn)S

In the 1950 and 1960's the major research emphasis in II-VI compounds had been on photoluminescence derived from deep luminescence centers in ZnS and photoconductivity in CdS. The basic physics and chemistry of zinc and cadmium sulfides have been reviewed by Aven and Prener[35] and in the book by Ray.[36] Mixed crystals of CdS and ZnS were studied for changes in photoelectronic properties by adjusting the composition of the solid solution. Cherin, Lind and Davis[37] found that (Cd,Zn)S forms a continuous solid solution with a wurtzite crystal structure over the entire composition range from CdS to ZnS. Davis and Lind[38] measured the bandgap of (Cd,Zn)S crystals and found it to vary smoothly from ~2.4 eV for CdS to ~3.7 eV for ZnS. Aven and Mead[39] determined the electron affinity of ZnS to be ~1 eV less than that of CdS. By choosing the correct composition for (Cd,Zn)S, electron affinity matching with Cu_2S may be achieved resulting in a higher V_{oc} as given by Equation 1.6. Note, however, that by

increasing the ZnS content to greater than the optimum composition ($\Delta X = 0$), a conduction band spike ($\Delta E_c > 0$) may be formed.

c. Crystal Growth Techniques for (Cd,Zn)S

The growth of Cd and Zn chalcogenide films by vacuum evaporation has been summarized by Holt.[40] Because of the good thermal expansion and lattice parameter matches between (Cd,Zn)S and GaAs (see Table 1.1), initial experiments in this study were performed on (111) GaAs substrates. The requirements for heteroepitaxial growth and characterization of the deposited films has been extensively reviewed by Matthews.[41] Previous studies of heteroepitaxial growth of CdS and ZnS on GaAs have included using the close-spaced deposition technique[42,43] and by vapor phase growth.[44-48]

(111) Ge substrates have also been used due to its structural and electrical properites (see Table 1.1). The heteroepitaxial growth of CdS and ZnS on Ge substrates has also been previously studied.[49-52]

Methods to deposit polycrystalline (Cd,Zn)S have included single-source evaporation,[53-57] multiple-source evaporation,[58-61] sputter deposition[62,63] and spray pyrolysis.[64-68] The heteroepitaxial growth of (Cd,Zn)S is more complex and most of the published results involved vapor phase chemical tansport onto (111) ZnS[69] and (111) GaAs substrates.[70] Hot-wall epitaxy has been successful in the deposition of IV-VI compounds and has been applied to II-VI materials to provide high quality films.[71,72] The hot wall epitaxial deposition technique has been reviewed by Lopez-Otero.[73]

II. EXPERIMENTAL PROCEDURE

2.1 Thin Film Growth and Characterization Methods

In order to obtain single crystal (Cd,Zn)S thin films for test devices a hot-wall vacuum deposition technique was adopted. The design of the growth apparatus was modified from that of Behrndt and Moreno[74] to include separate sources for simulatneous and/or sequential evaporation of ZnS and CdS (the difficulties experienced with single source evaporation of (Cd,Zn)S has been reported by Burton, Hench and Meakin[55]). One baffle was placed between the two sources to prevent cross contamination and another between the sources and substrate to prevent spitting from the evaporating charges. A longitudinal cross section of the apparatus is shown in Fig. 2.1 Chromel-alumel thermocouples were placed against the alumina cylinder wall and substrate holder to monitor temperatures. The temperatures of the two individual sources were controlled by varying the power delivered by separate constant current power supplies. The mass of the ZnS and CdS charges (each 99.999 percent pure sintered grains from Orion Chemical Company) were measured before and after each deposition run to give values for a normalized growth rate. A number of appropriate modifications were made later to the growth apparatus in order to achieve the desired results and are discussed in the following sections.

In operation the vacuum system containing the hot-wall apparatus was pumped down into the 10^{-6} torr range and the cylinder and substrate heated separately to 300-600°C. The substrate holder was

then lowered into position on the cylinder and allowed to equilibrate to the desired deposition temperature. The substrate was maintained at a temperature lower than the other parts of the growth chamber so that when the two sources are turned on, most of the vapor species would condense on the substrate and substrate holder. During the deposition the power to the sources and the temperatures of the cylinder wall and substrate were monitored.

Both (111) and off-(111) GaAs surfaces were used for the hetero-epitaxial growth of (Cd,Zn)S because of the good thermal expansion and lattice parameter matches. The (111) GaAs substrates were Zn-doped with $\rho = 1x10^{-3}$ Ω-cm and 14° off-(111) substrates Si-doped with $\rho = 1x10^{-3}$ Ω-cm, both from Laser Diode Laboratories, Inc. Later samples were grown on (111) GaAs O_2 doped with $\rho = 1x10^{-3}$Ω-cm from Crystal Specialties. For Hall measurements, (111) GaAs Cr-doped substrates and off-(111) (12° towards (110)) with $\rho > 10^{7}$Ω-cm were purchased from Crystal Specialties. The (111) Ge substrates were n-type Sb-doped with $\rho \sim 5$-9 Ω-cm from Eagle-Picher.

For the initial growth experiments on (111) GaAs the following surface preparation was performed: (1) 1-3 mins. etch in $4:1:1/H_2SO_4:H_2O_2:H_2O$, (2) distilled water rinse, (3) CH_3OH rinse, (4) 1 min. 2%Br:CH_3OH, (5) CH_3OH rinse and (6) dried with N_2. For the unpolished GaAs substrates the surfaces were polished using 0000 grit paper and final lapping done with 1 μm and 1/4 μm diamond paste on a polishing wheel. After polishing the substrates were etched using a microcloth saturated with either 5.25 percent

sodium hypochlorite or a Br:CH_3OH solution. The different surface preparations for these samples are detailed in Section 3.3. The (111) Ge substrates were etched in several percent HF, rinsed in distilled water and dried in N_2 prior to placement in the vacuum system.

Cherin, Lind and Davis have found[37] that (Cd,Zn)S forms a continuous series of solid solutions over the composition range from CdS to ZnS. They also reported a definitive calibration for lattice constants in which the variation of lattice parameters with composition was found to obey Vegard's law. This relationship was used to determine the composition of the grown films by measuring the d-spacings obtained from X-ray diffractometer scans. X-ray scans were performed on a Picker Model 3488K diffractometer using either CuK_α or FeK_α radiation. The surface morphology and composition profiles were examined using an AMR1000 Scanning Electron Microscope with EDAX attchment. Electron microprobe measurements were performed on a Materials Analysis Company system.

2.2 Electrical and Optical Measurement Apparatus

Two methods for Cu_xS formation were used in this study: (1) the solid-state "dry" process and (2) the reactive sputter deposition of Cu_xS. Figure 2.2 shows a schematic cross-section of a completed device. The steps in producing this structure from the (Cd,Zn)S film grown on GaAs for the "dry" Cu_xS were as follows: (1) The surface of the film was mechanically polished to provide a planar interface, provided the film was thick enough ($\geq$10 μm) to withstand this treatment. (2) The surface was given a short etch in dilute HCl.

(This step was not performed for early cells.) (3) CuCl was vacuum evaporated onto the surface through a mask contacting the (Cd,Zn)S film. (4) The cell was heated in an argon or argon +2 percent H_2 atmosphere for times from 30 min. to 2 hrs. at temperatures between 130°C and 175°C. (5) The reaction products were washed off the surface in water and in methanol. (6) At this point silver paint contacts were formed on the Cu_xS layer overlapping the (Cd,Zn)S to maximize the exposed Cu_xS area, and to the GaAs to check that the device worked. (7) If the device gave a photovoltaic response in the "front-wall" mode in step 6, the GaAs was masked at the edges with enamel and etched away from the back of the (Cd,Zn)S film in 5.25 percent sodium hypochlorite. (8) Finally, the silver paint contacts were remade.

A few remarks about the ohmic contacts are in order here. The silver paint was adequate for contacting the Cu_xS layer; although when the Cu_xS was too thin there was a measurable photovoltaic response from the paint which formed a Schottky barrier with the mixed crystal. The contact to the (Cd,Zn)S presented more of a problem, however. The GaAs could be contacted satisfactorily with silver paint, but since the GaAs-(Cd,Zn)S interface (at least with Zn-doped, p-type GaAs) behaved as a "leaky" diode, the overall contact resistance was too high. Indium was used to contact the front of the mixed crystal, but such contacts were not more effective because the film resistivity was too high to collect "in-plane" currents efficiently.

In order to use the substrate as an ohmic back contact for front-wall cells, n-type GaAs was used. It was not known if the n-CdS/n-GaAs heterojunction would be ohmic because of the uncertainty in the values of electron affinity (from Table 1.1 ΔE_c = .43-.80 eV) and also because of the effect of interface states. Experiments with n-GaAs substrates determined that this heterojunction also acted as a "leaky" diode. Ohmic junctions were obtained for CdS grown on n-type Ge substrates allowing for front-wall cell construction. In-Ga was used as the back contact to Ge and silver paint the front contact to Cu_xS.

Cu_xS was deposited by reactive sputtering onto the CdS and (Cd,Zn)S thin films by the Lawrence Livermore Laboratory for comparison with the dry process. The sputtering parameters in forming these Cu_xS films are described elsewhere.[34] The same device structure was used as for the "dry" processed Cu_xS cells in the front-wall mode. Cell current-voltage characteristics were measured with a Tektronix Type 502A oscilloscope and a Waveforms 401 H sine wave generator as shown in Fig. 2.3. Measurements were taken under tungsten lamp illumination and also in sunlight.

A rather sophisticated apparatus for obtaining electrical and photo-electrical measurements on CdS/Cu_xS or (Cd,Zn)S/Cu_xS heterojunctions is desirable because of the well-known difficulties involved in making reliable measurements of the properties of these devices (e.g., nonlinear "two-beam" effects[23] and also long-lived trapping states[75]).

Figure 2.4 shows a block diagram of the apparatus used for spectral response measurements. The system controller is an 8080-based microprocessor with a resident BASIC interpeter which allows great flexibility in control of the different experimental variables. The light source consists of a tungsten halide lamp, usuable to wavelengths down to ~350 nm, whose intensity is under program control. The light beam is focused onto the entrance slit of the double grating monochromator which is driven by a motor. The motor also drives a variable resistor connected to a transresistance amplifier to provide a voltage precisely proportional to the wavelength setting of the monochromator. The wavelength range and wavelength change per step are inputted through the teletype. The double grating monochromator (Oriel 7244) is used to achieve very low stray light to insure that the spectral response measured in the absence of bias illumination is indeed the monochromatic response.

The beam emerging from the exit slit of the monochromator is incident on both the cell being tested and a thermopile (Sensors, Inc., Model L22-18) whose sensitivity is wavelength independent (within a few percent, in the range from 450 to 9000 nm, limited by its CaF_2 window material). The beam is split using a beam scanning galvanometer driven by a power oscillator. This configuration is used to achieve a stable chopping frequency to provide a high signal-to-noise ratio of the short-circuit current and thermopile (light intensity) signals. The thermopile output is amplified by a Keithley "lock-in" amplifier and monitored by the controller as V(1) (see Fig. 2.4). The output of the

test cell is connected to an operational amplifier circuit of very low input impedance (<1Ω) to approximate short-circuit conditions. This signal is then phase-sensitively detected in the same manner as the thermopile signal. This d.c. voltage, proportional to the a.c. short-circuit current, is recorded by the controller as V(2).

The BASIC program for control of the steady-state spectral response measurements was written so that a set of ten readings of the short-circuit current, with a variable time delay between readings, was taken at a given wavelength (see Figs. 2.5-2.7). The mean and standard deviation of this data group were then calculated by the micro-processor. A second set of ten readings along with the mean and standard deviation was subsequently taken. The data was considered stable only if the difference between the means of the two sets of readings was less than the sum of the standard deviations; if not, the program initiated another set of measurements. The same procedure was used for obtaining thermopile readings to determine the normalized short-circuit current. The wavelength at which the readings were taken, the average thermopile signal and its standard deviation, the average of the last twenty stable readings of the short-circuit current and its standard deviation, and normalized short-circuit current were then printed on the teletype and magnetic tape. There was also provision for an on-line plot of the spectral respone using an analog divide module and an X-Y recorder as shown in Fig. 2.4.

Also shown in Fig. 2.4 are the components to be used for I-V-Temperature measurements. The environmental chamber for the test

cell consists of an evacuated sample holder immersed in a liquid nitrogen dewar with a heater and thermocouple to allow program control of the sample temperature. An available bias voltage from 0 to 1V is shown in the Analog Driver Power Supply. Difficulties in producing cells of low enough series resistance limited the use of the I-V-T measurement portion of the apparatus.

Hall effect measurements were performed using standard equipment at room temperature with a magnetic field of 6 Kgauss. To study the effects of magnetoresistance magnetic fields between 2-6 Kgauss were used.

2.3 Auger Electron Spectroscopy System

A Physical Electronics Industries Model 590 Scanning Auger Microscope (SAM) with a Multiple-technique Analytical Computer System (MACS) was utilized for surface composition studies. A 1.0 μm primary beam diameter with E_p = 3kV was used. The base pressure during surface analysis was approximately $2x10^{-9}$ torr. Profiling was accomplished using either 3kV or 5kV Ar^+ ions with an Ar ambient resulting in a base pressure of approximately $5x10^{-5}$ torr. Multi-point analysis was performed to evaluate the reproducibility of the data.

Two different interfaces were to be studied by Auger electron spectroscopy; the interface between (Cd,Zn)S and Cu_xS as formed by the solid state ion exchange reaction and by reactive sputtering. The

Zn content in the base film was varied to also follow subsequent changes in the Cu_xS formation. The two films used for examination were $Cd_{0.79}Zn_{0.21}S$ (Film 5239) and ZnS/CdS (Film 8319).

The Cu_xS layer formed by the dry process involved evaporating CuCl through a mask with a circular opening of either 0.125" or 0.073" diameter onto the (Cd,Zn)S or ZnS surface and then heat treating. Sample 5239 was heat treated for 2.75 hrs at 60°C in Ar. The ZnS sample (Film 8319) was heat treated for 2 hrs. at 100°C (the higher temperature was necessary because of the lower diffusivity of Zn^{++} as compared to Cd^{++}). The reactively sputtered Cu_xS layers were deposited by the Lawrence Livermore Laboratory and heat treated at 200°C or 175°C in air or Ar for several minutes.

III. FILM GROWTH AND CHARACTERIZATION RESULTS

3.1 Initial Growth Experiments

The initial growth runs were conducted using the hot-wall apparatus as shown in Fig. 2.1 to determine the conditions necessary for single crystal (Cd,Zn)S growth on (111) GaAs substrates. It was found that cross-heating between the evaporation sources in the growth chamber was negligible. Therefore, it was hoped that by determining the growth rates of CdS and ZnS separately these results could be used as a first approximation to the correct evaporation conditions for a given Cd-Zn ratio in a co-deposition. A very simple model was found to give a good fit to the growth of CdS deposits under several different growth conditions. However, it was then discovered that, although there was no thermal interaction of the sources, enough Zn vapor found its way around the baffles to the CdS source to drastically affect the CdS vaporization rate. This finding has also been reported by researchers at the University of Delaware Institute of Energy Conversion.[55] To circumvent this problem, an iterative procedure was used in which a given combination of source temperatures was tried and the resulting film composition determined from the X-ray diffractometer peaks. The temperatures were then changed in the appropriate directions for the next deposition in order to approach the desired composition.

In addition to the X-ray diffractometer measurement which gave a fairly precise determination of the surface layer composition and an idea as to the degree of polycrystallinity, the film composition as a function of depth was measured by two other means. The more precise

of these was the electron microprobe which was used to scan an angle-lapped section of the film. Figure 3.1a shows the results of such a scan on an early film having large composition gradients. When reasonable care was taken, this kind of measurement gave relative accuracies of the order of 1 percent.

A more qualitative, but also much more readily performed, measure of the transverse film composition was provided by the energy dispersive X-ray analyzer (EDAX) in the scanning electron microscope (SEM) with the vertical deflection of the beam-scan turned off. Using this technique, one could observe the composition profile at a cleaved edge of the film. Figure 3.1b is an example of such an experiment performed on the same sample as shown in Fig. 3.1a. Seen in Fig. 3.1b is a triple exposure of the same area of the specimen, at the same magnification, but in two operating modes. The two white lines graphically depict the film composition versus depth, i.e., the vertical displacement is proportional to the weight percent of the element being analyzed. The background "picture" is a normal SEM micrograph taken after the line scans in which the darkened band shows where the electron beam was repeatedly swept for the composition analysis. Note that the electron microprobe and SEM-EDAX analysis are in excellent qualitative agreement.

Figures 3.2a and b show respectively an EDAX profile of the cleaved edge and a low-magnification SEM micrograph of the top surface of a later grown film. It can be seen that this film is much more nearly uniform than that of Fig. 3.1. The X-ray diffractometer scan of the

sample of Fig. 3.2 showed evidence of some polycrystallinity in the film. It was discovered that the irregular shapes visible primarily on the tips of the hexagonal pyramids of Fig. 3.2b were responsible for the extra X-ray peaks. The morphology of the cleaved surface suggested that the misoriented grains existed only at the top surface of this sample.

Table 3.1 summarizes the experimental conditions and results for this initial group of films. The large scatter in thickness of the films grown under apparently similar conditions was thought to be due to escape of part of the charge at the seam between the hot-wall cylinder and the bottom end-plate. This view was supported by the observation that the background pressure outside the cylinder on some runs was much higher than for others where the resulting films were thicker.

One interesting result of these initial growth experiments concerns the differences in film growth on the Ga and As faces of the GaAs substrates. The GaAs wafers were supplied with one face polished, and this side was used for Films 10126 through 10266. However, when it was discovered that the wafers had all been polished on the same crystallographic face, the As $(\bar{1}\bar{1}\bar{1})$ or B-face, deposition on the opposite face, the Ga or A-face, was tried. It was found that growth on the Ga face has a greater tendency toward monocrystallinity (non-(002) peak heights were less) and, further, it seemed to proceed at a higher rate (see the results for Film 11036 in Table 3.1). However, because of the difficulties mentioned earlier, this latter

result was less certain. This difference in growth behavior is probably due to the difference in stacking sequence for films grown on A- or B-faces.

3.2 Growth on (111) Ga-face GaAs Substrates

In order to prevent the cross contamination of the CdS charge by the Zn vapor and also escape of the vapor at the seams, a quartz cylinder with integral baseplate and baffle was used for subsequent runs as shown in Fig. 3.3. The two sources, each containing a charge of sintered grains of CdS or ZnS, had quartz wool plugs and Ta baffles within the alumina crucibles to reduce splattering. Also shown in Fig. 3.3 is a metal block (initially Cr-plated copper and later Mo) positioned on top of the substrate to act as a heat sink for the GaAs. A thermocouple was placed within the heat sink to monitor the substrate temperature.

The results and the experimental conditions for the growth runs on the (111) Ga face are summarized in Table 3.2 These films were mostly epitaxial single crystals, as determined by X-ray diffractometry (those with some polycrystalline growth had off c-axis diffraction peaks with intensities at least two orders of magnitude less than that of the (002) peak). The composition of the films was determined from the (004) d-spacing.

It was observed that the perimeter region of the deposited film, which was shielded from the growth chamber by the substrate holder, showed different contrast in the SEM than the rest of the mixed crystal. This can be seen in Fig. 3.4a which is a micrograph of the

top of a (Cd,Zn)S specimen which was cleaved for transverse compositional analysis. The X-ray mapping technique of the SEM-EDAX was used to show the origin of this contrast difference. In the X-ray mapping mode the concentration of an element is related to the density of dots in each area on the display screen. Figure 3.4b is such a map of the same specimen as in Fig. 3.4a with the X-ray analyzer set up to detect Cd. Enhanced concentration of Cd in the perimeter region can be seen. A more precise measurement by X-ray diffraction determined this area to be "pure" CdS. This result can be explained by the higher surface diffusivity of Cd compared to that of Zn.

It was found that no cross-contamination of evaporation charges occurred due to the integral baffle in the quartz hot-wall cylinder. This has resulted in far better processing control of the mixed crystal films and also in compositional uniformity. Figure 3.5 shows the X-ray line scans of the cleaved cross-section of a grown film for Cd, Zn and S which are seen to be relatively uniform through the film thickness.

The SEM was also used to characterize different surface morphologies of the mixed crystal films. Figure 3.6a shows the rough surface of a polycrystalline film. In contrast, the surface of a single crystal film with a high growth rate (Film 4267) is shown in Fig. 3.6b. In most of the deposited films cracks were observed. Fine randomly oriented cracks were found for Film 5247, as seen in Fig. 3.7. Long cracks propagating along the $\langle 11\bar{2}0 \rangle$ crystallographic directions were observed for Film 6077 (Fig. 3.8). Film growth over a crack, as seen in Fig. 3.9 (Film 5117), indicates that the cracks were formed

early during crystal growth. Cracks have also been observed for (Cd,Zn)S films grown on (111) GaAs substrates by the close-space transport method.[76]

In an effort to determine the origin of these cracks, Film 4197 was polished and then etched for 30 seconds in 1:1/HCl:H_2O. Figure 3.10 shows the result of this treatment and indicates that the cracks extend through the thickness of the (Cd,Zn)S film. X-ray diffraction analysis revealed that GaS was present under the film after the cracks were opened by etching, suggesting that a thin film of GaS forming between the GaAs substrate and mixed crystal may have been responsible for the development of these cracks. Further experiments were conducted to determine the origin of this problem as discussed in Section 3.3.

The dependence of film composition and growth rate on the experimental parameters was also studied. Both the growth rate and composition were found to be extremely sensitive to the relative rates of evaporation of the ZnS and CdS charges. Figure 3.11 shows the variation of x, the ZnS mole fraction in the film, with θ, the ZnS fraction of spent charge. The data shown in this figure encompass substrate temperatures from 330 to 475°C, cylinder temperatures between 560 and 600°C and total charge loss rates from 3.96 to 28.68 mmole/hr. Almost all of the Ga-face films fall near the line shown in the figure. There is apparently a preferential incorporation of ZnS in the single crystal (002) films. In spite of (or possibly because of) this preference, the normalized growth rate, i.e., the growth rate divided by the total charge loss rate, shows a rapid decrease with increasing

θ as seen in Fig. 3.12. Figure 3.12 represents data for films grown with a 600°C cylinder temperature at various total charge loss rates and substrate temperatures. If the data of Fig. 3.12 are plotted vs. x, Fig. 3.13 is obtained, showing a somewhat weaker, but still remarkable, dependence of g on x. The mechanisms underlying this phenomenon are as yet not understood; however, there is perhaps an insight contained in the calculations of Gilmer and Bennema[77] based on comuter simulations of crystal growth. They found an exponential dependence of growth rate on the step formation energy. Since the bond strength of ZnS is greater than that of CdS, one might expect an increase in the surface step formation energy of (Cd,Zn)S crystals as the ZnS fraction increases.

3.3 Effect of GaAs Substration Preparation and Orientation

It was found that (Cd,Zn)S films grown on the (111) Ga face developed cracks propagating through the thickness of the film and also into the GaAs substrate. To eliminate this problem the effect of different etchants, substrate surface and substrate orientation on crack formation was studied. The substrate holder was also changed from stainless steel to Ta to prevent any possible contamination. These results are summarized in Tables 3.2 and 3.3A. The various substrate conditions examined were:

(1) (111) Ga face polished for ~10 sec on a microcloth saturated with 5.25 percent sodium hypochlorite (Films 5247 through 6277).

(2) (111) Ga face polished for ~30 sec on a microcloth saturated with 2 percent Br:CH_3OH (Films 7297 through 8317).

(3) $(\bar{1}\bar{1}\bar{1})$ As face etched for 15 minutes in 4:1:1/H_2SO_4:H_2O_2:H_2O followed by a 1 minute 2 percent Br:CH_3OH etch (Films 9017 through 9077).

(4) 14° off - $(\bar{1}\bar{1}\bar{1})$ As face etched as in (3) (Films 9097 through 9297).

All GaAs deposition surfaces were initially mechanically polished with 1μ and 1/4 μ diamond grit before etching. Prior to placement in the vacuum system all substrates were washed in CH_3OH and then blown dry with N_2.

All (Cd,Zn)S single crystal films grown on the (111) Ga face were cracked regardless of the etchant. It was believed that a thin film of GaS formed between the GaAs and the growing film. X-ray and electron diffraction, and EDAX analysis confirmed the presence of this sulfide. This film could be formed during the substrate preheating procedure or in the early stages of the deposition. There is some evidence in the literature to support this interpretation: Auger electron and X-ray photoemission spectroscopy have shown there is an excess of Ga after a Br:CH_3OH etch of the GaAs surface.[78] Weinstein and Wolff[44] determined that for CVD expitaxial growth of CdS on the (111) Ga-face of GaAs the S-atom always attached first to the substrate surface. This allows minimization of the electrostatic interfacial energy.[79] Therefore, with the (111) Ga-face substrates used in the present study the Ga-rich surface layers after etching may incorporate sulfur leading to the formation of a GaS layer which does not form with CVD because of <u>in situ</u> substrate etching. To prevent

cracking of the mixed crystal film the $(\bar{1}\bar{1}\bar{1})$ As face was used as the deposition surface. Since, on this face, the first incorporated species is the cation, and etching does not leave a gallium excess; there is no GaS formation, and the films were uncracked.

Crack-free films have also been produced on substrates tilted 14° away from (111). An interesting feature of film growth on these tilted substrates is that they do not show as dramatic a dependence of composition on the relative source evaporation rates as do the exact (111) substrates. The extreme sensitivity of film composition to deposition parameters for (111) substrates was discussed in the previous section. Furthermore, as might be expected for higher step-density substrates, the growth rates were higher with the tilted substrates. However, it was observed that many of the films deposited on the As face showed polycrystalline growth which may have been a result of the higher growth rates.

Figures 3.14 through 3.16 show SEM micrographs of films grown on tilted substrates. Figure 3.14 shows the cleaved edge of a film where the cleavage steps are seen to be parallel to the substrate <111> direction, just as in the case of exact (111) substrates. In Fig. 3.15 (Film 9207) elongated hexagonal faces are seen on the top surface. A markedly different surface morphology showing ledges is seen in Fig. 3.16 (Film 9107) in which the normalized growth rate was lower. These ledges were perpendicular to the axis of rotation away from the (111) substrate plane.

To eliminate the possibility of further variations in substrate surface condition, sputter-etching equipment was installed. Also to obtain a cleaner vacuum (mainly reduction in hydrocarbons present) a turbomolecular pump (Leybold-Heraeus 450 Turbovac) was used to replace the oil diffusion pump. Experiments using the sputter-etch procedure (Films 12067 thrugh 1118) were conducted on the following two GaAs surfaces:

(1) ~14° -off $(\bar{1}\bar{1}\bar{1})$ As face

(2) Cr-doped $(\bar{1}\bar{1}\bar{1})$ As face ($\rho > 10^6 \Omega$ -cm, Materials Research Corp.)

The latter substrates were to be used in making measurements of the film resistivity. Both sets of substrates were given the following etch procedure:

(1) 5 mins. $3:1/H_2SO_4:H_2O$

(2) 1 min. $5:1:1/H_2SO_4:H_2O_2:H_2O$

(3) 1 min. $7:1/H_2SO_4:H_2O$ (immediately preceding deposition)

All solutions were cooled in an ice bath. The substrates were washed in methyl alcohol and blown dry with N_2 prior to placement in the vacuum system.

In operation, to begin the sputter etching, argon was leaked into the chamber while the main gate valve was throttled so that the pressure was approximately 150 millitorr. D.C. voltages between 500 V and 2.6 KV were used for times of 2-10 minutes with a cathode-anode distance of approximately 2.5 cm. The substrate and cylinder were then heated and the usual deposition procedure initiated. A photograph of

the deposition apparatus with sputter-etch facilities is shown in Fig. 3.17.

Lower growth rates, between 11-30 Å/sec, were used for both kinds of substrates. All films grown on sputter-etched substrates had both (002) and off c-axis diffraction peaks as found by x-ray diffraction. Single crystal and polycrystalline regions on the same film were observed in the SEM as shown in Fig 3.18. A summary of film growth experiments using the sputter-etch procedure is given in Table 3.3A.

A possible explanation for the polycrystalline growth is extensive ion damage to the substrate surface from the sputter-etch procedure which would create heterogeneous nucleation sites. Figure 3.19 shows the growth of randomly oriented CdS grains from the shortened deposition Run 1118. Films 1138 and 1178 were deposited under similar conditions as the previous three runs but without the sputter-etch procedure. The improved epitaxy resulting in a highly specular surface is shown in Fig. 3.20.

Since growth on Ga face GaAs substrates was found to be greater than on the As face and epitaxy more readily achieved deposition Runs 1208 through 3098 were grown on 14°-off (111) Ga face substrates (see Table 3.3B). Some (Cd,Zn)S films were too thin (<1 μm) for analysis as can be seen in Table 3.3B. This was due to the very sensitive dependence of growth rate on the relative evaporation rates of CdS and ZnS, as discussed in the previous section.

3.4 Films Grown in Van der Pauw Geometry

In order to correlate the structural perfection of the grown films with their electrical properties, Hall effect experiments were performed to determine values for carrier concentration and mobility. CdS films in the Van der Pauw geometry[80] (see Fig. 3.21) were deposited onto insulating ($\rho > 10^7$ Ω-cm, chromium doped) (111) and 12°-off (111) towards (110) GaAs substrates. It was found that CdS films grown on the As face were polycrystalline (with the higher source power settings) and films grown on the Ga face were single crystal. An order of magnitude difference in Hall mobility was found for these samples as discussed in Section 4.1.

Yoshikawa and Sakai[81] reported that CdS films grown on GaAs substrates in H_2 gas by the close-spaced technique resulted in films with low resistivity and carrier concentration as high as 5×10^{19} cm^{-3}. They determined for films grown at substrate temperatures of 740°C for 10 mins. that the dominant donor species was Ga which had diffused from the GaAs substrate. CdS films for Hall effect measurements were grown on quartz and Corning 7059 substrates to investigate the effects of autodoping. It was found, however, that all films grown on these substrates were non-adherent even after altering several processing parameters and substrate preparation techniques. The results for films grown in the Van der Pauw geometry for Hall effect measuements are summarized in Table 3.4.

3.5 Films Grown on (111) Ge Substrates

Single crystal CdS and (Cd,Zn)S films were grown on GaAs substrates because of the good thermal expansion and lattice parameter match. However, current-voltage measurements of the n-CdS/n-GaAs heterojunction showed a non-ohmic characteristic. Efforts were made to etch the GaAs from the grown single crystal film for backwall cell construction, but the thickness of the films (usually less than 10 μm) made handling extremely difficult (see the results for films grown on GaAs substrates in Tables 3.3A and 3.3B).

To facilitate front-wall cell construction, a semiconductor substrate forming an ohmic back contact was sought. Growth experiments were conducted on (111) n-Ge substrates because of the good thermal expansion and lattice parameter matching and its larger electron affinity than GaAs (see Table 1.1). CdS and (Cd,Zn)S films were deposited on Ge substrates under growth conditions similar to those for GaAs substrates. These films, however, were non-adherent. Abdalla, Holt and Wilcox[51] observed no CdS film growth on Ge substrates heated above 550°C which they attributed to sulfur attack of the Ge resulting in a pitted surface. Epitaxial CdS films were grown on Ge by lowering the substrate temperature to approximately 320°C at the beginning of the deposition. Good quality single crystal films of CdS were grown at the lower substrate temperatures but upon addition of Zn, the (Cd,Zn)S and further CdS films were cracked as shown in Fig. 3.22. In some cases the films cracked during growth and etching of the Ge occurred through the cracks (Fig. 3.22a) resulting in non-adherent

films. These growth results are summarized in Table 3.5A. (The values for substrate temperature indicates the temperature at the start of the deposition and the additional heating due to the sources).

Since cracking only occurred after a ZnS evaporation, it was believed that the exclusion of Zn from the growth chamber would eliminate this problem. An extensive cleaning and out-gassing procedure was conducted before each growth run. Uncracked single crystal CdS films were then routinely deposited. (Cd,Zn)S films were grown by initially depositing a CdS layer (see Table 3.5B). Because the hot-wall cylinder was cleaned before each growth run, the effect of cylinder wall temperature on growth rate could be more accurately determined as shown in Fig. 3.23.

An effect of supersaturation on surface morphology was also observed. Figure 3.24a shows the top surface of a single crystal CdS film grown on (111) Ge in which the surface morphology is dominated by hexagonal pyramids. Christmann, Jones and Olsen (CJO)[82] found for CdS grown epitaxially on SrF_2 substrates that the hexagonal pyramids were associated with an excess amount of cadmium, and that they could be formed by growth around a cadmium droplet. Cadmium droplets formed when conditions existed which did not allow the cadmium adatoms sufficient time to diffuse to their equilibrium positions.
Figure 3.24b is a SEM micrograph of a single crystal CdS film grown at a lower cylinder temperature in which the supersaturation was less than in the previous example. Hexagonal flat-tops are dominant which is in agreement with CJO who showed that this morphology was the equilibrium growth form produced by two-dimensional nucleation.

IV. ELECTRICAL AND OPTICAL MEASUREMENTS

4.1 Hall Effect Results

Hall effect experiments were conducted on CdS films grown in the Van der Pauw geometry to obtain values of Hall mobility parallel to the substrate surface ("in-plane"), carrier concentration, and resistivity. The results are summarized in Table 4.1. The measurements were performed at room temperature with a magnetic field of 6 Kgauss.

An order of magnitude variation in Hall mobilities was measured with the lower values obtained from the polycrystalline samples. Because of the differences between substrate orientation and growth conditions, more specific relationships could not be determined. Kazmerski, Berry and Allen have discussed the role of grain boundaries and surfaces[83] and stacking faults[84] on the electrical properties of polycrystalline CdS. An empirical model was developed to explain the scattering effects of these defects. It was concluded that the fabrication parameters, especially the deposition rate and substrate temperature, determined the nature of the crystalline imperfections and therefore the electrical properties.

Yoshikawa and Sakai[81] reported that CdS films grown on GaAs substrates in H_2 gas by the close-spaced technique resulted in films with low resistivity and carrier concentrations as high as 5×10^{19} cm^{-3} as a result of autodoping. In this study Hall measurements made on single crystal and polycrystalline films grown on GaAs substrates showed carrier concentrations in the 10^{16}-10^{17} cm^{-3} range. This data along with the fact that the films were grown at substrate

temperatures 300°C lower than that used by Yoshikawa and Sakai would indicate that autodoping was not occurring.

Hall mobility measurements of two samples were made at different magnetic fields to determine the effects of magnetoresistance. Figures 4.1 and 4.2 show the change in Hall mobility with magnetic field for samples 6208 (single crystal CdS) and 6218 (polycrystalline CdS), respectively. Note that the curves take the same form for both single crystal and polycrystalline samples. Beer and Willardson,[85] by taking into account mixed scattering from acoustic phonons and ionized impurities, have reported this same type of behavior for single crystal Ge. Since these measurements were taken at room temperature, scattering from both of these processes were probably present.

4.2 Current-Voltage Measurements

The I-V characteristics of a representative sample of cells using GaAs substrates are summarized in Table 4.2 As noted in the previous chapter, difficulties were encountered in using both p- and n-type GaAs substrates because of the non-ohmic back junction for front-wall cells. This affected the illuminated I-V characteristics resulting in a "reverse-knee" as shown in Fig. 4.3 for cell 3088-1. Front wall tungsten lamp and sunlight I-V curves for cell 6167-1 using an In contact to the (Cd,Zn)S are shown in Figs. 4.4a and b, respectively. No attempt was made to simulate any sunlight-equivalent condition with the tungsten lamp. It was intended only as a reproducible experimental condition for comparison between cells. As discussed in the following

section on spectral response measurements, the low currents measured were partly due to the insufficient thickness of the Cu_xS layers.

Many of the cells produced by the dry process using heat treatment temperatures greater than 100°C resulted in shorted devices. Figure 4.5 is an SEM micrograph of the top surface of a (Cd,Zn)S film (Run 9258) converted to Cu_xS by heat treating at 135°C for 1 hour. The cracks which were observed only after the conversion process are due to the difference in lattice parameters as reported by Singer and Faeth,[86] and Cook, Shiozawa and Augustine.[87] It is believed that these cracks provide a fast diffusion path for Cu resulting in short-circuits through the cell. Non-shortened cells using the dry process were possible for the thicker CdS or (Cd,Zn)S films. To circumvent the shorting problems associated with the dry process and to compare with cells using the same (Cd,Zn)S base film , devices were also formed by reactive sputtering of Cu_xS. Some of these results are summarized in Table 4.2.

Other experiments were performed in which the heat treatment temperature and time used for the dry conversion process was varied. Figure 4.6 shows the original CdS and converted regions using a heat treatment temperature of 60°C for 1/2 hour. No cracks were observed in this case for the entire surface. The converted Cu_xS region was verified using EDAX. Figure 4.7a is the EDAX spectrum of the area marked as CdS in Fig. 4.6, showing the characteristic lines for the elements S, Cd and Ge (from the underlying substrate). Figure 4.7b shows the presence of Cu which was detected only in the evaporated CuCl

region which was converted to Cu_xS. The I-V characteristics of this cell are shown in Fig. 4.8b. When the conversion process was performed at 60°C for 1 hour on a different CdS film (8249), the short-circuit current increased while the open-circuit voltage decreased as shown in Fig. 4.8a. This may be explained by a thicker Cu_xS layer and hence larger generation of carriers but a higher shunt conductance was measured, resulting in a lower V_{oc}. The results for devices using Ge substrates are summarized in Table 4.3.

4.3 Spectral Response Measurements

Figure 4.9 shows the room temperature front-wall mode spectral response of cell 6167-1. This measurement indicates that the Cu_xS layer was too thin since there was a large mixed crystal response at ~400 nm in spite of the good long wavelength response; this contributes to the low measured short-circuit current. The shape of the long wavelength response indicates good stoichiometry of the Cu_xS; a moderately thick chalcocite (Cu_2S) layer, however, would be opaque at 400 nm. Spectral response measurements of cells for which the Cu_xS was formed by reactive sputtering showed very similar characteristics with a large response from the CdS or (Cd,Zn)S as shown in Fig. 4.10.

V. AUGER ELECTRON SPECTROSCOPY STUDIES

5.1 Introduction

Auger electron spectroscopy (AES) has become an established analytical technique for obtaining the chemical composition of solid surfaces. The basic advantages of this technique are its high sensitivity for chemical analysis in the 5-20Å region near the surface, a rapid data acquisition speed and the ability to detect all elements above He.[88] When surface chemical analysis by AES is carried out simultaneously with inert gas sputtering, composition depth profiles may be obtained.[89]

The basic physical mechanism of the Auger process involves the ionization of an electron in a solid in which the relaxation energy from filling the inner shell is transferred to a second, or Auger electron. When a primary electron ionizes an inner electron shell, e.g., the K-shell, an outer electron, e.g. the L_1 electron, may drop to the lower energy level. The energy released by this transition is either emitted as a photon or given to another electron. If this energy is sufficient, an electron, e.g., at $L_{2,3}$, may be ejected from the atom resulting in the $KL_1L_{2,3}$ Auger transition. The energy released for this transition is exactly $E_K - E_{L_1}$, but the ejected electron must expend the energy $(E'_{L_{2,3}} + \phi)$ to escape the atom where ϕ is the work function and $E'_{L_{2,3}} \neq E_{L_{2,3}}$ due to the extra positive charge of the atom. Because of the positive charge, $E'_{L_{2,3}}$ should be approximately equal to the $L_{2,3}$ ionization energy of the next heavier element, or $E'_{L_{2,3}}(Z) = E_{L_{2,3}}(Z+\Delta)$, where Z is

the atomic number and $\Delta \simeq 1$ to account for the extra charge. The energy of the ejected electron is then:

$$E(Z) = E_K(Z) - E_{L_1}(Z) - E_{L_{2,3}}(Z + \Delta) - \phi. \qquad (5\text{-}1)$$

Equation (5-1) may be generalized to any Auger event involving the levels $W_o X_p Y_q$; also the actual measured energy will have an additional term $-(\phi_A - \phi)$, which is the difference in work functions between the analyzer and the material being examined. This results in:

$$E_{WXY}(Z) = E_W(Z) - E_X(Z) - E_Y(Z+\Delta) - \phi_A \qquad (5\text{-}2)$$

By taking into account quantum mechanical exchange effects, refinements in Eqn. (5-2) results in values of E_{WXY} that agree with experiment to within ≤ 1 percent for the simpler families of Auger transitions.[90] The strongest transitions observed experimentally are of the type WXY with X,Y = W or (W+1), where (W+1) is the next higher level. This "selection rule" follows from the fact that electron-electron interactions are strongest between electrons whose orbitals are closest together.

The Auger electrons are observed as small peaks in the total energy distribution function N(E) but become more pronounced by electronic differentiation which removes the large background. This background consists mainly of backscattered primary electrons and inelastically scattered Auger electrons.[88] The principal Auger transitions are

listed[91] so that rapid identification of peaks in an Auger spectrum may be performed.

5.2 Experimental Results

Figure 5.1 shows the differentiated AES spectrum for a reactively sputtered Cu_xS layer deposited onto (Cd,Zn)S film 5239 after sputtering for 10 mins. using 3kV Ar^+ ions. The AES spectrum of the original surface showed the presence of carbon, oxygen and nitrogen. Figure 5.2 shows the atomic concentration versus sputtering time (following the original 10 min. sputtering) for the elements S, Cu, Zn and Cd in which the sample was sputter-etched using 5 kV Ar^+ ions (the higher energy ions were considered necessary because of the low sputtering rate obtained at 3kV). The AES spectrum for the resulting surface after 8 mins. of sputtering is shown in Fig. 5.3, indicating the presence of only S, Zn and Cd. In examining the AES spectrum and the resulting atomic composition depth profile as determined by the Multiple-technique Analysis Computer System (MACS), it is apparent that several errors exist.

To determine the relationship between the Auger electron signal and atomic concentration the method used in the MACS program was to compare the Auger peak-to-peak height from the sample element with that from a pure silver standard. The atomic concentration of element x is defined as

$$C_x = \frac{\frac{I_x}{S_x\, d_x}}{\sum_{i=1}^{n} \frac{I_i}{S_i\, d_i}} \qquad (5\text{-}3)$$

where

I_x = peak-to-peak Auger amplitude of element x,

S_x = relative sensitivity factor (compared to silver),

$d_x = L_x\, E_{m,x}\, I_{p,x}$,

L_x = lock-in sensitivity for element x,

$E_{m,x}$ = peak-to-peak modulation amplitude for element x, and

$I_{p,x}$ = primary beam current for element x.

This results in the following expression for the atomic concentration:

$$C_x = \frac{\frac{I_x}{S_x\, L_x\, E_{m,x}\, I_{p,x}}}{\sum_{i=1}^{n} \frac{I_i}{S_i\, L_i\, E_{m,i}\, I_{p,i}}} \qquad (5\text{-}4)$$

It was assumed that the primary beam current was the same for all i (this was experimentally maintained) and that L_i was fixed for all i so that L_i may be replaced with N_i, the number of sweeps for element i. The formula implemented by the MACS computer is then:

$$C_x = \frac{\frac{I_x}{S_x N_x E_{m,x}}}{\sum_{i=1}^{n} \frac{I_i}{S_i N_i E_{m,i}}} \qquad (5\text{-}5)$$

The tabled values used for the atomic concentration calculation are:

Element	Auger Peak (eV)	S_i	$E_{m,i}$
S	152	.80	3
Cu	920	.22	6
Zn	994	.17	6
Cd	376	.98	3

West has studied the statistical reproducibility of quantitative chemical compositions calculated from Auger spectra.[92] He concluded that the absolute compositions could be determined to within ±20 percent when reciprocal sensitivity factors based on pure elements was used. The main assumption in these calculations is that the sensitivity factor for element i is the same for the pure element and in a mixture which implies small "matrix effects." These matrix effects will change the Auger peak energy and shape and has been discussed by Chang.[93]

Another error in these calcuations occurs in determining the peak-to-peak height for elements in which there is no signal at the prescribed energy value and the background noise is taken to be the intensity. This can be seen in the atomic concentration value obtained for Zn in Fig. 5.2 for sputter time = 0, whereas the Auger spectrum of Fig. 5.1 indicates no presence of Zn at 994 eV (the peak-to-peak Auger

signals from which these calculations were done is shown in Fig. 5.4). An erroneous atomic concentration of 7 percent Zn was determined. The AES spectrum after 8 mins. of sputtering however shows Zn to be present and results in 12 atomic percent Zn. This compares well with the bulk value of $Cd_{0.79}Zn_{0.21}S$ (10.5 atomic percent Zn) as determined by X-ray measurements. Also shown in Fig. 5.2 are several atomic percent of Cd present at the surface of the Cu_xS layer and Cu throughout the (Cd,Zn)S layer which are probably artifacts of the computing process (the solid solubility limits of Cd and Zn in Cu_xS are about 5 x 10^{19} cm^{-3} or less[94]).

The peak-to-peak Auger signal profile of the heterojunction formed by the reactive sputter deposition of Cu_xS (Fig. 5.4) may be compared with that formed by the solid-state ion exchange method (Fig. 5.4) in which the same (Cd,Zn)S base film was used. The interface between the Cu_xS and (Cd,Zn)S is more diffuse than that formed by reactive sputtering in which a relatively high concentration of Zn and Cd is still present for the interface region between the sputtering times of 4 and 6 mins. (there is still the problem of a computed Zn concentration in which the AES spectrum indicates no Zn Auger peak for sputter time = 0). The peak-to-peak and atomic concentration ratios of Zn/Cd for the interface region and the (Cd,Zn)S film are given below:

Sputtering Time	Zn/Cd Ratio Peak-to-Peak	Atomic Concentration
4	0.48	1.41
5	0.22	0.58
6	0.19	0.53
7→20	0.16	0.42
Bulk X-ray Data		0.26

For the interface region an enhanced Zn concentration was found indicating that the heterojunction formed between Cu_xS and (Cd,Zn)S by the dry process results in either a (Cd,Zn)S interface layer with a higher Zn content than that measured in the initial base material and/or the precipitation of Zn.

Compositional depth profiling was also performed for Cu_xS formed by reactive sputtering and the ion-exchange method on a ZnS/CdS/Ge structure (the intermediate CdS film was necessary in order to prevent etching of the Ge substrate as discussed in Section 3.5). Lower energy Ar^+ ions (3kV) were used for sputter etching to reduce the possibility of introducing artifacts due to ion bombardment. An increased sputtering rate from the previous two samples (sputtered at 5kV) was achieved by changing the sample tilt angle. Some of the problems associated with inert gas sputtering has been discussed by Coburn[95] and Wehner.[96] Figure 5.6 is the peak-to-peak Auger signal profile of a reactively sputtered Cu_xS film on the single crystal ZnS/CdS structure. The Cu_xS layer was initially sputtered with 3kV Ar^+ ions for 30 sec. to remove surface contaminants (C and O were detected on the original surface). The interface between the reactively sputtered Cu_xS and ZnS is very sharp as was found for the sputtered Cu_xS layer onto a (Cd,Zn)S surface. The interface between

the ZnS and CdS appears diffuse which may be explained by a mixed crystal layer since Cd and Zn are mutually soluble. A rough estimate in converting sputtering time to depth may be done by assuming the same sputtering rates for the different compounds and that of a Ta_2O_5 standard. A sputtering rate of approximately 400 Å/min. was found for the Ta_2O_5 standard using 3kV Ar^+ ions which would indicate a Cu_xS layer thickness of approximately 2600 Å (this was within the thickness range estimated by the group at the Lawrence Livermore Laboratory).

For Cu_xS formed by the dry process on the ZnS/CdS structure, a very different peak-to-peak Auger signal profile was obtained as shown in Fig. 5.7. A 30 sec. 3kV pre-profile sputter etch was performed initially to remove surface contaminants. The atomic concentration profile as determined by the MACS program is shown in Fig. 5.8. The region labeled 1 in Fig. 5.8 indicates the dry process formed Cu_xS; region 2 an interfacial region; region 3 ZnS and (Cd,Zn)S; and region 4 CdS. Because of the difficulties in obtaining an accurate measure of the atomic concentrations, more detailed calculations were made using two different analyses.

Since the atomic concentrations calculated by the MACS program resulted in errors due to the background noise, it was assumed that no Zn or Cd existed throughout region 1 of Fig. 5.8 (as verified by the AES spectrum before and after the initial 30 sec. sputter etch). To determine the amount of Zn present in region 2, the concentrations of Cu_xS and ZnS were calculated using the ratios of Cu/S and Zn/S as

measured in regions 1 and 3, respectively. The Zn/S ratio measured for a sputtering time of 6 mins. (Zn/S = 1.13) compares well with the value found for ZnS from Fig. 5.6 (Zn/S = 1.16). The tabled relative sensitivity factors were used in determining the element concentrations.

Other data was also used to refine the calculations. Craig and Kullerud[97] studied the phase relations for the Cu–Zn–S system and found no ternary phases. They also determined that the solid solubilities of ZnS in Cu_xS (x=2) and Cu_xS in ZnS were less than 1 weight percent below 100°C. Assuming only the existence of ZnS and Cu_xS in region 2, on thermodynamic grounds, an excess of Zn was found as shown in Table 5.1. Also shown in Table 5.1 is the original data as calculated from the MACS program.

The second compositional analysis was based on the knowledge of several fixed compositions. Adjusted relative sensitivity factors were calculated using sulfur as a standard in Eqn. 5–5 and assuming Cu/S = 2 for sputter time = 0, Zn/S = 1 for sputter time = 6 min. (ignoring background Cu and Cd), and Cd/S = 1 for sputter time = 20 min. The same solubility requirements were used as applied for the previous case. The calculated relative sensitivity factors are: $S_S = 1.0$, $S_{Cu} = 0.36$, $S_{Zn} = 0.24$, and $S_{Cd} = 0.89$. The revised depth profile is shown in Fig. 5.9 (the dashed lines indicate the estimated composition profiles) and the atomic concentrations are listed in Table 5.2. Note that there is an excess of Zn measured in region 2 as in the previous calculations. To confirm the validity of

the revised relative sensitivity factors, the data from Fig. 5.5 was recalculated using the adjusted values. The revised data is listed in Table 5.2 and plotted in Fig. 5.10 in which the retention of Zn at the interface was also found.

Iwami, Kim, Matsuo and Hiraki[98] studied the growth mechanism of Cu_xS on CdS substrates also using Auger electron spectroscopy. They found by depth profile measurements that the junction formed by the dry process (~40 min. at ~200°C) had a diffuse interface composed of Cu, Cd and S with a thickness of ~500Å. They also found that Cu and Cd atoms diffused into the CdS substrate and Cu_xS, respectively, with the Cu diffusion being rather deep (~500Å). This Cu "tail" into the CdS and formation of a compensated region has also been observed by Meakin.[99]

An interesting change in the sulfur Auger signal was reported by Iwami et al., from that observed for the Cu_xS layer and CdS substrate.[98] The S peak from the Cu_xS showed a splitting which was explained by a chemical shift resulting from the hybridization of the valence s- and p-like electrons with the host metal d-band.[100] This effect was studied for reactively sputtered Cu_xS and Fig. 5.11 shows the S signal obtained from sample 8319, in which no splitting was found. However, when the Cu_xS surface was sputter etched for 30 sec. with 3 kV Ar^+ ions, splitting of the S peak was observed as shown in Fig. 5.12. It should be noted that Iwami et al., first cleaned their surfaces by ion sputter etching (2 kV Ar^+ ions with a beam current

density of ~10 $\mu A/cm^2$) and that the splitting may be an artifact of this sputter process. This may possibly be explained by the change in valence state of the sulfur due to ion bombardment.

VI. DISCUSSION

6.1 Thin Film Growth

A number of different single crystal semiconductor surfaces were used as substrates for the heteroepitaxial growth of CdS and (Cd,Zn)S; each of which presented its own unique set of problems. The single crystal films were necessary in order to approach a planar interface between the II-VI compound and epitaxial Cu_xS. The problems associated with grain boundary intrusion of Cu_xS in polycrystalline samples was therefore avoided.

It was found experimentally that both the composition and growth rate of single crystal (Cd,Zn)S films depended very strongly upon the ratio of ZnS to CdS evaporated as shown in Figs. 3.11-3.13. These graphs may be used as guidelines for the vapor growth of (Cd,Zn)S thin films of a desired composition. These same experiments also indicated the importance of eliminating cross-contamination between the CdS and ZnS sources. Due to the higher diffusivity of Cd, it was also observed that for lateral uniformity of the film composition it was necessary to eliminate temperature gradients across the substrate surface.

Film growth experiments on the (111) Ga or As faces and off-(111) orientations provided information about growth mechanisms and the effects of interfacial layers. The exposed substrate surface (either A or B face) resulted in a different stacking sequence of the deposited film. The presence of an interfacial GaS layer was found to affect the stresses in the multilayered structure resulting in cracking. An

accelerated growth rate was observed for the higher step-density (off-(111)) substrates.

It was found the GaAs substrates were unsuitable for front-wall test cell construction because of the non-ohmic junction with CdS. Film growth experiments were transferred to (111)n-Ge substrates which did form an ohmic isotype heterojunction. For (Cd,Zn)S film growth an intermediate layer of CdS was found necessary to avoid attack of the Ge substrate. Conditions for the heteroepitaxial growth of (Cd,Zn)S on Ge substrates were determined.

6.2 Electrical and Optical Characteristics

Test devices were fabricated to evaluate the effects of different processing parameters on resulting electrical and optical properties. Hall effect experiments showed electron mobilities in the vapor grown CdS films to be comparable with other published results.

The current voltage characteristics of cells formed by the solid state ion-exchange and reactive sputtering processes showed low short-circuit current densities. This was partly due to the inadequate thickness of the Cu_xS resulting in lower absorption of photons as observed in the spectral response measurements. Cells formed by the ion-exchange method also had low shunt resistances resulting in poor fill factors. Note that no extensive optimization of the cell characteristics was attempted and that relatively poor soft characteristics has also been reported on single crystal cells by Oktik, Russell and Woods.[101] These results indicated that the fabrication process used would produce functional devices allowing for comparisons between cells.

To improve the performance of these test cells several aspects of the cell construction could be altered. The total series resistance of the cell could be lowered by doping the CdS or (Cd,Zn)S films with In and also by the development of a better front contact structure to prevent current crowding. Another critical improvement would be the optimization of Cu_xS thickness and stoichiometry.

6.3 Auger Studies

The compositional depth profiles of Cu_xS formed by the dry ion-exchange process on single crystal (Cd,Zn)S and ZnS films indicates a very complex interface. For both heterojunctions with Cu_xS an enhanced concentration of Zn was found.

Burton[94] has by atomic absorption spectroscopy measured the concentrations of Cd and Zn in the Cu_2S/(Cd,Zn)S heterojunction formed by the wet ion-exchange process. He found excess Zn under the interface and concluded that approximately 75 percent of the available Zn particpated in the ion-exchange reaction. Assuming that no precipitation of Cu occurs (this implies that the ion-exchange reaction will only proceed with the formation of a Cd or Zn cation vacancy), the revised data for sample 5239 from Table 5.2 results in an interfacial region consisting of Cu_xS, (Cd,Zn)S and precipitates of both Cd and Zn. This would suggest that in addition to the modification of the heterojunction band structure due to the enhanced Zn concentration in the (Cd,Zn)S interfacial layer, the precipitation of Zn and Cd also requires consideration. Burton concluded that the actual (Cd,Zn)S composition under the interface differed from that of the starting film

and could result in a potential spike at the interface and/or reduced values of mobility and electric field. This would then result in the observed reduction of photogenerated current.

For the Cu_xS/CdS cell, the presence of Cd in the Cu_xS layer has been observed. The Cd/Cu ratios found for an approximately 6 μm thick Cu_xS layer formed by the wet ion-exchange process was found to be 0.24 percent as determined by atomic absorption.[99] Because of this low value the Cd in Cu_xS was not thought to adversely affect the cell response. It should be noted that the Cd/Cu ratios determined was the average for the Cu_xS layer thickness and did not reflect the likely presence of a Cd gradient.

Burton, Dwight and Zeller[102] have performed AES compositional studies of the polycrystalline Cu_xS/(Cd,Zn)S heterojunction and found an anomalously high Zn concentration in the Cu_xS; especially at the top surface (the Cu_xS was formed by the dry ion-exchange process and the reaction products not removed). It is difficult to determine from their results if there is enhancement or precipitation of Zn since their polycrystalline sample probably consisted of Cu_xS penetrating down grain boundaries. This would result in an averaging of bulk and grain boundary converted Cu_xS depending upon the grain size of the sample and the incident electron beam size.

The AES results from this study are in agreement with more recent data[103] and may be extended by making several assumptions. If the concentrations of Cd and Zn in Cu_xS are assumed to be much less than 1 atomic percent and may be ignored, then an excess of Cd and Zn

in the form of a second phase is present in the interfacial region. This was calculated by accounting for the sulfur required to form Cu_xS and assuming that the remaining sulfur would be used to form (Cd,Zn)S. For sample 5239 the atomic percent S remaining for sputter time t = 3 through 6 sec (see Table 5.2) is less than the sum of the Cd and Zn atomic percent. The precipitation of Zn at the Cu_xS/ZnS interface was more evident.

Boer[104] in his model of the Cu_xS/CdS heterojunction proposed that for reasons of charge compensation and localized stress field near the interface dislocations, a substantially increased solubility of Cd ions in Cu_2S was expected. The estimated density of interstitial cadmium near the sulfur bonds at the mismatch dislocation field would be extremely large (sulfur dangling bond density $>10^{14}$ cm^{-2}). A model was proposed to explain the observed increase in V_{oc} and decrease in I_{sc} when the lattice mismatch is reduced due to the widening of the potential spike at the barrier thereby reducing the tunneling current (this model involves a valence band-edge jump and a potential spike resulting from a dipole layer and not from the differences in electron affinity). The effect of Zn in the (Cd,Zn)S/Cu_xS cell may be greater than Cd in the CdS/Cu_xS cell because of the reduced values of solubility and diffusion coefficients of Zn^{++} relative to those of Cd^{++} in Cu_xS.

6.4 Suggestions for Future Work

Single crystal films of CdS and (Cd,Zn)S were grown to study their planar interface with Cu_xS to better understand the possible

mechanisms affecting cell performance. It was found that the precipitation of Cd and Zn occurs which alters the heterojunction properties. A model has been proposed in which the mismatch dislocation field accomodates these ions and explains the observed electrical properties of these cells. It is apparent that a detailed structural study along with chemical analysis is required to correlate these imperfections with their electrical properties.

An initial transmission electron microscopy (TEM) study of the films grown in this work indicated the presence of inclined dislocations perpendicular to the substrate.[105] These dislocations, however, did not seriously affect the bulk electrical properties as measured by Hall effect experiments but may be extremely detrimental during the heterojunction formation or heat treatment (this may explain the low shunt resistance measured for some cells). A TEM cross-section of a processed cell would clarify the precipitation occurring at the interface and the presence of other structural imperfections.

It was also found that the reactively sputtered Cu_xS formed epitaxially on single crystal CdS. The AES study in this work showed an abrupt junction which suggests that this may be the preferred processing technique for the formation of Cu_xS. To further understand the limitations and effects of different processing of these heterojunctions, studies on the correlation between structural, chemical and electrical properties needs to be continued.

REFERENCES

1. See for example:
   (a) Records of the Photovoltaic Specialists Conferences which have been sponsored by the IEEE (IEEE Press, New York, 1961-1982), Volumes 1-16.
   (b) H. J. Hovel, Solar Cells, Semiconductors and Semimetals, edited by R. K. Willardson and A. C. Beer (Academic Press, New York, 1975).
   (c) R. C. Neville, Solar Energy Conversion (Elsevier Scientific, New York, 1978).
   (d) R. Hill in Active and Passive Thin Film Devices, edited by T. J. Coutts (Academic Press, New York, 1973), p. 487.
2. A. M. Barnett, J. A. Bragagnolo, R. B. Hall, J. E. Phillips and J. D. Meakin, Proc. 13th IEEE Photovoltaic Spec. Conf. (IEEE Press, New York, 1978), p. 419.
3. W. Palz, J. Besson, T. W. Duy and J. Vedel, Proc. 10th IEEE Photovoltaic Spec. Conf. (IEEE Press, New York, 1973), p. 69.
4. T. M. Peterson, Ph.D. Thesis, University of California, Berkeley (1975), LBL-3985.
5. A. Banerjee, S. R. Das, A. P Thakoor, H. S. Randhawa and K. L. Chopra, Solid-State Electron. 22, 495 (1979).
6. R. B. Hall, R. W. Birkmire, J. E. Phillips and J. D. Meakin, Appl. Phys. Lett. 38, 925 (1981).
7. L. C. Burton, Solar Cells 1, 159 (1979).
8. R. L. Anderson, IBM J. Res. and Dev. 4, 283 (1960).

9. R. L. Anderson, Solid-State Electron. 5, 341 (1962).

10. W. Shockley, Electrons and Holes in Semiconductors (Van Nostrand, Princeton, 1950), p. 309.

11. W. G. Oldham and A. G. Milnes, Solid-State Electron. 7, 153 (1964).

12. A. R. Riben and D. L. Feucht, Solid-State Electron. 9, 1055 (1966).

13. L. J. Van Ruyven, in Annual Review of Materials Science, Vol. 2, edited by R. A. Huggins (Annual Reviews, Palo Alto, 1972), p. 501.

14. T. L. Tansley, in Semiconductors and Semimetals, Vol. 7, Part A, edited by R. K. Willardson and A. C. Beer, (Academic Press, New York, 1971), p. 294.

15. A. L. Fahrenbruch and J. Aranovich, in Topics in Applied Physics, Vol. 31, edited by B. O. Seraphin (Springer-Verlag, New York, 1979), p. 257.

16. A. G. Milnes and D. L. Feucht, Heterojunctions and Metal-Semiconductor Junctions (Academic Press, New York, 1972).

17. D. C. Reynolds, G. Leies, L. L. Antes and R. E. Marburger, Phys Rev. 96, 533 (1954) and D. C. Reynolds and S. J. Czyzak, Phys. Rev. 96, 1705 (1954).

18. R. Williams and R H. Bube, J. Appl. Phys. 31, 968 (1960).

19. H. G. Grimmeiss and R. Memming, J. Appl. Phys. 33, 2217 and 3596 (1962).

20. D. A. Cusano, Solid-State Electron. 6, 217 (1963).

21. A. E. van Aerschodt, J. J. Capart, K. H. David, M. Fabbricotti, IEEE Trans. ED-18, 471 (1971).

22. A. G. Stanley, in Applied Solid State Science, Vol. 5, edited by R. Wolfe (Academic Press, New York, 1975), p. 251.

23. W. D. Gill, Ph.D. Thesis, Stanford University (1969).

24. S. Martinuzzi and O. Mallem, phys. stat. sol. (a) 16, 339 (1973).

25. L. D. Partain, G. A. Armantrout and J. Leong, J. Electron. Mater. 9, 467 (1980).

26. A. Rothwarf and A. M. Barnett, IEEE Trans. ED-24, 381 (1977).

27. M. Savelli and J. Bougnot in Topics in Applied Physics, Vol. 31, edited by B. O. Seraphin (Springer Verlag, New York, 1979) p. 213.

28. B. J. Mulder, phys. stat. sol. (a) 18, 633 (1973).

29. W. R. Cook, Jr., Ph.D. Thesis, Case Western Reserve University (1971).

30. E. H. Roseboom, Jr., Am. Mineral. 47, 1181 (1962).

31. L. R. Shiozawa, F. Augustine, G. A. Sullivan, J. M. Smith and W. R. Cook, Clevite Corp. Final Report U.S. Air Force AF 33 (615) 5224 (1969); L. R. Shiozawa, G. A. Sullivan and F. Augustine, Proc. 8th IEEE Photovoltaic Spec. Conf. (IEEE Press, New York, 1968), p. 39.

32. T. S. teVelde, Energy Conversion 15, 111 (1975).

33. J. D. Meakin, First Quarterly Progress Report, E (49-18)-2538 PR 76/1, Institute of Energy Conversion, University of Delaware (1976).

34. G. A. Aramtrout, D. E. Miller, K. E. Vindelov and T. G. Brown, J. Vac. Sci. Technol. 16, 212 (1979).

35. M. Aven and J. S. Prener, editors, Physics and Chemistry of II-VI Compounds (North-Holland, Amsterdam, 1967).

36. B. Ray, II-VI Compounds (Pergamon Press, Oxford, 1969).

37. P. Cherin, E. L. Lind and E. A. Davis, J. Electrochem. Soc. 117, 233 (1970).

38. E. A. Davis and E. L. Lind, J. Phys. Chem. Solids 29, 79 (1968).

39. M. Aven and C. A. Mead, Appl. Phys. Lett. 7, 8 (1965).

40. D. B. Holt, Thin Solid Films 24, 1 (1974).

41. J. W. Matthews, editor, Epitaxial Growth Parts A and B (Academic Press, New York, 1975).

42. A. Yoshikawa and Y. Sakai, J. Appl. Phys. 45, 3521 (1974).

43. M. Bettini and G. Brandt, J. Appl. Phys. 50, 6938 (1979).

44. M. Weinstein and G. A. Wolff, Crystal Growth: Proc. Int. Conf. on Crystal Growth (Pergamon Press, Oxford, 1967), p. 537.

45. B. J. Curtis and H. Brunner, J. Crystal Growth 6, 269 (1970).

46. O. Igarashi, J. Appl. Phys. 42, 4035 (1971).

47. W. M. Yim and E. J. Stofko, J. Electrochem. Soc. 119, 381 (1972).

48. M. Moulin, A. Huber and M. Dugue, J. Crystal Growth 17, 212 (1972).

49. H. V. Dijk and J. Goorissen, Crystal Growth: Proc. Int. Conf. on Crystal Growth (Pergamon Press, Oxford, 1967), p. 531.

50. P. J. Peasley, S.J.T. Owen and P. W. Webb, J. Mater. Sci. 5, 1054 (1970).

51. M. I. Abdalla, D. B. Holt and D. M. Wilcox, J. Mater. Sci. 8, 590 (1973).

52. C. Paorici, C. Pelosi, G. Bolzoni and G. Zuccalli, J. Mater. Sci. 10, 2117 (1975).

53. V. D. Vankar, S. R. Das, Prem Nath and K. L. Chopra, phys. stat. sol.(a) 45, 665 (1978).

54. S. Martinuzzi, J. Oualid, D. Sarti and J. Gervais, Thin Solid Films 51, 211 (1978).

55. L. C. Burton, T. L. Hench and J. D. Meakin, J. Appl. Phys. 50, 6014 (1979).

56. P. Domens, M. Cadene and G. W. Coton, phys. stat. sol.(a) 59, 201 (1980).

57. C. M. Mbow, G. W. Cohen-Solol and D. Laplaze, Thin Solid Films 87, 141 (1982).

58. W. Kane, J. P. Spatt, L. W. Hershinger and I. H. Khan, J. Electrochem. Soc. 113, 136 (1966).

59. D. Bonnet, phys. stat. sol.(a) 11 K135 (1972).

60. L. C. Burton and T. L. Hench, Appl. Phys. Lett. 29, 612 (1976).

61. N. Romeo, G. Sberveglieri and L. Tarricone, Appl. Phys. Lett. 32, 807 (1978).

62. J. B. Snelling, Sandia Laboratories Report SAND 75-0466, (1975).

63. D. B. Fraser and H. D. Cook, J. Vac. Sci. Tech. 11, 56 (1976).

64. R. S. Feigelson, A. N'Diaye, S-Y Yin and R. H. Bube, J. Appl. Phys. 48, 3162 (1977).

65. U. P. Agnihotri and B. K. Gupta, Japan. J. Appl. Phys. 18, 317 (1979).

66. H. I. Kwok and Y. C. Chau, Thin Solid Films 66, 303 (1980).

67. V. P. Singh and J. F. Jordan, IEEE Electron Device Letters 6, 137 (1981).

68. A. Banerjee, Prem Nath, V. D. Vankar and K. L. Chopra, phys. stat. sol.(a) 46, 723 (1978).

69. Y. Sakurai, Y. Kokubun, H. Watanabe and M. Wada, Japan. J. Appl. Phys. 16, 1455 and 2115 (1977).

70. P. Franzosi, C. Ghezzi and E. Gombia, J. Crystal Growth 51, 314 (1981).

71. A. Lopez-Otero and W. Huber, J. Crystal Growth 45, 214 (1978).

72. J. Humenberger, H. Sitter, W. Huber, C. Sharma and A. Lopez-Otero, Thin Solid Films 90, 101 (1982).

73. A. Lopez-Otero, Thin Solid Films 49, 3 (1978).

74. M. E. Behrndt and S. C. Moreno, J. Vac. Sci. Tech. 8, 494 (1971).

75. P. F. Lindquist, Ph.D. Thesis, Stanford University (1970).

76. P. Franzosi, C. Ghezzi and E. Gombia, J. Crystal Growth 44, 306 (1978).

77. G. H. Gilmer and P. Bennema, J. Appl. Phys. 43, 1347 (1972).

78. C. C. Chang, P. H. Citrin and B. Schwartz, J. Vac. Sci. Tech. 14, 943 (1977).

79. M. Cardona, M. Weinstein and G. A. Wolff, Phys. Rev. 140, A633 (1965).

80. L. J. van der Pauw, Philips Research Reports 13, 1 (1958).

81. A. Yoshikawa and Y. Sakai, Japan. J. Appl. Phys. 14, 1547 (1975).

82. M. H. Christmann, K. A. Jones and K. H. Olsen, J. Appl. Phys. 45, 4295 (1974).

83. L. L. Kazmerski, W B. Berry and C. W. Allen, J. Appl. Phys. 43, 3515 (1972).

84. L. L. Kazmerski, W. B. Berry and C. W. Allen, J. Appl. Phys. 43, 3521 (1972).

85. A. C. Beer and R. K. Willardson, Phys. Rev. 110, 1286 (1958).

86. J. Singer and P. A. Faeth, Appl. Phys. Lett. 11, 130 (1967).

87. W. R. Cook, L. Shiozawa and F. Augustine, J. Appl. Phys. 41, 3058 (1970).

88. A. Joshi, L. E. Davis and P. W. Palmberg in Methods of Surface Analysis, edited by A. W. Czanderna, (Elsevier, New York, 1975), p. 159.

89. P. W. Palmberg, J. Vac. Sci. Tech. 9, 160 (1971).

90. C. C. Chang, in Characterizaton of Solid Surfaces, edited by P. F. Kane and G. B. Larrabee (Plenum Press, New York, 1974), p. 509.

91. L. E. Davis, N. C. MacDonald, P. W. Palmberg, G. E. Riach and R. E. Weber, Handbook of Auger Electron Spectroscopy, 2nd Ed. (Physical Electronics Industries, Prarie, MN, 1976).

92. L. A. West, J. Vac. Sci Technol. 13, 198 (1976).

93. C. C. Chang, Surf. Sci. 48, 9 (1975).

94. L. C. Burton, Appl. Phys. Lett. 35, 780 (1979).

95. J. W. Coburn, J. Vac. Sci Technol. 13, 1037 (1976).

96. G. K. Wehner, in Methods of Surface Analysis, edited by A. W. Czanderna, (Elsevier, New York, 1975), p. 5.

97. J. R. Craig and G. Kullerud, Minerol. Deposita 8, 81 (1973).

98. M. Iwami, S. Kim, I. Matsuo and A. Hiraki, J. Cryst. Growth 45, 467 (1978).

99. J. D. Meakin, Proc. International Workshop on Cadmium Sulfide Solar Cells and Other Abrupt Heterojunctions, (IEC, University of Delaware, 1975). p. 75.

100. A. Hiraki, S. Kim, W. Kammura and M. Iwami, Appl. Phys. Lett. 34, 194 (1979).

101. S. Oktik, G. J. Russell and J. Woods, Solar Cells 5, 231 (1982).

102. L. C. Burton, D W. Dwight and M. V. Zeller, Proceedings of Photovoltaic Material and Device Measurements Workshop, Arlington, VA (Solar Energy Research Institute, Golden, CO, 1979), p. 53.

103. P. N. Uppal, L. C. Burton, L. Rivaud and J. E. Greene, J. Appl. Phys. 54, 982 (1983).

104. K W. Boer, phys. stat. sol.(a) 49, 455 (1978).

105. B. L. Chin, T. M. Peterson, U. Dahmen, K. Seshan, L. E. Sindelar and J. Washburn, Final Report of Research on Cu_xS/(Cd,Zn)S Photovoltaic Solar Energy Converters, March 1980, LBL-10791.

Table 1.1 Semiconductor Properties

Material	Crystal Structure	Lattice Constant (Room Temp.) (Å)	Linear Thermal Expansion Coefficient (RT → 800°C) (10^{-6}/°C)	Electron Affinity (eV)
CdS	Wurtzite	a = 4.137[a]	⊥ c 5.0[b]	4.5[d]
		c = 6.716	∥ c 2.5	4.87[e]
ZnS	Zincblende	a = 5.409[a]	6.5 - 8.5[b]	3.9[f]
GaAs	Zincblende	a = 5.654[d]	6.72[b]	4.07[d]
			5.7 - 7.3[c]	
Ge	Diamond Cubic	a = 5.658[d]	6.2[b]	4.13[d]
			5.7 - 7.6[c]	

References:

a W. L. Roth, in Physics and Chemistry of II-VI Compounds, edited by M. Aven and J. S. Prener (North-Holland, Amsterdam, 1967), pp. 127-128.
b W. M. Yim and E. J. Stofko, J. Electrochem. Soc. 119, 381 (1972).
c Thermophysical Properties of Matter, Volume 12, edited by Y. S. Touloukian (IFI/Plenum, New York, 1970).
d A. G. Milnes and D. L. Feucht, Heterojunctions and Metal-Semiconductor Junctions, (Academic Press, New York, 1972), Table 1.2, p. 8.
e J. A. Van Vechten, Phys. Rev. 187, 1007 (1969).
f R. K. Swank, Phys. Rev. 153, 844 (1967), Surface Value.

Table 3.1. Initial Film Growth Experiments

Run	ZnS Current (amps)	CdS Current (amps)	Run Duration (minutes)	Cylinder Temp. (°C)	Substrate Temp. (°C)	Crystallinity s = single p = poly	Thickness (μm)	Composition y in $Cd_{1-y}Zn_yS$ for (hkl)	Substrate
10126	46	30	60	600	495	p	30	(002) y = .15, .86 (103) y = .26 (004) y = .22	($\bar{1}\bar{1}\bar{1}$) As
10136	46	25	60	600	480	p	30	(002) y = .10, 1.0 ZnS (102) y = .08 (103) y = .10	($\bar{1}\bar{1}\bar{1}$) As
10156	43	25	60	600	485	-	-	Non-uniform	($\bar{1}\bar{1}\bar{1}$) As
10186	41	23	60	600	470	p	~24	(002) y = .13 (102) y = .20 (103) y = .15 (104) y = .10	($\bar{1}\bar{1}\bar{1}$) As
10206	37	20	90	600	460	p	7	(002) y = 1.0 ZnS (102) y = .31 (103) y = .29	($\bar{1}\bar{1}\bar{1}$) As
10246	37	20	90	550	420	s	~2	(002) y = 1.0 ZnS	($\bar{1}\bar{1}\bar{1}$) As
10256	39	23	90	550	420	s	~3	(002) y = 0.70 Broad X-ray peak	($\bar{1}\bar{1}\bar{1}$) As
10266	39	24	180	560	430	p	~11	(002) y = .80 (102) y = .28 (103) y = .29	($\bar{1}\bar{1}\bar{1}$) As
11036	39	24	110	560	430	p	10	(002) CdS (101) y = .10 (102) y = .13 (103) y = .13	($\bar{1}\bar{1}\bar{1}$) As
						p	10-45	(002) y = .10 (102) y = .12 (103) y = .15 (004) y = .15	(111) Ga (unpolished)
11056	39	24	110	560	430	p	12-20	(102) y = .10 (103) y = .11	(111) Ga (polished)
11096	37	22	180	560	420	"s"	<1-13	(002) y = .15 (002) y = .75	(111) Ga (polished)
11176	37	22	180	560	395	-	<1	-	Baffle 2 used
11226	38	22	180	600	450	s	<1	(002) ZnS (004) ZnS	(111) Ga (unpolished)

Table 3.2. Film Growth Experiments on (111) Ga-Face Substrates

Run	ZnS Power (watts)	CdS Power (watts)	Run Duration (minutes)	Cylinder Temp. (°C)	Substrate Temp. (S.S.)* (°C)	ZnS Rate R_{ZnS} (mmole/hr)	CdS Rate R_{CdS} (mmole/hr)	ZnS Mole Fraction	Θ (R_{ZnS}/R_{Total})	Thickness τ (μm)	$d\tau/dt$ (Å/sec)	Growth Rate g (Å/μmole)
2047	304	120	60	560	(430)	6.05	13.31	0.29	.312	37.5	104.2	19.37
2097	343	102	30	560	(430)	8.17	16.72	0.29	.328	5.2	28.89	4.18
2107	400	99	60	560	(440)	14.62	14.06	0.90	.510	15.0	41.67	5.23
2167	395	96	60	510	(450)	10.38	10.65	0.90	.493	5.7	15.83	2.71
3087	267	96	60	560	(445)	3.83	10.00	0.24	.277	8.0	22.22	5.79
3297	225	93	60	560	(440)	2.64	13.80	1.00	.161	2.0	5.56	1.22
4017	269	92	60	560	(455)	3.93	11.64	0.82	.253	1.0	2.78	0.64
4057	244	90	60	560	(465)	1.19	2.77	0.31	.301	1.0	2.78	2.53
4077	300	119	60	600	(500)	4.98	8.32	0.82	.374	2.5	6.94	1.88
4137	250	105	60	560	(420)	0.96	4.40	0.17	.180	6.3	17.5	11.74
4197	240	105	120	560	(420)	0.83	3.59	0.22	.187	9.0	12.5	10.18
4267	270	112	120	560	440	1.77	5.44	0.19	.245	23.0	31.94	15.94
5247	258	100	120	560	425	1.29	4.34	0.15	.230	17.0	23.61	15.1
6067	300	100	60	600	475	4.24	4.63	1.00	.478	<1.0	---	---
6077	260	102	60	600	470	2.11	8.24	0.24	.204	3.5	9.72	3.38
6147	262	102	60	600	420	1.98	5.54	0.27	.263	3.5	9.72	4.65
6167	266	105	60	600	460	1.66	9.61	0.19	.148	5.0	13.89	4.44
6177	190	88	90	600	330	0.41	5.25	0.11	.073	9.0	16.67	10.6
6207	182	89.6	90	600	460 → 400	0.53	5.30	0.11	.901	10.0	18.52	11.4
6217	212	89.6	90	600	490 → 420	0.88	5.92	0.17	.130	6.0	11.11	5.88
6237	212	89.6	90	600	340	1.15	4.76	0.17	.195	5.0	9.26	5.64
6277	199	89.6	90	600	340	---	3.72	0.07	---	12.0	22.22	---
7297	0	86.8	90	600	360	0	4.08	0	0	4.0	7.41	6.54
8107	215	89	90	600	340	0	7.06	0	0	15.0	27.78	14.16
8187	216	89.6	90	600	400	0.89	0	1.0	1.0	<1.0	---	---
8317	228	89.6	90	600	370	1.03	6.77	0.05	.135	21.6	40.0	18.47

* (S.S.) = temperatures in parentheses were measured directly on stainless steel holders.

Table 3.3A. Effects of GaAs Substrate Preparation and Orientation

Run	ZnS Power (watts)	CdS Power (watts)	Run Duration (minutes)	Cylinder Temp. (°C)	Substrate Temp. (°C)	ZnS Rate R_{ZnS} (mmole/hr)	CdS Rate R_{CdS} (mmole/hr)	ZnS Mole Fraction	Θ (R_{ZnS}/R_{Total})	Thickness τ (μm)	$d\tau/dt$ (Å/sec)	Growth Rate g (Å/μmole)	Substrate
9017	0	136	30	590	385	0	13.22	0	0	20.0	111.1	30.25	$(\bar{1}\bar{1}\bar{1})$B
9067	0	120	30	585	400	0	8.25	0	0	10.0	55.55	24.24	$(\bar{1}\bar{1}\bar{1})$B
9077	232	102	60	600	410	0	8.31	0	0	27.5	76.39	33.11	$(\bar{1}\bar{1}\bar{1})$B
9097	232	78	60	600	380	0	5.67	0	0	18.0	50.00	31.75	Off $(\bar{1}\bar{1}\bar{1})$B
9107	232	65	60	600	410	0	2.64	0	0	6.6	18.33	24.96	Off $(\bar{1}\bar{1}\bar{1})$B
9127	236	67.5	60	600	420	0.72	3.27	0.05	0.18	18.7	51.94	46.92	Off $(\bar{1}\bar{1}\bar{1})$B
9197	225	60	60	600	420	0.78	2.87	0.05	0.21	15.0	41.67	41.14	Off $(\bar{1}\bar{1}\bar{1})$B
9207	232	57.6	60	600	420	0.70	2.56	0.05	0.21	13.3	36.94	40.81	Off $(\bar{1}\bar{1}\bar{1})$B
9297	250	60	60	600	420	0.75	2.33	0.09	0.24	5.0	13.88	16.22	Off $(\bar{1}\bar{1}\bar{1})$B
9307	225	58	30	600	400	0.69	2.00	0.03	0.25	8.0	44.44	59.69	Off (111)A
12067	190	55.2	60	600	440	1.14	2.60	~0.14+	0.30	8.3	23.06	22.18	Off $(\bar{1}\bar{1}\bar{1})$B
12137	200	60	60	600	440	1.05	3.05	~0.12+	0.26	10.0	27.78	24.43	Off $(\bar{1}\bar{1}\bar{1})$B
12167	184	51.7	60	600	450	0	2.60	0	0	10.0	27.78	38.42	$(\bar{1}\bar{1}\bar{1})$B
12197	127	34.2	60	600	440	0	1.18	0	0	5.0	13.89	42.24	$(\bar{1}\bar{1}\bar{1})$B
1078	172	27.2	90	600	460	0	1.47	0	0	10.0	18.52	45.43	Off $(\bar{1}\bar{1}\bar{1})$B
1098	164	32.4	60	600	440	0	1.09	0	0	4.0	11.11	38.81	Off $(\bar{1}\bar{1}\bar{1})$B
1118	170	39.9	35	600	440	0	---	0	0	A	A	A	Off $(\bar{1}\bar{1}\bar{1})$B

+ = No X-ray data available, estimated from EDAX.

A = Aborted run.

Table 3.3B. Effects of GaAs Substrate Preparation and Orientation

Run	ZnS Power (watts)	CdS Power (watts)	Run Duration (minutes)	Cylinder Temp. (°C)	Substrate Temp. (°C)	ZnS Rate R_{ZnS} (mmole/hr)	CdS Rate R_{CdS} (mmole/hr)	ZnS Mole Fraction	Θ (R_{ZnS}/R_{Total})	Thickness τ (μm)	$d\tau/dt$ (Å/sec)	Growth Rate g (Å/μmole)	Substrate
1138	184	39	60	600	490	0	1.22	0	0	6.0	16.67	49.25	Off $(\bar{1}\bar{1}\bar{1})$B
1178	175	41	60	600	520	0	1.32	0	0	6.0	16.67	45.38	Off $(\bar{1}\bar{1}\bar{1})$B
1208	188	38	60	600	500	0	1.68	0	0	15.0	41.67	89.54	Off (111)A
1248	192	38	60	600	500	1.10	1.59	0.23	0.41	9.0	25.00	33.54	Off (111)A
1278	204	40	60	600	500	0	1.76	0	0	15.0	41.67	85.31	Off (111)A
1308	126	32	60	600	525	0	0.71	0	0	9.0	25.00	127.47	Off (111)A
2028	152	33	60	600	560	0.43	1.21	0.03	0.26	12.3	34.17	74.89	Off (111)A
2078	158	34.2	60	600	550	0.37	0.84	0.15	0.31	10.6	29.44	87.82	Off (111)A
2098	164	32.4	60	600	530	0.28	0.98	0.03	0.22	11.3	31.47	90.41	Off (111)A
2278	137	30	60	600	420	0	0.32	0	0	3.0	8.33	94.22	Off (111)A
2288	122	30	60	600	460	0.12	0.35	*	0.26	*	*	*	Off (111)A
3028	136	40	60	600	490	0.15	0.62	*	0.20	*	*	*	Off (111)A
3088	134	40	60	600	480	0.08	0.66	0.03	0.11	5.5	15.28	74.35	Off (111)A
3098	136	42	65	600	480	0.09	0.75	*	0.11	*	*	*	Off (111)A
5268	118	38	60	600	490	0	0.57	0	0	*	*	*	$(\bar{1}\bar{1}\bar{1})$ As
5308	140	35	60	600	470	0	0.42	0	0	*	*	*	$(\bar{1}\bar{1}\bar{1})$ As
6028	130	44	60	600	480	0	0.64	0	0	*	*	*	$(\bar{1}\bar{1}\bar{1})$ As
6068	140	44	60	600	480	0	0.69	0	0	2.0	5.56	28.9	(111)Ga
6088	130	55	60	600	485	0	0.87	0	0	2.4	6.67	27.5	(111)Ga
8298	152	74	120	600	480	0	1.03	0	0	6.5	9.03	31.5	(111)Ga
8308	216	93	120	600	420	0.85	1.58	0.08	0.35	8.0	11.1	16.5	(111)Ga
8318	261	93	120	600	420	1.62	0	1.00	1.00	*	*	*	(111)Ga
9078	161	48	60	600	430	0	0.81	0	0	3.5	9.72	43.2	(111)Ga

* = Film thickness less than 1 μm; difficult to analyze.

Table 3.4 Films Grown in Van der Pauw Geometry

Run	ZnS Power (watts)	CdS Power (watts)	Run Duration (minutes)	Cylinder Temp. (°C)	Substrate Temp. (°C)	ZnS Rate R_{ZnS} (mmole/hr)	CdS Rate R_{CdS} (mmole/hr)	ZnS Mole Fraction	θ (R_{ZnS}/R_{Total})	Substrate
2148	113	34.2	60	600	480	0	0.34	0	0	(111)Ga
2158	136	33	60	600	420	0.10	0.37	*	0.22	(111)Ga
6148	130	70	60	600	465	0	1.29	0	0	$(\bar{1}\bar{1}\bar{1})$ As
6158	126	60	90	600	480	0	1.25	0	0	$(\bar{1}\bar{1}\bar{1})$ As
6198	122	53	90	600	460	0	1.22	0	0	Off (111)Ga
6208	122	59	60	600	470	0	0.79	0	0	Off (111)Ga
6218	133	57	120	600	460	0	0.64	0	0	$(\bar{1}\bar{1}\bar{1})$ As
7258	119	57	60	600	470	0	0.87	0	0	Quartz
7268	135	70	60	600	460	0	1.40	0	0	Quartz
7278	137	70	60	600	470	0.13	1.25	0.03	0.10	Quartz
8018	145	73	60	600	440	0.13	1.20	0.03	0.10	Quartz
8148	164	74	60	600	440	0	1.29	0	0	Corning 7059
8168	148	81	60	600	420	0	1.47	0	0	Corning 7059
8178	202	73	60	600	450	0	1.37	0	0	Corning 7059
8288	130	70	120	500	350	0	---	0	0	Corning 7059

* = Film thickness less than 1 μm; difficult to analyze.

Table 3.5A. Film Growth Experiments on (111)Ge Substrates

Run	ZnS Power (watts)	CdS Power (watts)	Run Duration (minutes)	Cylinder Temp. (°C)	Substrate Temp. (°C)	ZnS Rate R_{ZnS} (mmole/hr)	CdS Rate R_{CdS} (mmole/hr)	ZnS Mole Fraction	Θ (R_{ZnS}/R_{Total})	Thickness τ (μm)	$d\tau/dt$ (Å/sec)	Growth Rate g (Å/μmole)
9148	157	50	60	600	420 → 450	0	---	0	0	NA	NA	NA
9158	144	60	60	600	400 → 440	0	0.66	0	0	NA	NA	NA
9198	165	52	60	600	415 → 450	0.13	0.66	---	0.17	NA	NA	NA
9218	154	51	60	540	320 → 420	0	0.17	0	0	*	*	*
9228	158	65	90	530	300 → 420	0	0.24	0	0	*	*	*
9258	190	73	60	520	300 → 410	0.18	0.71	0.08	0.21	1.0	2.78	11.1
9298	192	84	120	520	315 → 410	0.17	0.81	0.08	0.18	2.5	3.47	12.7
10038	184	84	60	520	320 → 400	0.15	0.72	0.16	0.18	1.0	2.78	11.4
11038	184	84	60	560	320 → 420	0	1.80	0	0	3.9	10.83	21.7
11078	264	99	60	570	320 → 430	1.10	1.58	0.27	0.41	3.0	8.33	11.2
11088	239	97	60	545	330 → 400	0.45	1.09	0.20	0.29	2.0	5.56	13.0
11218	209	96	120	520	290 → 360	0.09	0.63	LS1	LS1	1.0	LS1	LS1
11288	255	96	150	510	310 → 390	0.42	0.64	LS1	LS1	*	LS1	LS1
11298	255	96	180	500	320 → 375	0.44	1.27	LS1	LS1	4.2	LS1	LS1
12058	258	96	180	510	320 → 350	0.88	0.75	LS1	LS1	4.2	LS1	LS1
12158	220	96	120	500	300 → 380^{SS}	0.28	0.76	---	0.27	NA	NA	NA
1159	220	96	120	500	300 → 390^{SS}	0.31	0.97	---	0.24	NA	NA	NA

NA = Non-adherent film

* = Film thickness less than 1 μm, difficult to analyze

LS1 = Layer Structure 1; (Cd,Zn)S/ZnS/Ge

SS = Stainless steel substrate holder used

Table 3.5B. Film Growth Experiments on (111)Ge Substrates using Outgassing Procedure

Run	ZnS Power (watts)	CdS Power (watts)	Run Duration (minutes)	Cylinder Temp. (°C)	Substrate Temp. (°C)	ZnS Rate R_{ZnS} (mmole/hr)	CdS Rate R_{CdS} (mmole/hr)	ZnS Mole Fraction	θ (R_{ZnS}/R_{Total})	Thickness τ (μm)	$d\tau/dt$ (Å/sec)	Growth Rate g (Å/μmole)
4209	108	124	180	500	300 → 400	0	1.30	0	0	4.0	3.70	10.3
4249	111	122	210	560	320 → 450	0	2.66	0	0	12.0	9.52	12.9
5019	114	109	180	600	330 → 450	0	1.75	0	0	10.0	9.26	19.1
5179	128	93	150	580	335 → 450	0.06	1.02	~0	0.06	4.0	4.44	14.8
5239	240	111	120	600	340 → 500	1.57	3.74	0.21	0.30	15.0	20.83	14.1
5309	190	92	150	580	320 → 460	0.49	2.30	0.17	0.18	10.0	11.11	14.3
6269	244	118	180	580	340 → 480	1.02	1.80	LS2	LS2	14.0	LS2	LS2
8249	105	120	180	580	330 → 390	0	2.05	0	0	8.0	7.41	13.0
8319	270	68	180	550	340 → 490	1.26	1.33	LS3	LS3	2.9	LS3	LS3
9269	105	120	180	530	320 → 400	0	1.68	0	0	1.7	1.57	3.4
1040	100	108	180	580	320 → 360	0	1.21	0	0	6.0	5.56	16.6

LS2 = Layer Structure 2: $(Cd_{0.83}Zn_{0.17})S/CdS/Ge$
LS3 = Layer Structure 3: ZnS/CdS/Ge

Table 4.1 Hall Effect Measurements

Sample	Substrate	Growth Rate (Å/μmole)	Crystallinity	Hall Mobility (cm^2/V-sec)	Carrier Concentration (cm^{-3})
2148	(111) Ga face	--	Single Crystal	44.6	10^{16}–10^{17}
6208	12° off (111) Ga face	65.89	Single Crystal	128.5	1.4×10^{17}
6158	$(\bar{1}\bar{1}\bar{1})$ As face	21.40	Polycrystalline	13.8	2.7×10^{16}
6218	$(\bar{1}\bar{1}\bar{1})$ As face	23.30	Polycrystalline	20.3	5.2×10^{16}
a	(111) Ga face	(~ 3,000 Å/min)	Single Crystal	125 - 154	$5x4x10^{17}$–$1.7x10^{19}$
b	Corning 7059	(40-400 Å/min)	Polycrystalline	11.1 - 16.0	10^{15}–10^{16}

References

a - A. Yoshikawa and Y. Sakai, Japan. J. Appl. Phys. 13, 547 (1974).

b - L. L. Kazmerski, W. B. Berry and C. W. Allen, J. Appl. Phys. 43, 3515 (1972).

Table 4.2 Summary of Device Experiments for Films Grown on GaAs Substrates

Cell No.	Polish	Etch time/HCl conc.	Heat Tr. time-temp. (hrs.-°C)	I^*_{sc} W-lamp or (sunlight)	Voc* W-lamp or (sunlight)	ZnS fraction	Cu_xS Formation D = Dry Process S = Sputtered	Comments
10046-1	none	none	1.0 - 137 ± 3	.50 mA F .16 mA B	.41 V F .34 V B	0	D	CdS film
2047-2	1 μm C	5 min/25%	2.0 - 135	---	---	.29	D	Shorted
5247-1	none	none	0.5 - 170	~10 μA F	~.1 V F	.15	D	Unstable-shorted after appl. of ~10 V bias
6167-1	none	5 sec/10%	0.5 - 180	24 μA F ~1.2 mA/cm^2 (15 μA F)	.48 V F (.38 V F)	.19	D	In contact to (Cd,Zn)S
6167-2	none	5 sec/10%	2.0 - 185	---	---	.19	D	Shorted
6177-1	none	5 sec/10%	2.0 - 185	---	---	.11	D	Shorted
6271-1	none	5 sec/10%	2.0 - 185	~1 μA	---	.17	D	High (~.6V) barrier
1208-1	none	5 sec/10%	2.0 - 185	200 μA F ~10 mA/cm^2	.50 V F	0	D	Non-ohmic back contact - High R_s
9077-1	none	none	(3 min in Air @200°C)	21 μA F	.34 V F	0	S	Polycrystalline CdS
9077-1	none	none	(Add. 3 min in Air @200°C)	40 μA F	.34 V F	0	S	Additional Heat Treatment
3088-1	none	none	(3 min in Ar 200 °C)	2 mA/cm^2 F	.42 V F	.03	S	"Reverse-knee"

* F = Front-wall
B = Back-wall

Table 4.3 Summary of Device Experiments for Films Grown on Ge Substrates

Cell No.	Heat Treatment	I_{sc} (mA) W-lamp	V_{oc} (v) W-lamp	ZnS Fraction	Cu_xS Formation D = Dry Process S = Sputtered
11038-1	5' @175°C in Air	0.57 2.96 mA/cm²*	0.46 0.46*	0	S
11088-1	5' @175°C in Air Additional 5'	0.15 0.25	0.26 0.46	0.20	S
5019-1	60' @60°C in Ar	1.25	0.34	0	D
5179-1	30' @60°C in Ar	1.25	0.42	~0	D
8249-1	150' @60°C in Ar	1.85	0.28	0	D
9269-1	15' @60°C in Ar	1.15	0.26	0	D
5179-L	5' @175°C in Air	0.41	0.31	~0	S
1040-A	30' @60°C in Ar	0.55	0.35	0	D
-B	60' @60°C in Ar	0.55	0.21		D
-C	120' @60°C in Ar	0.75	0.24		D
-D	300' @60°C in Ar	0.90	0.15		D

* Measured under Sunlight

Table 5.1 AES Measurements of Dry Proceessed Cu_xS on ZnS/CdS (Sample 8319)

I. MACS Computation

Sputter Time(min.)	Peak-to-Peak Height S	Cu	Zn	Cd	Cu/S Ratio	Zn/S Ratio	Excess Zn
0	39.8	58.0	2.5	2.5	1.46	--	--
1	39.8	60.5	3.3	2.1	1.52	--	--
2	39.0	59.5	4.0	2.5	1.53	--	--
3	40.0	51.0	4.3	2.0	1.50	0.48	1.42
4	47.0	20.2	19.0	3.3	1.50	0.48	2.91
5	49.3	17.7	22.2	3.7	1.50	0.48	4.20
6	56.0	5.2	27.0	4.2	--	0.48	--

II. MACS Computation

Sputter Time(min.)	Atomic Concentration S	Cu	Zn	Cd	Cu/S Ratio	Zn/S Ratio	Excess Zn
0	26.0	68.8	3.8	1.3	2.65	--	--
1	25.0	69.1	4.9	1.1	2.76	--	--
2	24.6	68.2	5.9	1.3	2.77	--	--
3	27.7	64.2	7.0	1.1	2.73	1.13	2.28
4	35.8	28.0	34.1	2.1	2.73	1.13	5.18
5	36.1	23.5	38.2	2.2	2.73	1.13	7.21
6	42.3	7.1	48.0	2.6	--	1.13	--

III. Revised Data (Analysis I)

Sputter Time(min.)	Atomic Concentration S	Cu	Zn	Cd	Cu/S Ratio	Zn/S Ratio	Excess Zn
0	27.4	72.6	0	0	2.65	--	--
1	26.6	73.4	0	0	2.76	--	--
2	26.5	73.5	0	0	2.77	--	--
3	28.0	64.9	7.1	0	2.73	1.13	2.31
4	36.6	28.6	34.8	0	2.73	1.13	5.30
5	36.9	24.1	39.1	0	2.73	1.13	7.36
6	43.4	7.3	49.2	0	--	1.13	--

Table 5.2 AES Measurements Using Adjusted Relative Sensitivity Factors (Analysis II)

I. Sample 8319 Dry Processed Cu_xS on ZnS/CdS

Sputter Time(min.)	Atomic Concentration S	Cu	Zn	Cd	Cu/S Ratio	Zn/S Ratio	Excess Zn
0	33.3	66.6	0	0	2.00	--	--
1	32.4	67.6	0	0	2.09	--	--
2	32.3	67.7	0	0	2.09	--	--
3	33.6	58.9	7.5	0	2.00	1.0	3.29
4	41.2	24.3	34.5	0	2.00	1.0	5.50
5	41.2	20.3	38.5	0	2.00	1.0	7.43
6	50.0	0	50.0	0	--	1.0	--
20	50.0	0	0	50.0	--	--	--

II. Sample 5239 Dry Processed Cu_xS on (Cd,Zn)S

Sputter Time(min.)	Atomic Concentration S	Cu	Zn	Cd	Cu/S Ratio	Zn/Cd Ratio
0	33.9	66.1	0	0	1.95	--
1	35.1	64.9	0	0	1.85	--
2	35.5	64.5	0	0	1.82	--
3	31.9	53.0	10.0	5.1	--	1.94
4	34.1	40.6	11.9	13.5	--	0.88
5	39.8	25.7	10.1	24.5	--	0.41
6	40.6	13.0	12.1	34.4	--	0.35
7→20 (Ave.)						0.29

ACKNOWLEDGEMENTS

I wish to express my appreciation to Professor Jack Washburn for his guidance and counsel during the course of this work. I am indebted to Dr. Terry Peterson for his invaluable help in initiating this project and developing the spectral response apparatus. My most sincere thanks to Dr. Uli Dahmen and Elisa and Zachariah Webb for their friendship, encouragement and moral support without whom this work may have never been completed. My appreciation goes to the technical staff of the Materials and Molecular Research Division for their expert assistance and to Dr. John Wang for performing the Auger spectroscopy work. For their helpful and friendly discussions, thanks to Drs. Ken Kubarych, Bob Drosd and Raj Mishra.

This work was done under the auspices of the U.S. Energy Research and Development Administration and the Division of Solar, Geothermal, Electric and Storage Systems, U.S. Department of Energy under Contract No. DE-AC03-76SF00098.

FIGURE CAPTIONS

Figure No.

1.1 Overview of experimental approach.

1.2 a) Energy-band diagram of two isolated semiconductors with differing bandgaps E_{gi}, and electron affinities χ_i.

b) Energy-band diagram of the two semiconductors in a) when brought into intimate contact.

2.1 Longitudinal cross-section of initial hot-wall deposition apparatus.

2.2 Schematic cross-section of single crystal (Cd,Zn)S/Cu_xS heterojunction structure used for test device measurements.

2.3 Schematic diagram of current-voltage measurement apparatus.

2.4 Schematic outline of spectral response apparatus with facilities for I-V-T measurements.

2.5-

2.7 Listing of BASIC program used for spectral response measurements.

3.1 a) Plot of ZnS fraction vs. depth in mixed crystal film as measured by electron microprobe scan of angle-lapped surface (Film 8136).

b) Scanning electron micrograph and EDAX line-scans of cleaved edge of the same film as in a).

3.2 a) EDAX line-scans of nearly uniform mixed crystal film (Film 11056).

b) Scanning electron micrograph of top surface of the same film as in a).

3.3 Longitudinal cross-section of revised hot-wall deposition apparatus showing integral quartz cylinder with baffle.

3.4 a) SEM micrograph of top surface of mixed crystal film (Film 2287).

b) Cd X-ray map of same surface as in a).

3.5 EDAX line-scans of cleaved surface of mixed crystal film (Film 4197).

3.6 a) SEM micrograph showing surface morphology of polycrystalline mixed crystal film (Film 5057).

b) SEM micrograph showing surface of high growth rate mixed crystal film (Film 4267).

3.7 SEM micrograph of mixed crystal film containing irregular cracks (Film 5247).

3.8 SEM micrograph of mixed crystal film containing cracks along the <1120> directions (Film 6077).

3.9 SEM micrograph of mixed crystal crack which has been bridged during growth (Film 5117).

3.10 SEM micrograph of cracked mixed crystal film after etching to reveal cracks in the GaAs substrate (Film 4197).

3.11 Graph of mixed crystal film composition vs. fraction of ZnS in source loss rate.

3.12 Graph of growth rate divided by total source loss rate vs. fraction of ZnS in source loss rate.

3.13 Graph of growth rate divided by total source loss rate vs. mixed crystal film composition.

3.14 SEM micrograph of cleaved cross section of CdS film grown on off-(111) GaAs substrate (Film 9097).

3.15 SEM micrograph of top surface of (Cd,Zn)S film grown on off-(111) GaAs substrate showing elongated hexagons (Film 9207).

3.16 SEM micrograph of top surface of CdS film grown on off-(111) GaAs substrate showing ledges (Film 9107).

3.17 Photograph of hot-wall deposition equipment showing sputter-etch apparatus configuration.

3.18 a) SEM micrograph of top surface of largely single crystal region of CdS film (Film 12167).

b) SEM micrograph showing polycrystalline growth for the same film as in a).

3.19 SEM micrograph of randomly oriented CdS grains on sputter-etched GaAs substrate (Film 1118).

3.20 SEM micrograph of top surface of CdS film grown on 14°-off (111) Ga face substrate showing ledges (Film 1178).

3.21 Photograph of CdS film grown in the Van der Pauw geometry onto insulating GaAs substrate.

3.22 a) SEM micrograph of top surface of (Cd,Zn)S film showing attack of the Ge substrate (Film 12158).

b) SEM micrograph of top surface of (Cd,Zn)S in which cracks extended into the Ge substrate (Film 1159).

3.23 Graph of normalized CdS growth rate vs. hot wall cylinder temperature.

3.24 a) SEM micrograph of top surface of CdS surface dominated by hexagonal pyramids (Film 8249).

b) SEm micrograph of top surface of CdS film grown at lower supersaturation than in a) dominated by hexagonal flat-tops (Film 9269).

4.1 Hall mobility vs. magnetic field for single crystal CdS (Film 6208).

4.2 Hall mobility vs. magnetic field for polycrystalline CdS (Film 6218).

4.3 Current-voltage characteristics of $(Cd_{.97}Zn_{.03})S/Cu_xS$ cell in which Cu_xS was reactively sputtered (Cell 3088-1).

4.4 Current-voltage characteristics of Cell No. 6167-1 under a) tungsten lamp and b) sunlight illumination.

4.5 SEM micrograph of the Cu_xS film formed on single crystal (Cd,Zn)S by the dry ion-exchange process at 135°C for 1 hr. (Film 9258).

4.6 SEM micrograph of converted and masked regions of CdS film formed by the dry process at 60°C for 1/2 hr. (Film 5179).

4.7 a) EDAX spectrum of masked region of CdS film in Fig. 4.6.

b) EDAX spectrum of converted region.

4.8 a) Current-voltage characteristics of Cell 8249-1 formed by the dry process at 60°C for 1 hr.

b) Current-voltage characteristics of Cell 5179-1 formed by the dry process at 60°C for 1/2 hr.

4.9 Spectral response of Cell 6167-1 (dry process Cu_xS).

4.10 Spectral response of Cell 5179 (reactively sputtered Cu_xS).

5.1 Differentiated AES spectrum of reactively sputtered Cu_xS on (Cd,Zn)S Film 5239.

5.2 Atomic concentration vs. sputter time for reactively sputtered Cu_xS on (Cd,Zn)S Film 5239 determined by MACS program.

5.3 Differentiated AES spectrum of (Cd,Zn)S Film 5239.

5.4 Peak-to-peak Auger signal vs. sputter time for reactively sputtered Cu_xS on (Cd,Zn)S Film 5239.

5.5 Peak-to-peak Auger signal vs. sputter time for dry processed Cu_xS on (Cd,Zn)S Film 5239.

5.6 Peak-to-peak Auger signal vs. sputter time for reactively sputtered Cu_xS on ZnS/CdS Film 8319.

5.7 Peak-to-peak Auger signal vs. sputter time for dry processed Cu_xS on ZnS/CdS Film 8319.

5.8 Atomic concentration vs. sputter time for dry processed Cu_xS on ZnS/CdS Film 8319 determined by MACS program.

5.9 Atomic concentraton vs. sputter time for dry processed Cu_xS on ZnS/CdS Film 8319 determined using adjusted relative sensitivity factors.

5.10 Atomic concentration vs. sputter time for dry processed Cu_xS on (Cd,Zn)S Film 5239 determined using adjusted relative sensitivity factors.

5.11 Differentiated AES spectrum of reactively sputtered Cu_xS on ZnS/CdS Film 8319 prior to sputtering with Ar^+ ions.

5.12 Differentiated AES spectrum of reactively sputtered Cu_xS on ZnS/CdS Film 8319 after 30 sec. sputter etch with 3 keV Ar^+ ions.

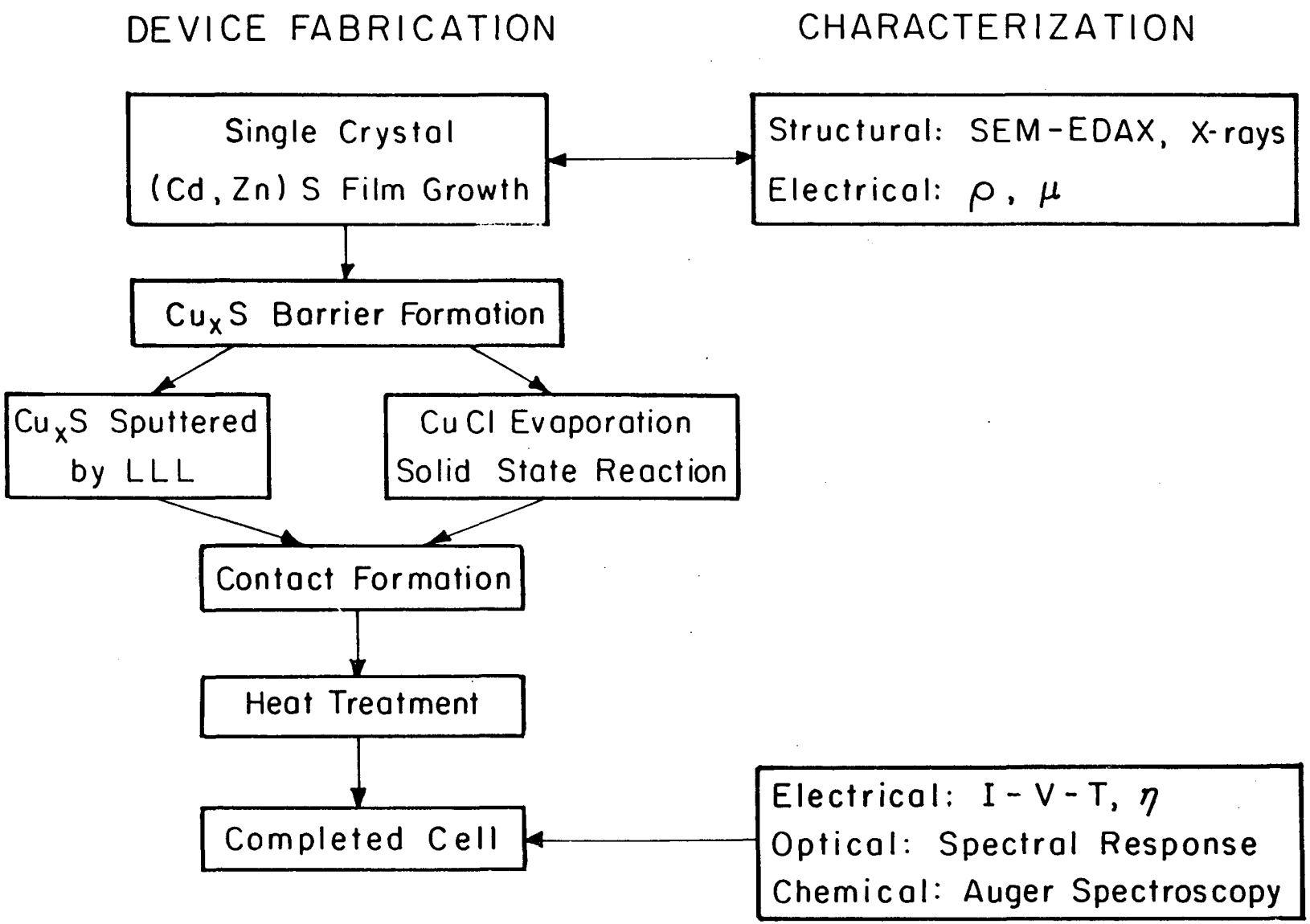
DEVICE FABRICATION
CHARACTERIZATION
Single Crystal
(Cd, Zn) S Film Growth
Structural: SEM-EDAX, X-rays
Electrical: ρ, μ
Cu_xS Barrier Formation
Cu_xS Sputtered
by LLL
CuCl Evaporation
Solid State Reaction
Contact Formation
Heat Treatment
Completed Cell
Electrical: I-V-T, η
Optical: Spectral Response
Chemical: Auger Spectroscopy
XBL 838-6224

Fig. 1.1

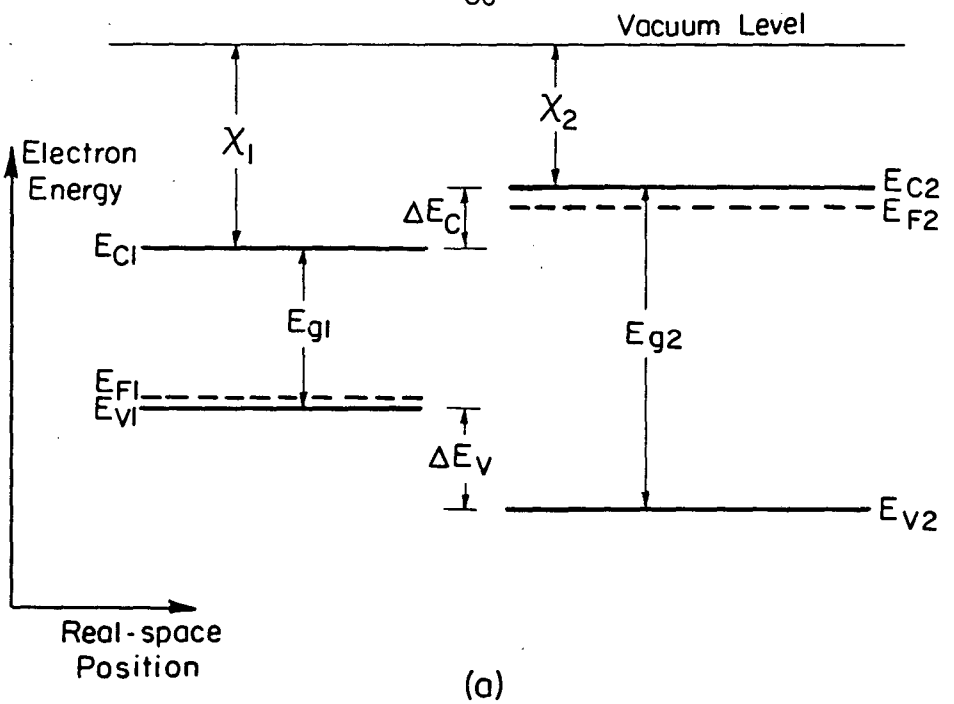

(a)

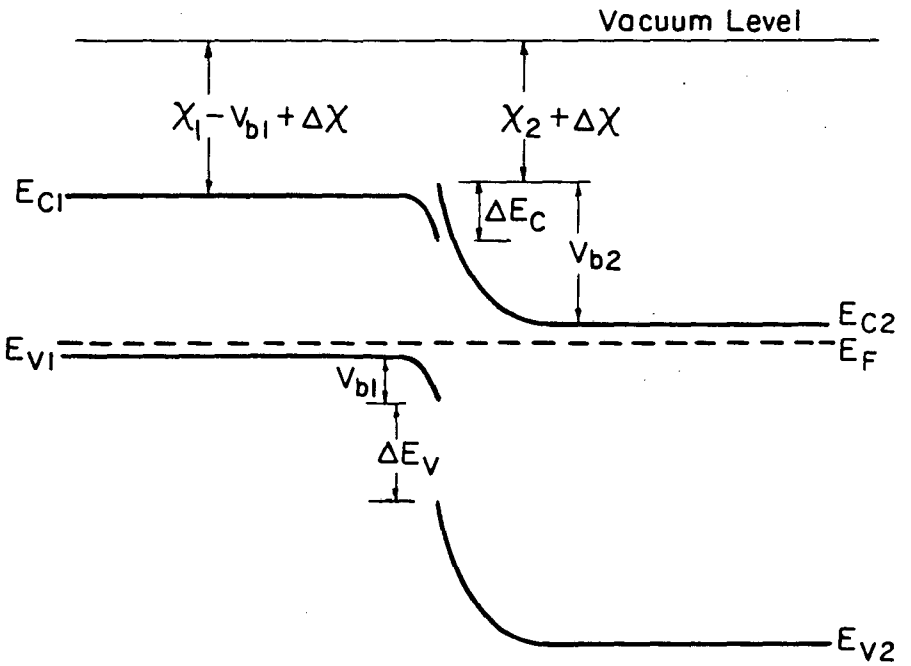

(b)

XBL 758-6974

Fig. 1.2

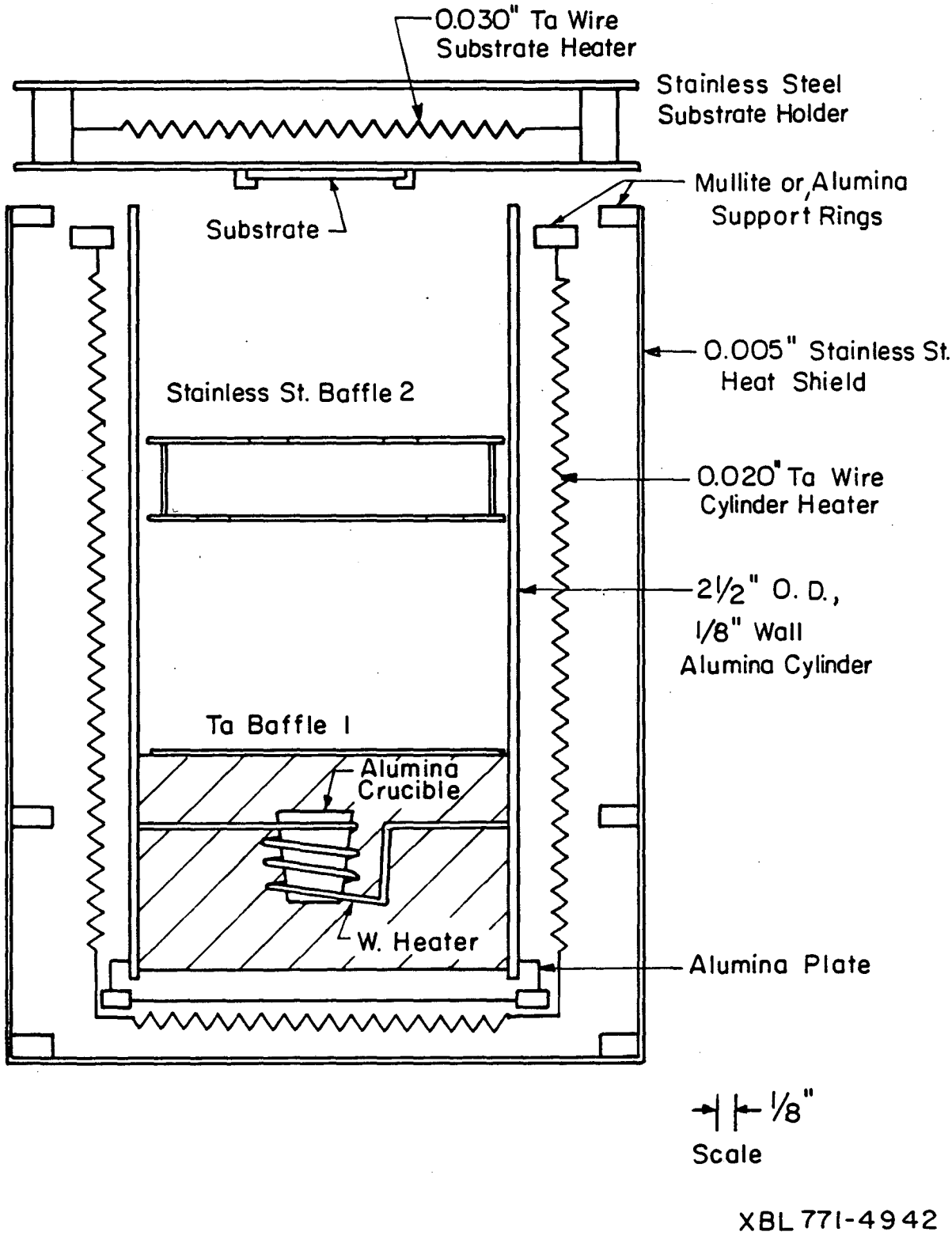
0.030" Ta Wire
Substrate Heater
Stainless Steel
Substrate Holder
Mullite or Alumina
Support Rings
Substrate
0.005" Stainless St.
Heat Shield
Stainless St. Baffle 2
0.020" Ta Wire
Cylinder Heater
2½" O. D.,
1/8" Wall
Alumina Cylinder
Ta Baffle 1
Alumina
Crucible
W. Heater
Alumina Plate
1/8"
Scale
XBL 771-4942

Fig. 2.1

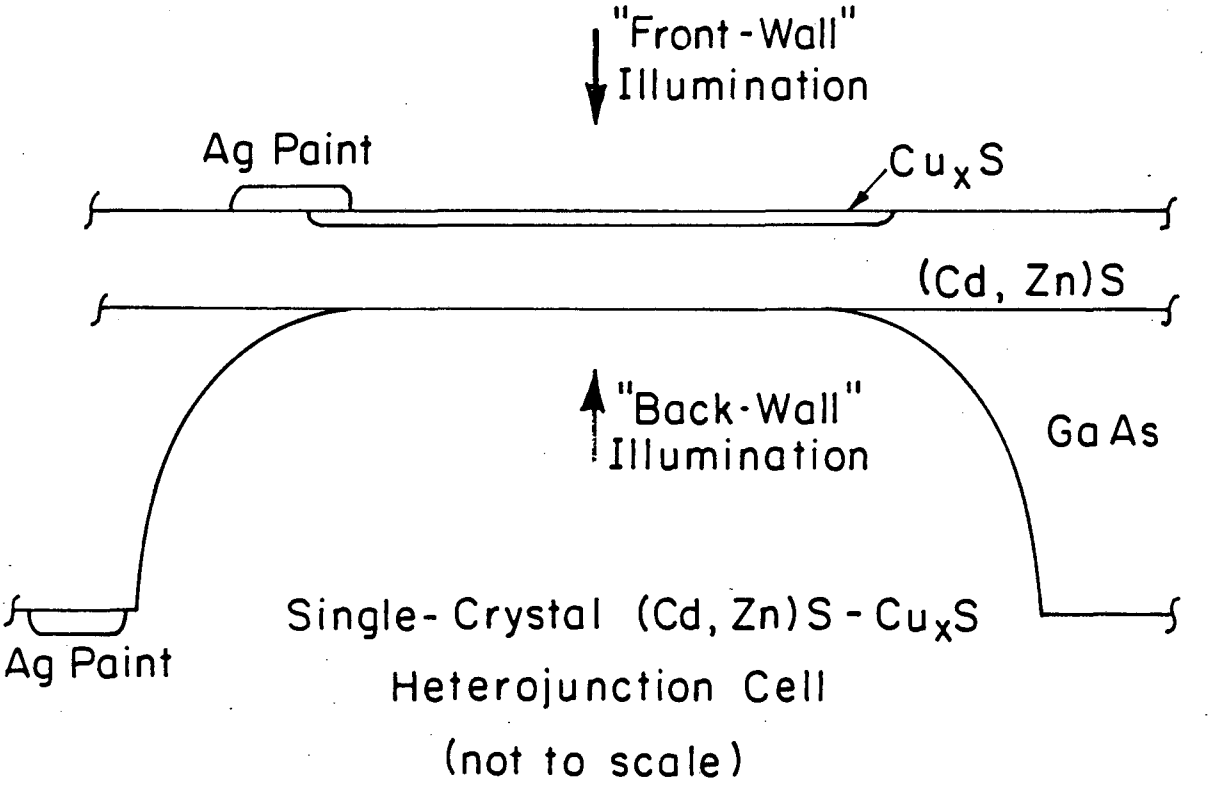
"Front-Wall"
Illumination
Ag Paint
Cu_xS
(Cd, Zn)S
"Back-Wall"
Illumination
GaAs
Ag Paint
Single-Crystal (Cd, Zn)S - Cu_xS
Heterojunction Cell
(not to scale)
XBL 838-6225

Fig. 2.2

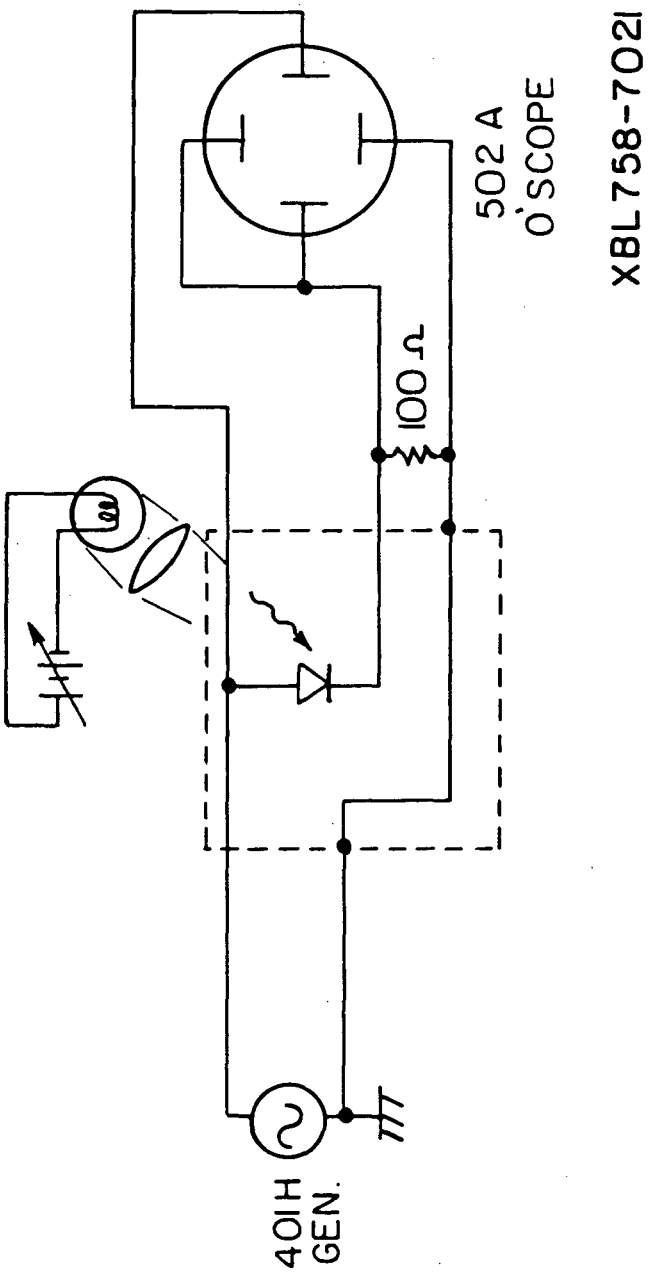

Fig. 2.3

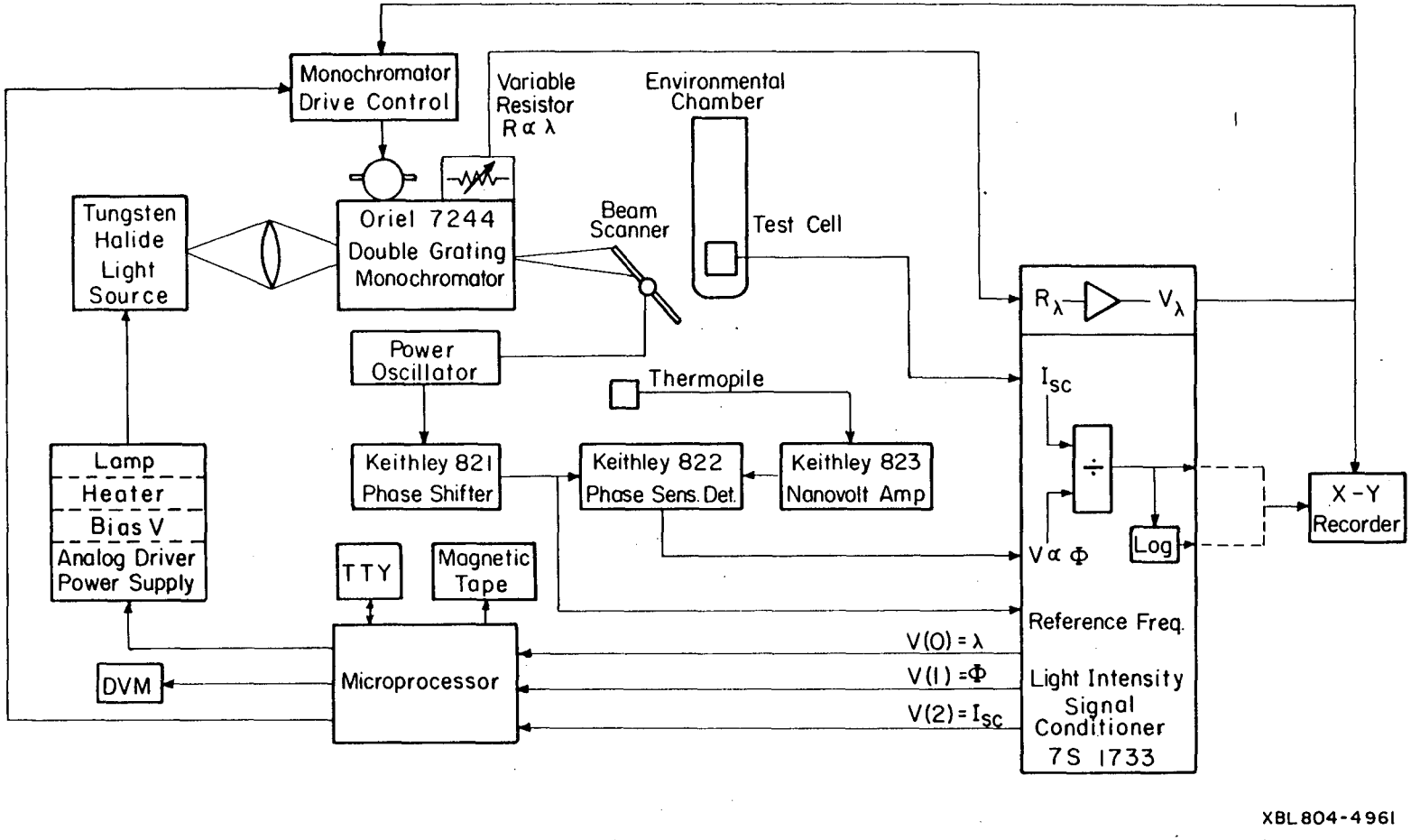

XBL804-4961

Fig. 2.4

```
 35 REM "SPECTRAL REPONSE PROGRAM"
 40DIMV(4)
 49REM" INIT. 8255'S"
 50CALL(13)
 51REM" TURN MOTOR OFF "
 52LETPUT(32)=1
 55REM"PORT 32 = MOTOR, 0=DN, 1=STOP, 2=UP"
 56LETPUT(43)=128
 57LETPUT(40)=1
100REM"CONNECT DVM TO MONO."
101REM" READ DVM TO CHECK STATUS"
104LETC9=1
106GOSUB2300
107PRINT" "
108PRINT"***************SPECTRAL RESPONSE PROGRAM*******************"
109PRINT"******************VERSION  7/24/79*****************************"
110PRINT"RUN IDENTIFIER?";
111CALL(14)
112GOSUB1000
115PRINT"GRATING RULING: 600 OR 1200L/MM";
116INPUTGO
117IFGO=600THEN119
118IFGO<>1200THEN115
119LETF=12E4/GO
130PRINT"INITIAL WAVELENGTH =";
132INPUTE1
134LETE1=E1/F
140PRINT"FINAL WAVELENGTH =";
142INPUTE9
143LETE9=E9/F
150PRINT"WAVELENGTH CHANGE PER STEP =";
152INPUTD
153LETD=D/F
154LETN=E9-E1
155LETN=N/D
160IFN>0THEN164
162LETN=-N
163LETD=-D
164LETN=N+1.00001
166PRINT"NUMBER OF STEPS=";N AS 3I
170PRINT"OFFSET CHECK: CURRENT READING OF MONOCHROMATOR =";
174INPUTE
176LETE=E/100
177LETC9=1
178GOSUB2300
180LETE=E-V
181PRINT"OFFSET=": E*F AS 6F2;"NM."
182PRINT"COMPENSATE? (0=NO, 1=YES)";
184INPUTY
186IFY=1THEN190
188IFY<>0THEN182
190LETE9=-E*Y
194PRINT
195PRINT" WAVE   LIGHT      STD.                    STD.       NORM."
196PRINT"LENGTH   INT.      DEV.       S.C.C.       DEV.       S.C.C."
197LETPUT(43)=128
198LETPUT(40)=255
200FORJ=1TON
202LETL=J-1
204LETE=D*L
206LETE=E+E1
207LETC9=1
208GOSUB2000
```

Fig. 2.5

```
210LETC9=4
212GOSUB3000
214LETV(3)=V
216 LET D2=S
220LETC9=2
222GOSUB3000
224LETV(2)=V
225LET D1=S
229LETV(0)=V(3)/V(2)
230 PRINT E*F AS 5I; V(2) AS9F4; D1 AS 12E3; V(3) AS12E3;
231 PRINT D2 AS 12E3; V(0) AS 12E3
232 REM "WRITE SAME PRINTED LINE ON MAGNETIC TAPE"
235 CALL(9)
240 PRINT E*F, V(2), D1, V(3), D2, V(0)
245 CALL (1)
250 NEXT J
255 LETPUT(18)=128+64
260 PRINT" "
265 LETPUT(18)=128
270 LETPUT(40)=1
302 PRINT "ANOTHER RUN?  (0=NO, 1=YES)";
305 INPUT Y
310 IF Y<>0 THEN 110
320 STOP
1000 REM "MAKE UP FOR NO EOR IN SUB 14"
1020 CALL(9)
1030 PRINT " "
1040 CALL (1)
1050 PRINT " "
1060 RETURN
2000REM"MOVE MONOCHROMATOR TO E+E9"
2002GOSUB2300
2005LETE0=E+E9
2018LETE3=E0-V
2020IFE3>0THEN2024
2021LETE3=-E3
2022IFE3>.05THEN2100
2024IFE3>.05THEN2030
2026GOTO2150
2030LETPUT(32)=2
2034GOSUB2330
2036IFE0-V>.025THEN2034
2040GOTO2150
2100LETPUT(32)=0
2110GOSUB2330
2115IFV-E0>.017THEN2110
2120GOTO2150
2150LETPUT(32)=1
2155GOSUB2330
2160LETE3=E0-V
2165LETM=2
2170IFE3>0THEN2180
2175LETE3=-E3
2177LETM=0
2180IFE3<.001THEN2190
2185LETT1=3
2186LETPUT(32)=M
2187GOSUB2200
2189GOTO2150
2190RETURN
2200REM" TIME DELAY=6MS*T1 "
2202FORK=1TOT1
2204NEXTK
2206RETURN
```

Fig. 2.6

```
2300REM"CONNECT AND READ DVM"
2302LETPUT(17)=C9
2304REM"WAIT FOR CONV. AND AUTO RANGE"
2306LETT1=300
2308GOSUB2200
2330REM"ENTRY TO BYPASS WAIT"
2332 CALL (4)
2336INPUTV
2338CALL(1)
2340RETURN
3000REM"OBTAIN STABLE DVM READ."
3001REM"ON RETURN: V=AVER. OF LAST 20 READ, S=STD. DEV. OF SAME"
3002GOSUB2300
3004GOSUB3200
3006FORL=2TO500
3008LETV0=V
3010LETS0=S
3015LETT1=.2E4
3020GOSUB2200
3025GOSUB3200
3030LETD0=V-V0
3035IFD0>0THEN3045
3040LETD0=-D0
3045IFD0>S+S0THEN3090
3050LETL=501
3090NEXTL
3095LETV=V+V0
3100LETV=V/2
3105 LET S=S+S0
3110 LET S=S/2
3140IFL<>500THEN3190
3145PRINT"STABILITY NOT REACHED, C9=";C9;" DV/S=";D0/S
3190RETURN
3198 PRINT"NEGATIVE VALUE: ANOTHER DATA SET TAKEN"
3200REM"TAKE 10 DVM READ. AND OBTAIN S"
3210LETM=0
3220LETS2=0
3230FORL=1TO10
3240GOSUB2330
3250LETM=M+V
3260LETV2=V*V
3270LETS2=S2+V2
3280NEXTL
3290LETV2=M*M
3300LETV2=V2/10
3310LETS2=S2-V2
3320LETX=S2/9
3330GOSUB4000
3335LETS=X
3340LETV=M/10
3350RETURN
4000REM"FIND SQRT OF X"
4005IFX=0THEN4086
4006 IF X<0 THEN 3198
4010LETX0=X
4015LETX1=X
4020LETX=X0/X1
4025LETX=X+X1
4030LETX=.5*X
4050IFX<>X1THEN4015
4086RETURN
4096PRINT"E R R O R - ARG. OF SQRT <0",X
4097STOP
22222END
```

Fig. 2.7

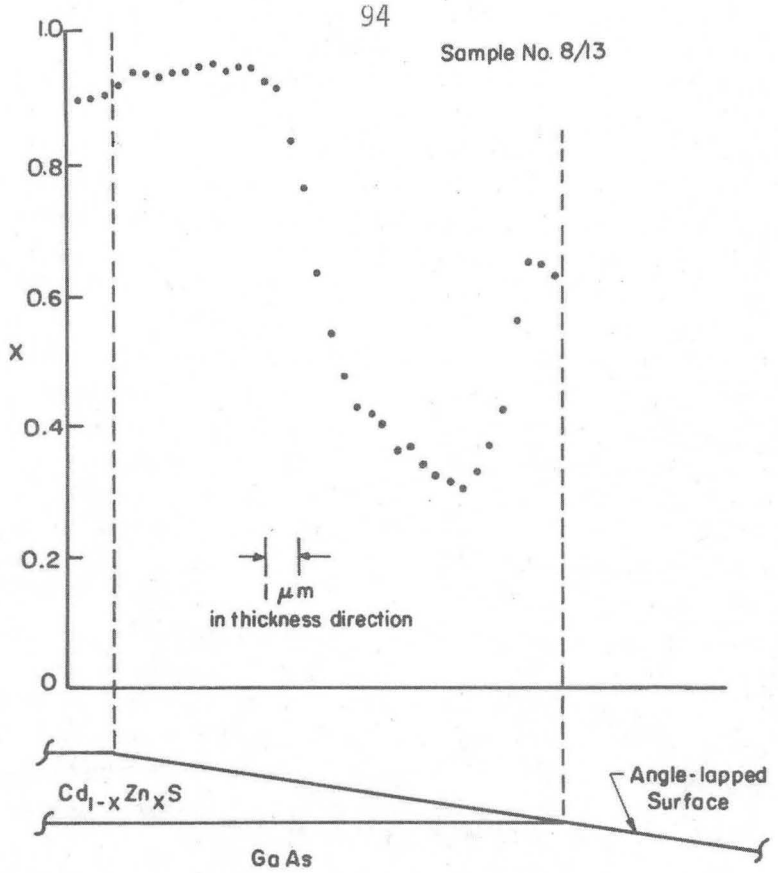

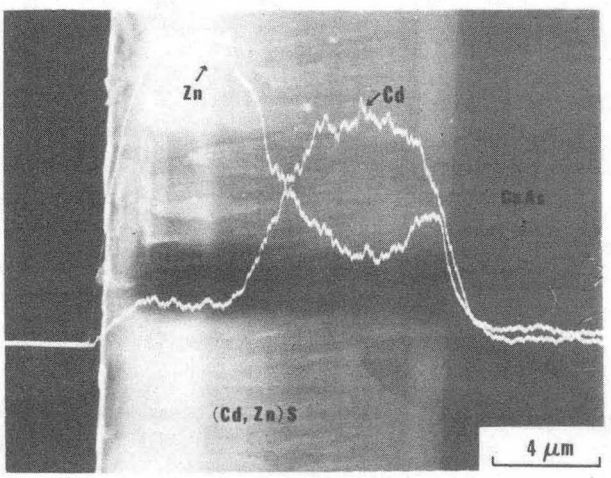

XBB 771 148

Fig. 3.1

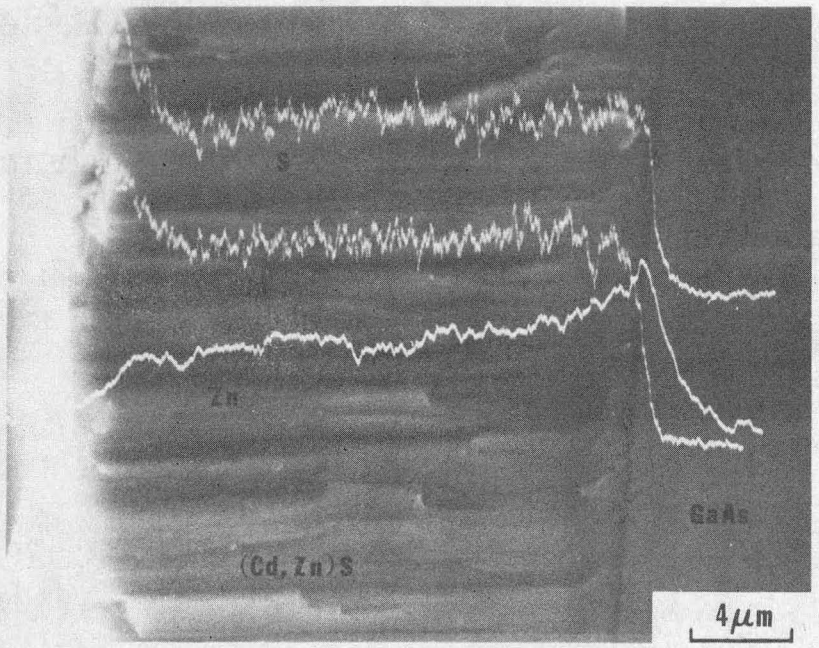

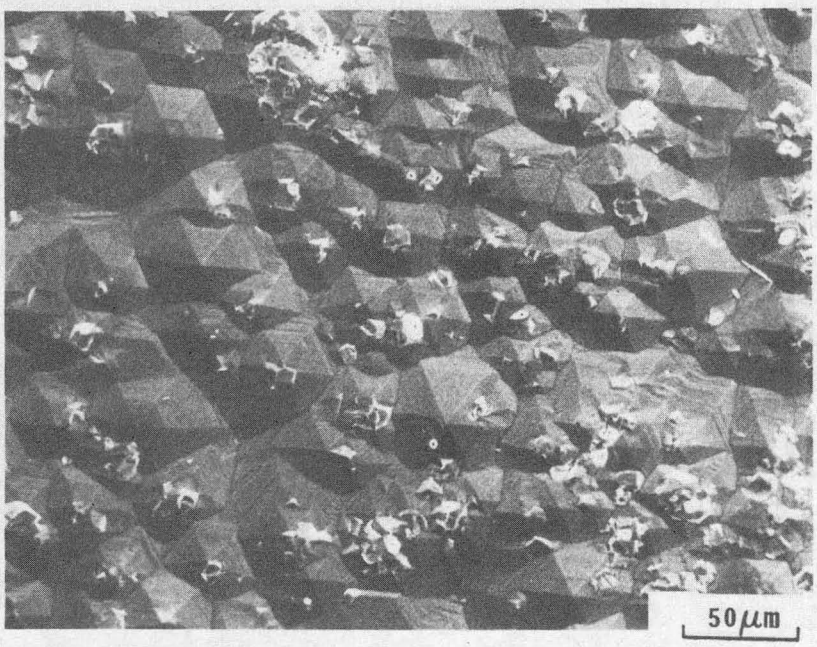

XBB 771 149

Fig. 3.2

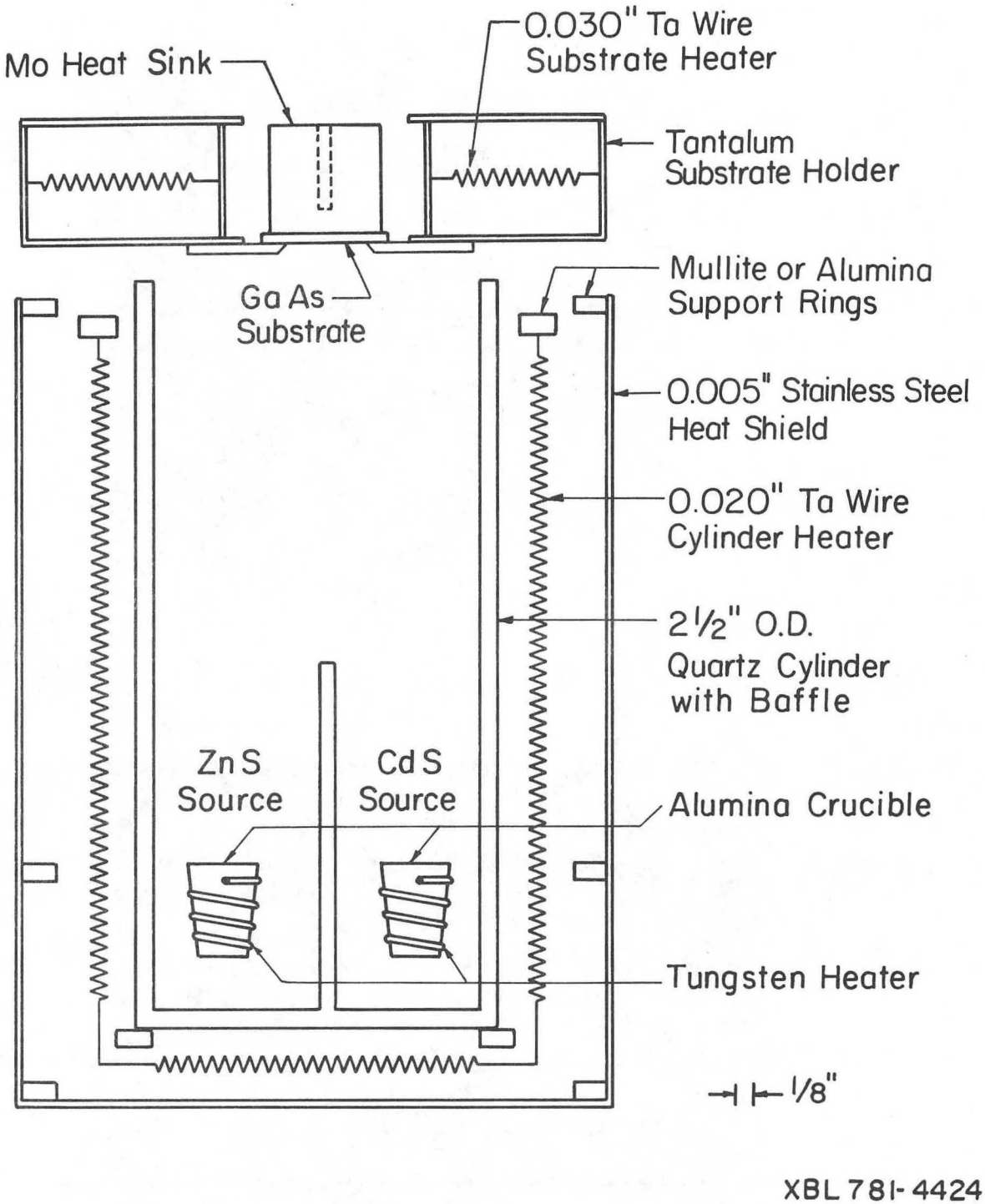
Mo Heat Sink
0.030" Ta Wire
Substrate Heater
Tantalum
Substrate Holder
Ga As
Substrate
Mullite or Alumina
Support Rings
0.005" Stainless Steel
Heat Shield
0.020" Ta Wire
Cylinder Heater
2 1/2" O.D.
Quartz Cylinder
with Baffle
Zn S
Source
Cd S
Source
Alumina Crucible
Tungsten Heater
1/8"
XBL 781-4424

Fig. 3.3

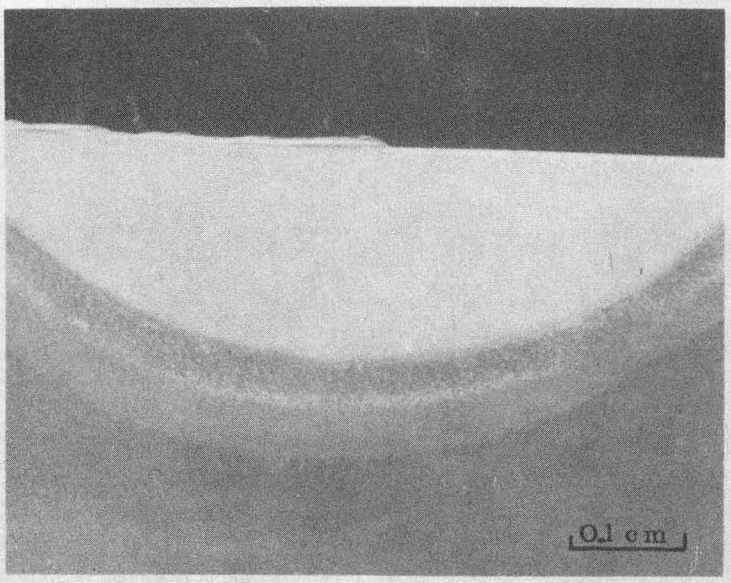

a



b

XBB 776 6043

Fig. 3.4

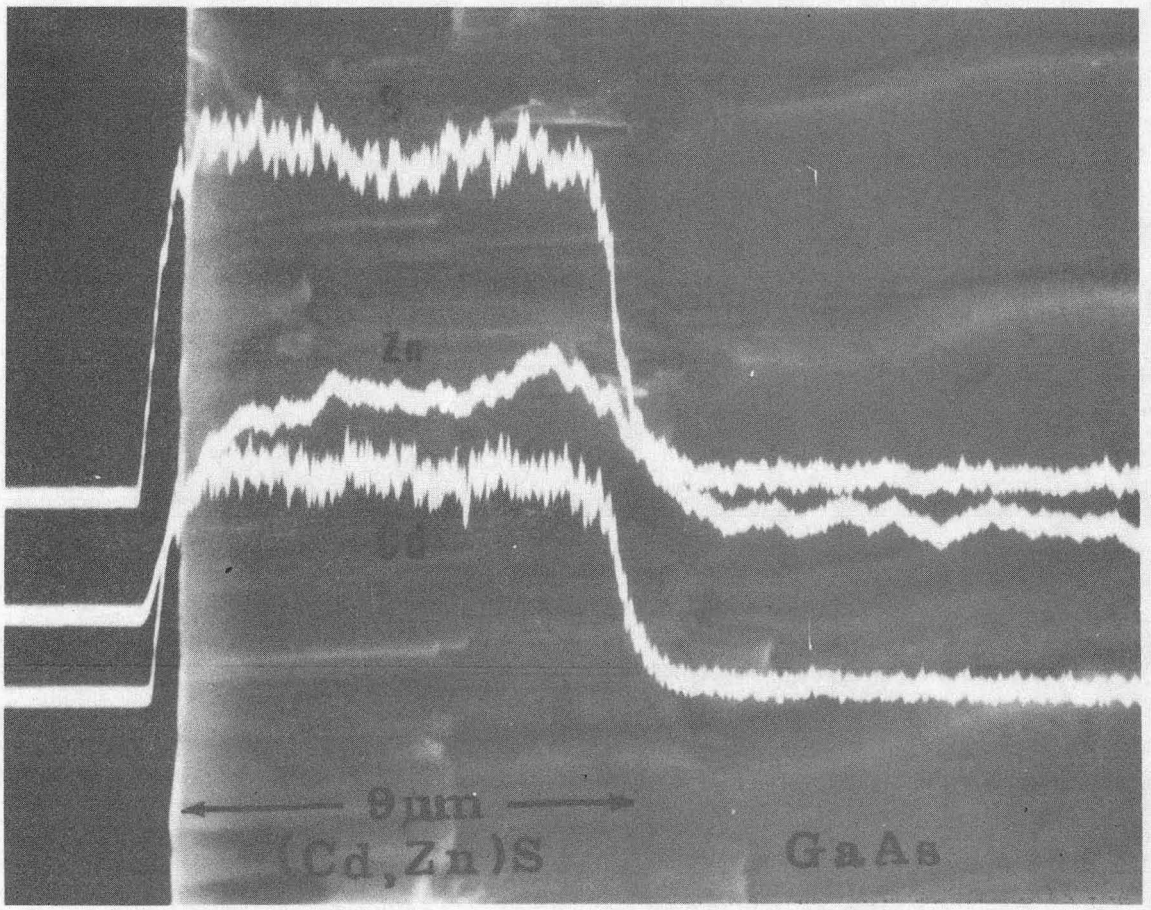

XBB 777 6727

Fig. 3.5

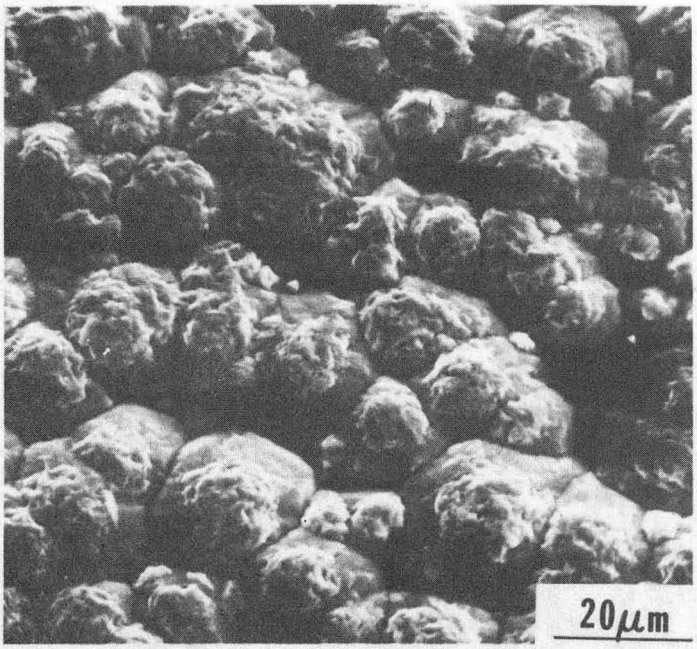

a

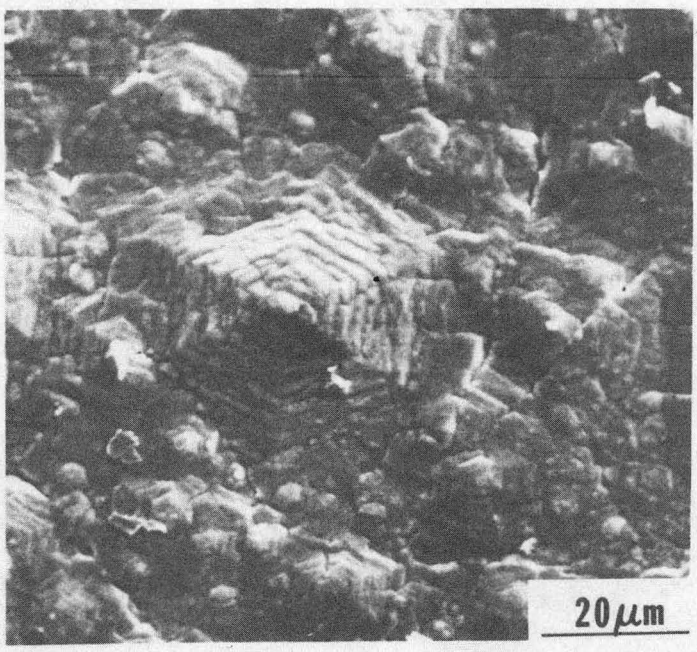

b

XBB 7911-15815

Fig. 3.6

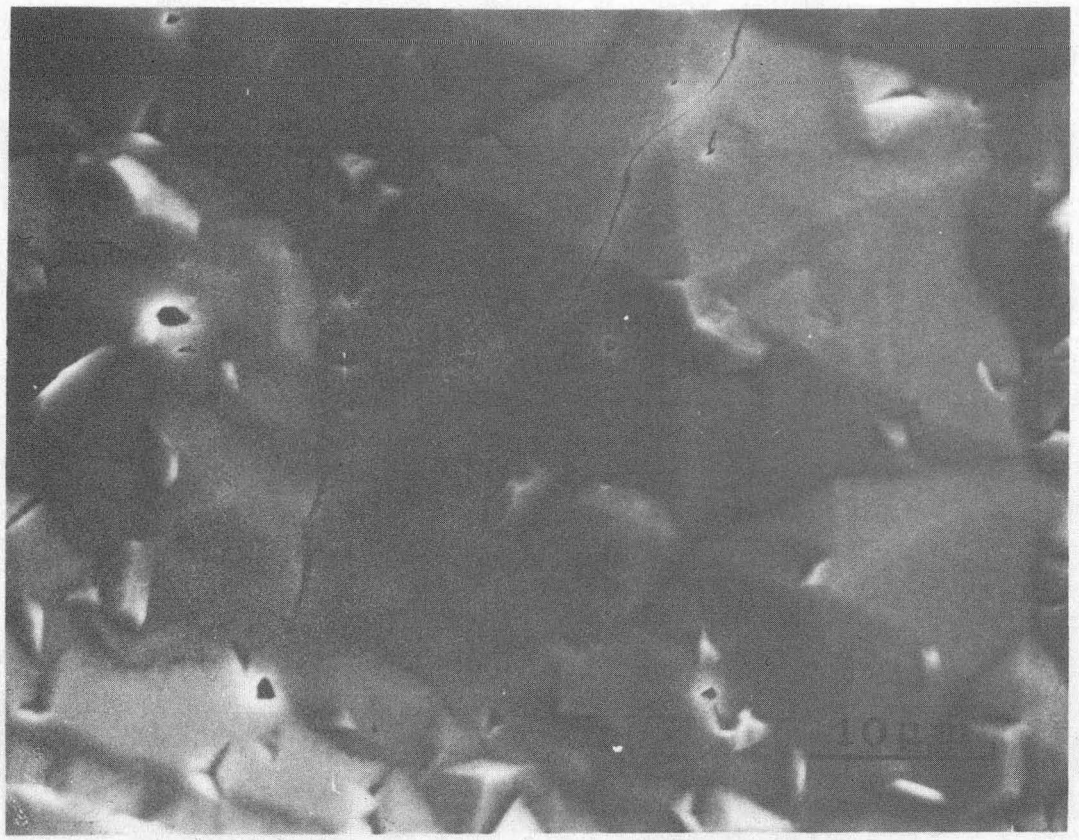

XBB 777 6726

Fig. 3.7.

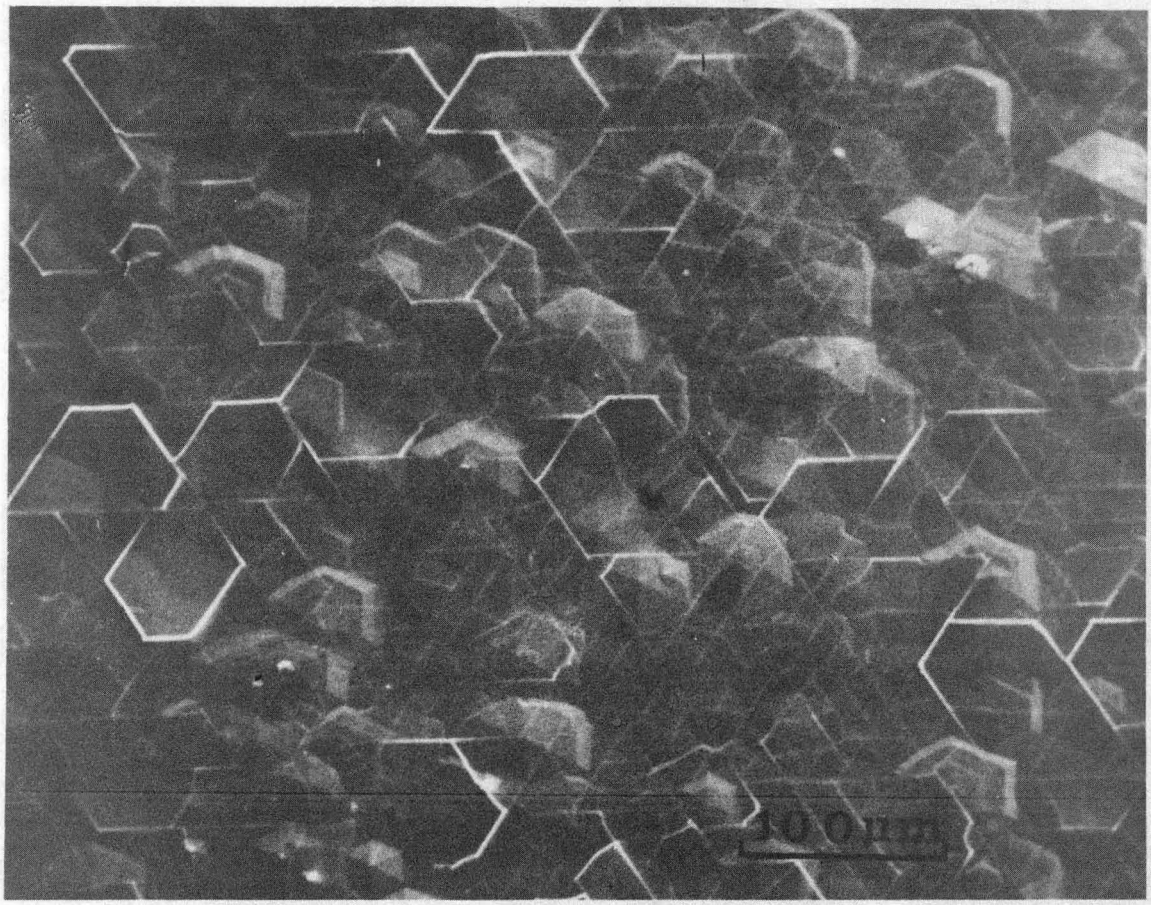

XBB 777 6725

Fig. 3.8

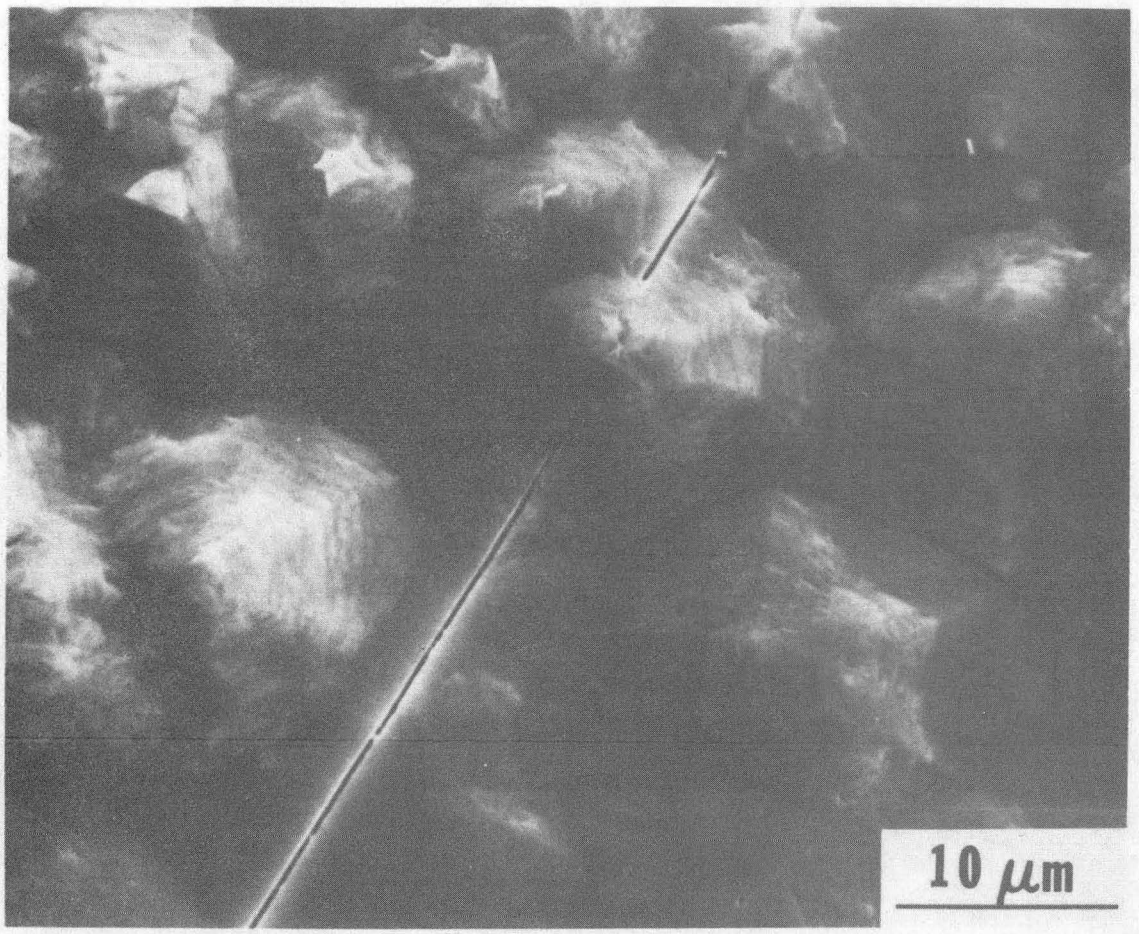

XBB 776 6047

Fig. 3.9

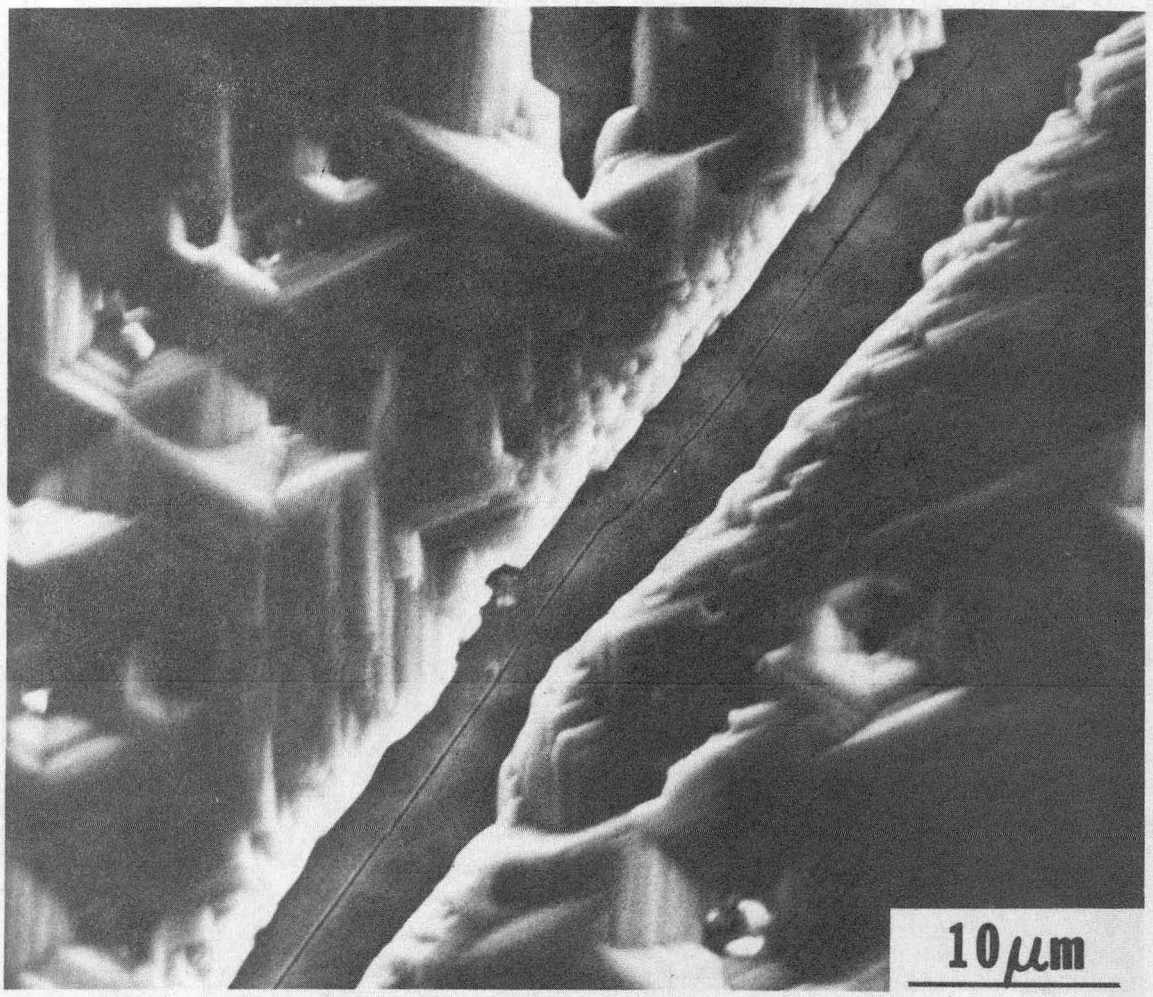

XBB 776 6046

Fig. 3.10

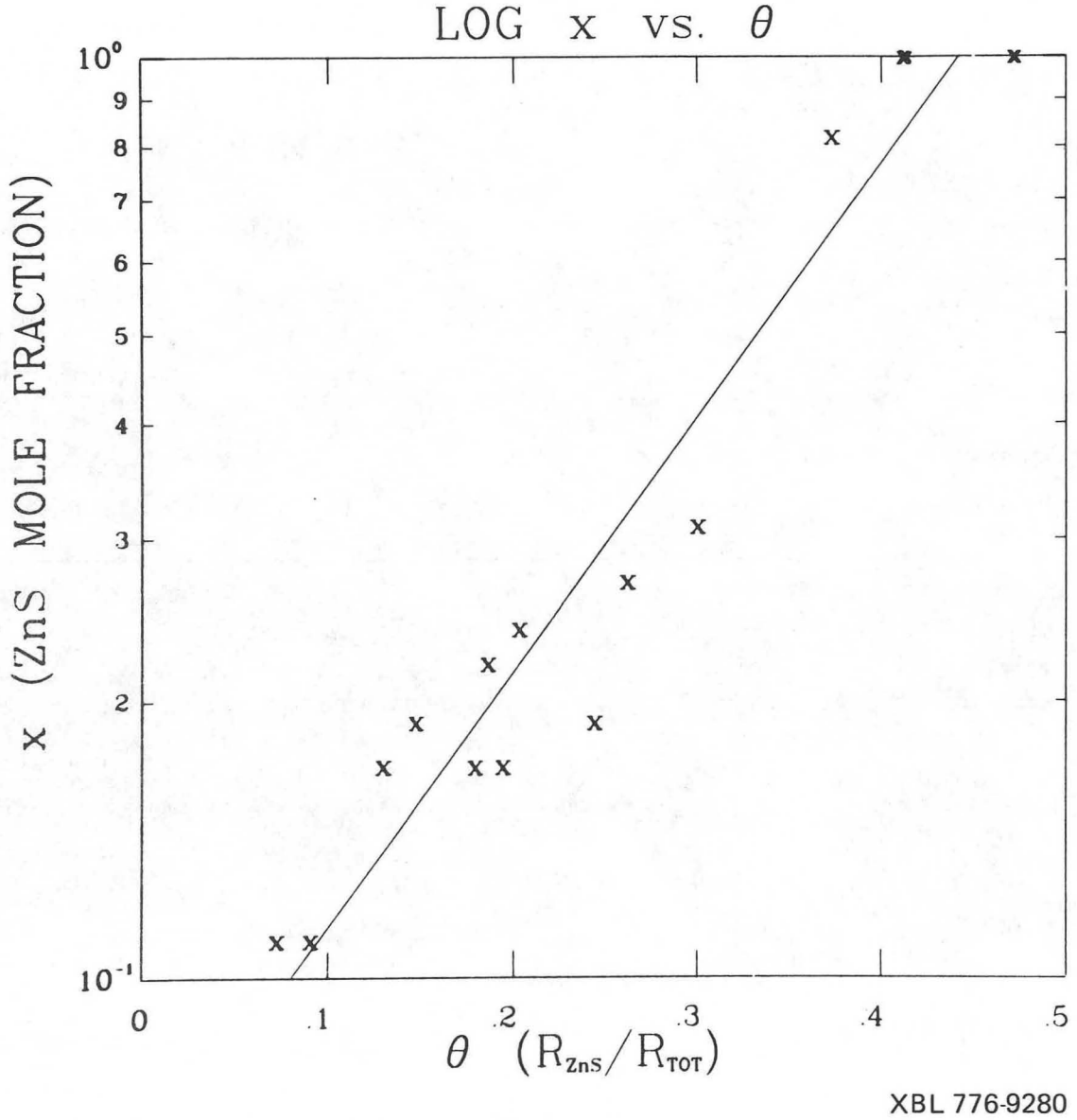
LOG x vs. θ
x (ZnS MOLE FRACTION)
10⁰
9
8
7
6
5
4
3
2
10⁻¹
0
.1
.2
.3
.4
.5
θ (R_ZnS/R_TOT)
XBL 776-9280

Fig. 3.11

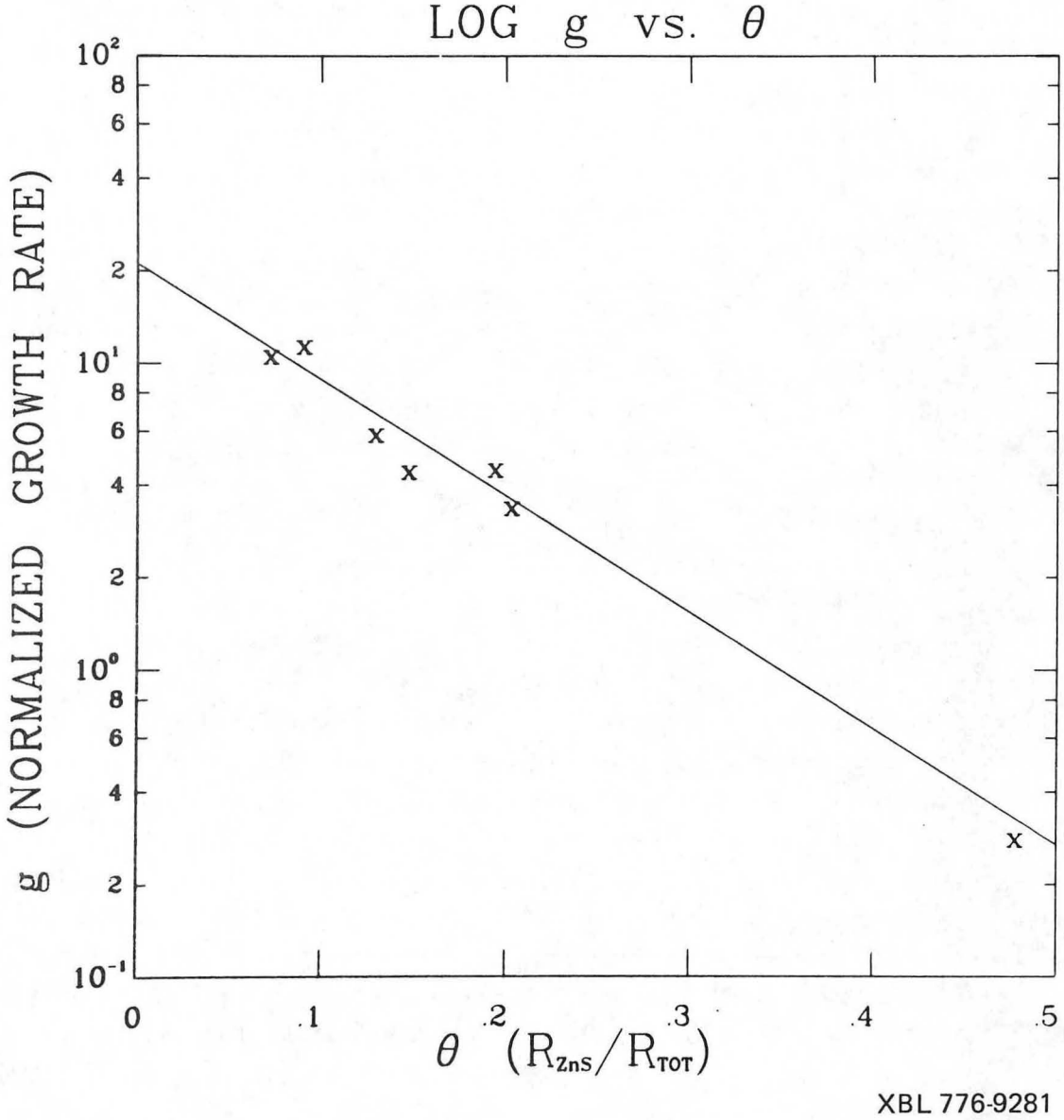

Fig. 3.12

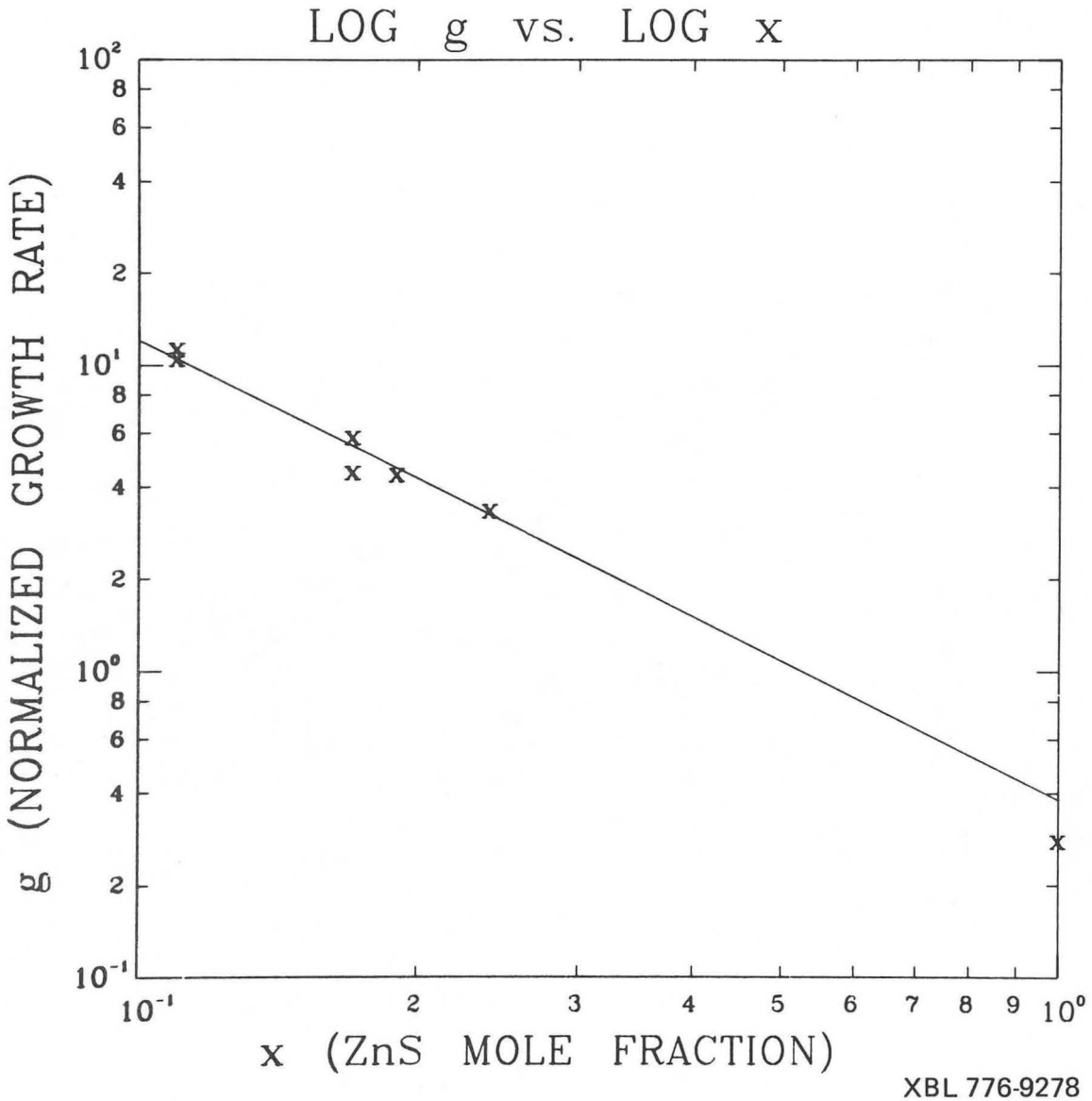
LOG g vs. LOG x
g (NORMALIZED GROWTH RATE)
x (ZnS MOLE FRACTION)
XBL 776-9278

Fig. 3.13

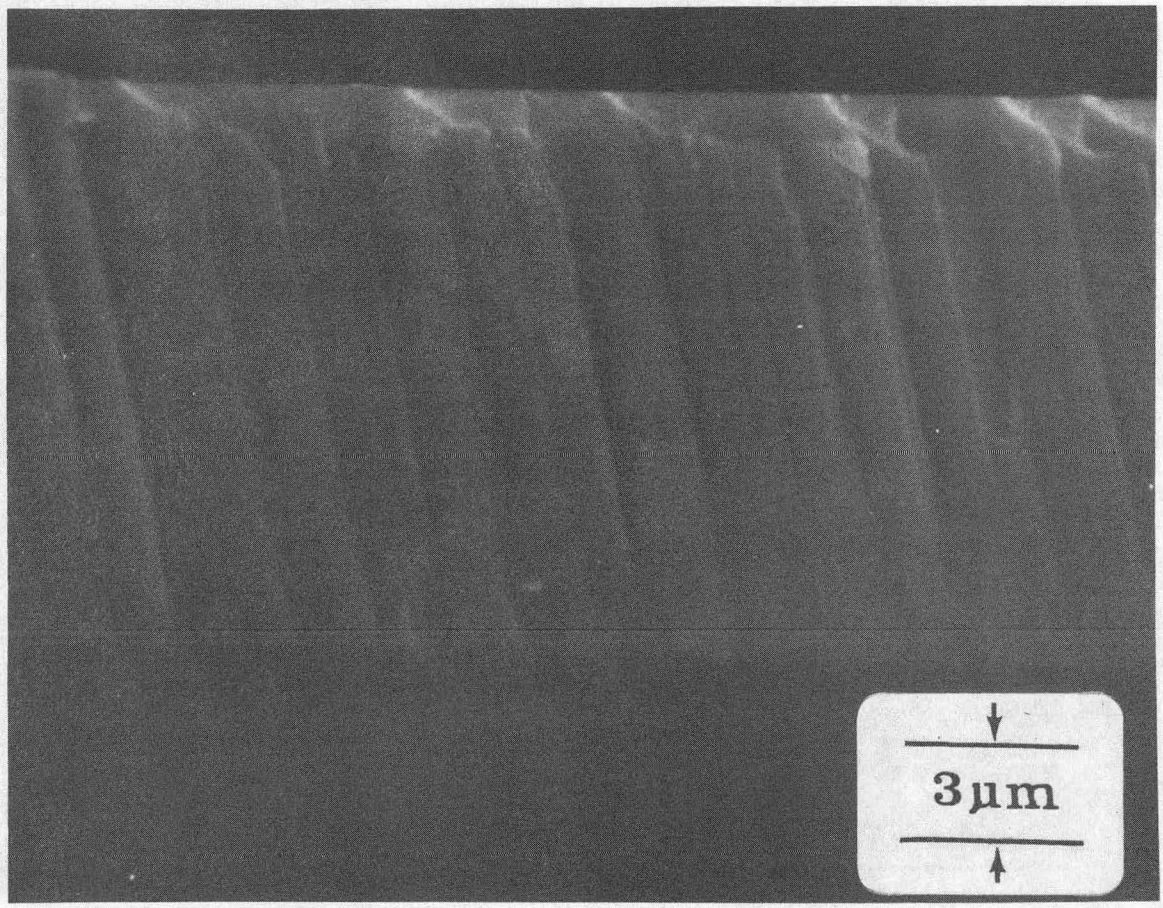

XBB 779 9107

Fig. 3.14

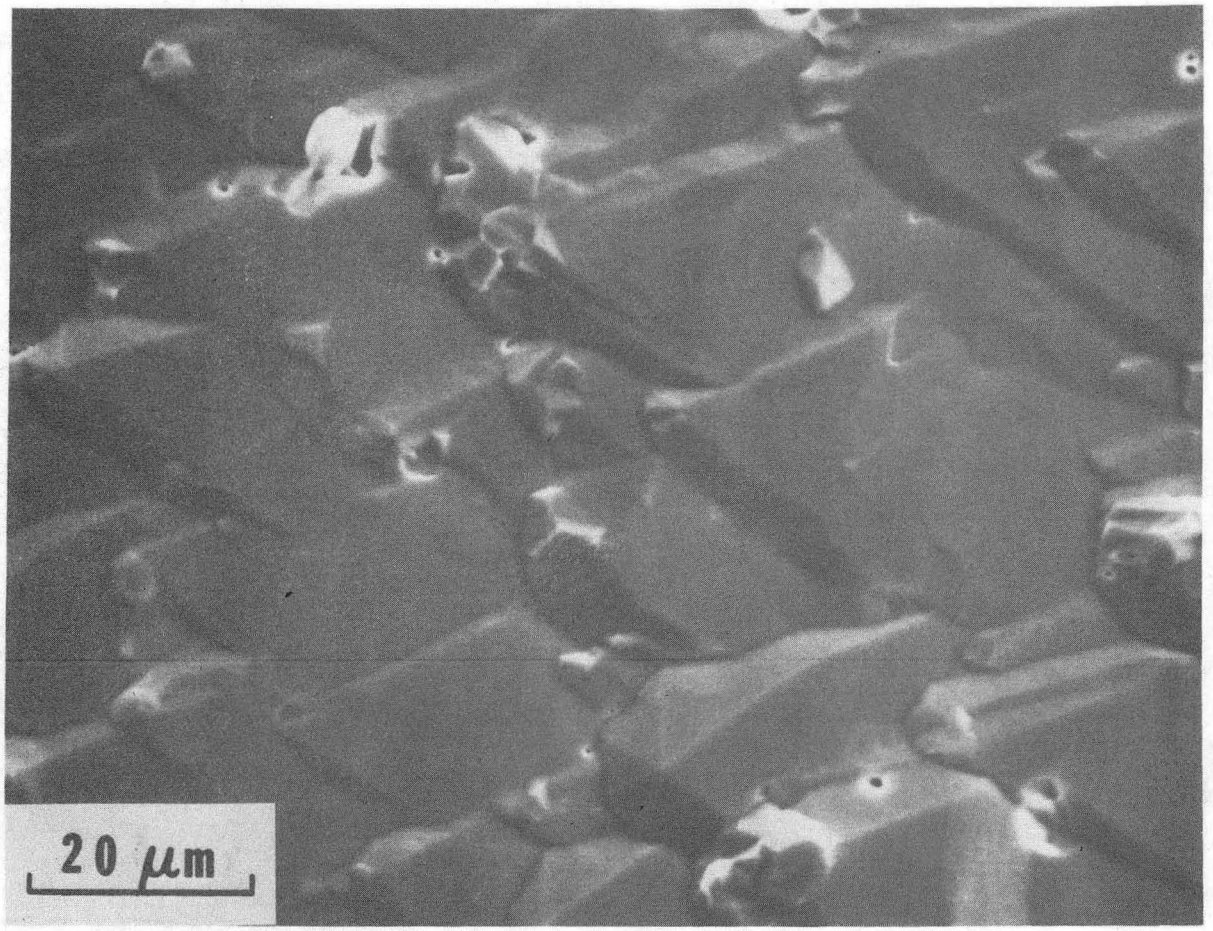

XBB 779 9474

Fig. 3.15

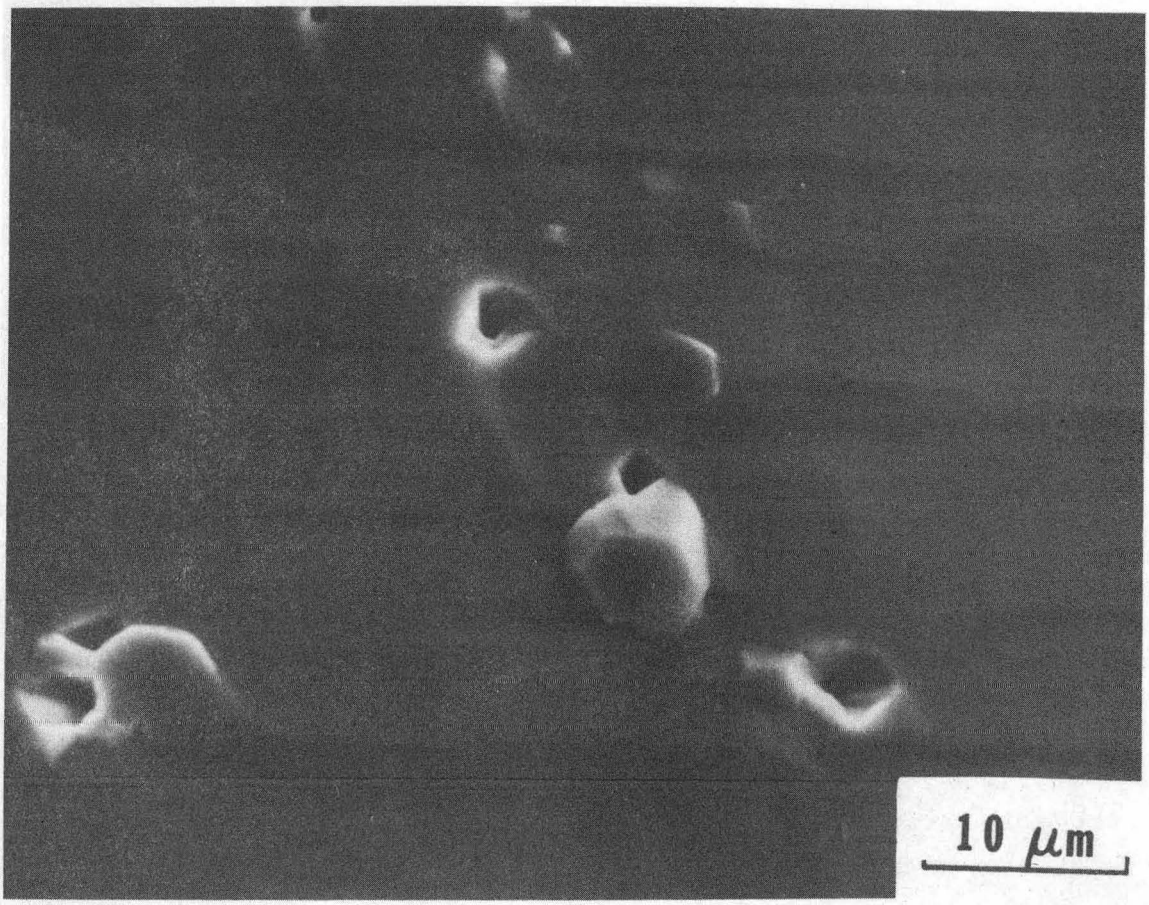

XBB 779 9106

Fig. 3.16

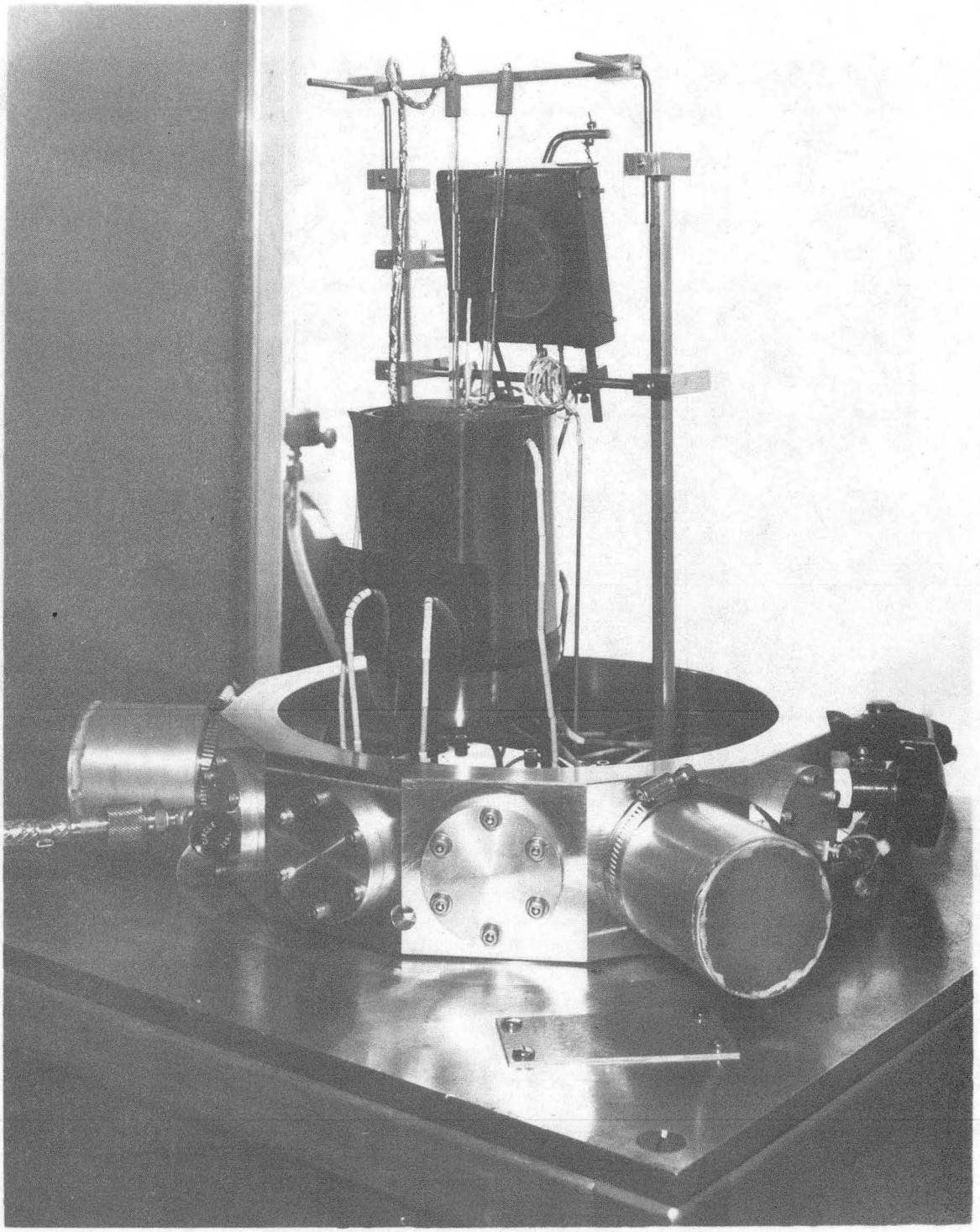

CBB 781 460

Fig. 3.17

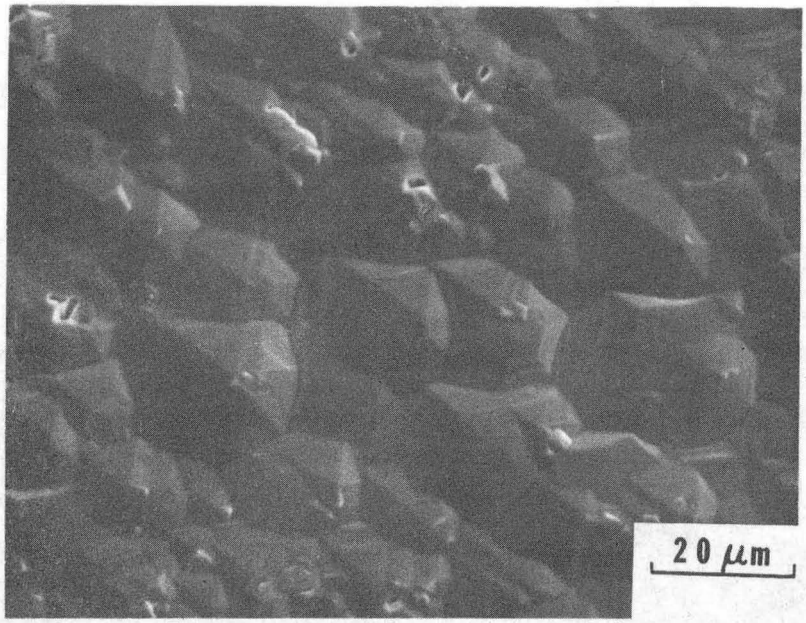

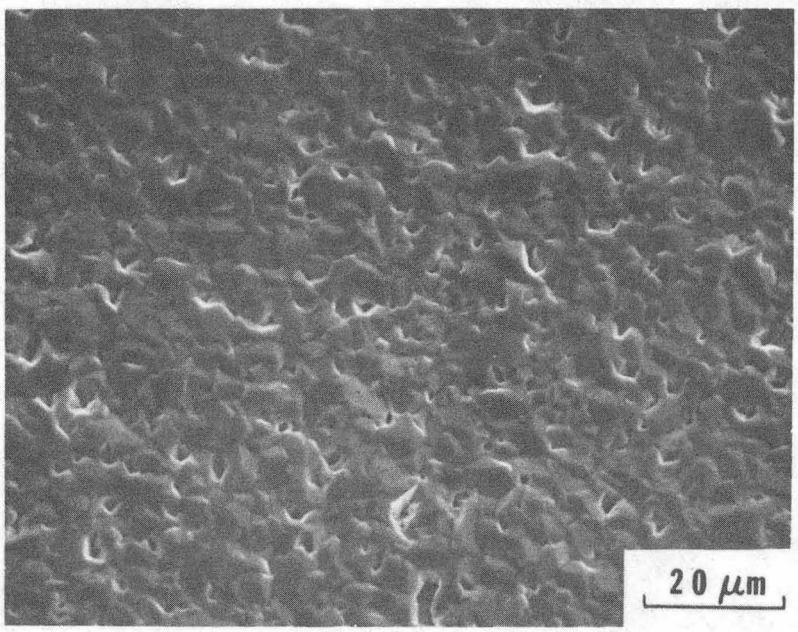

XBB 781 573

Fig. 3.18

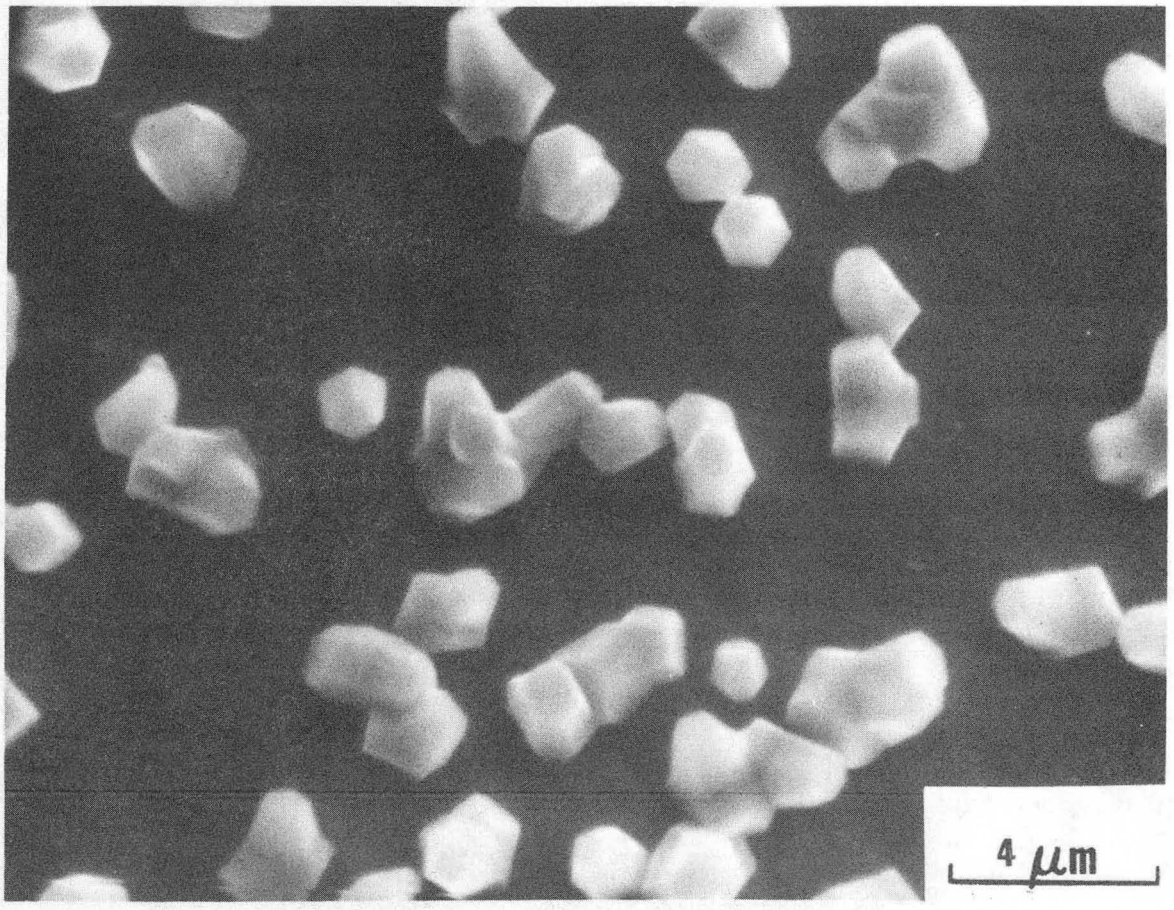

XBB 784 4137

Fig. 3.19

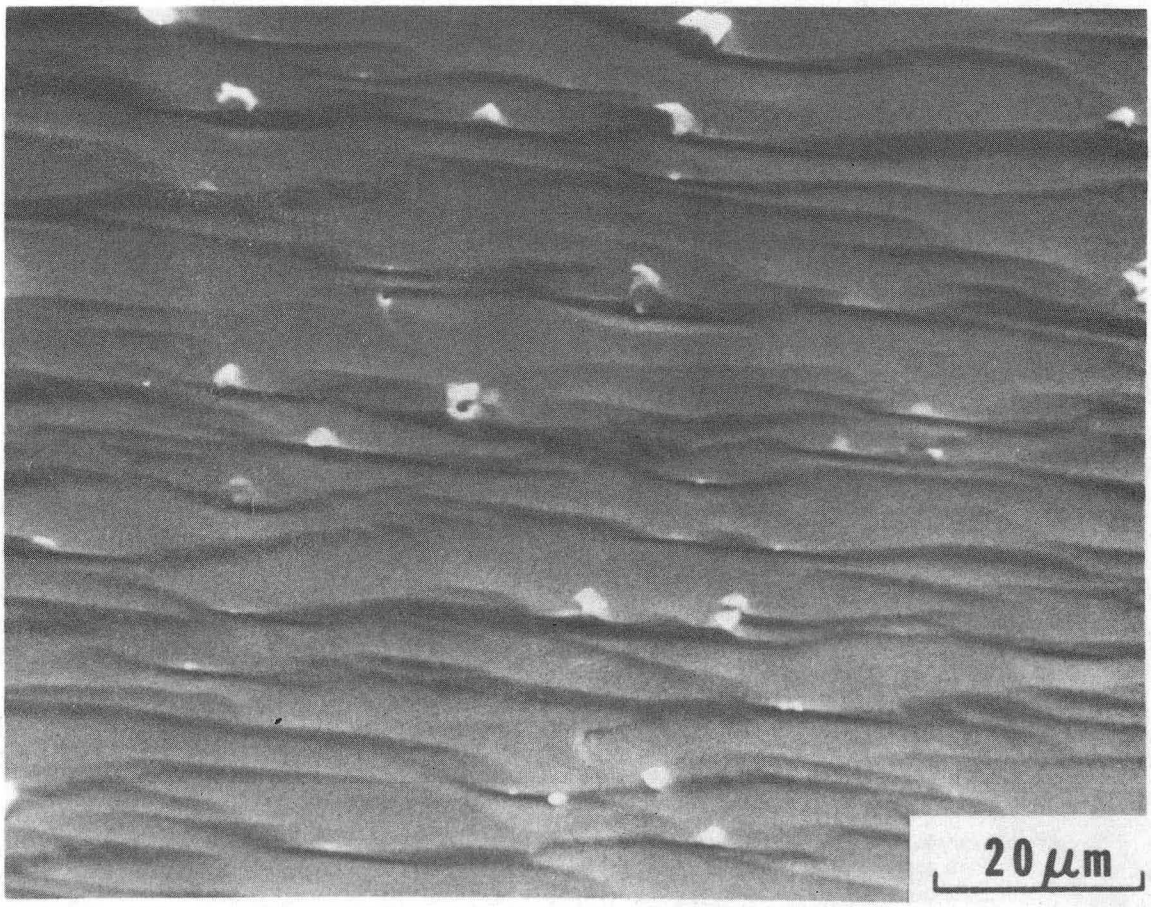

XBB 784 4138

Fig. 3.20

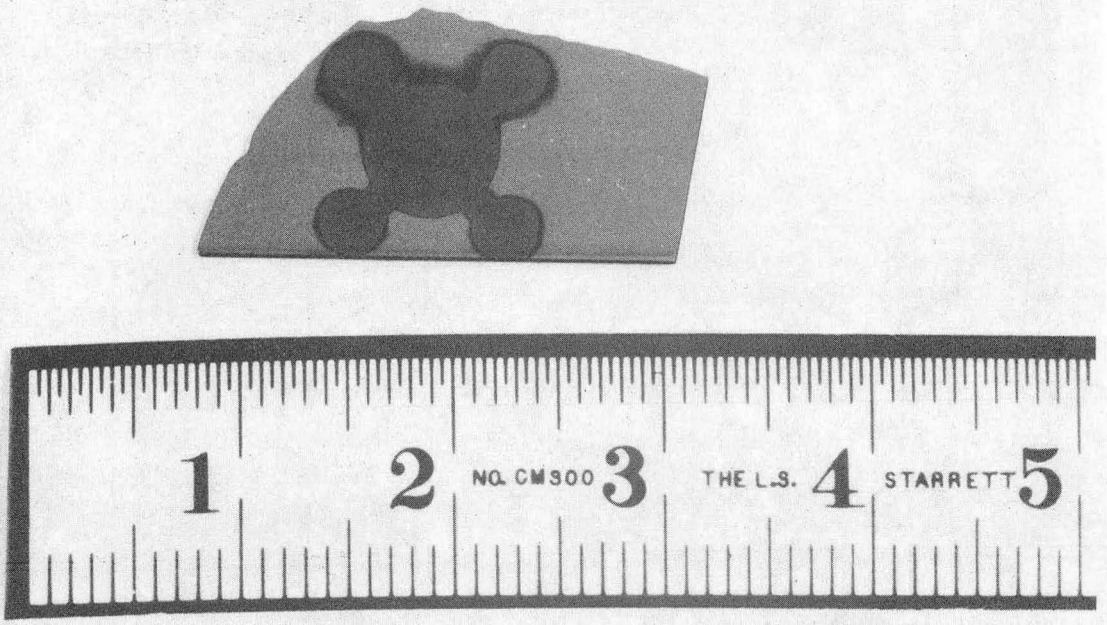

CBB 783 2708

Fig. 3.21

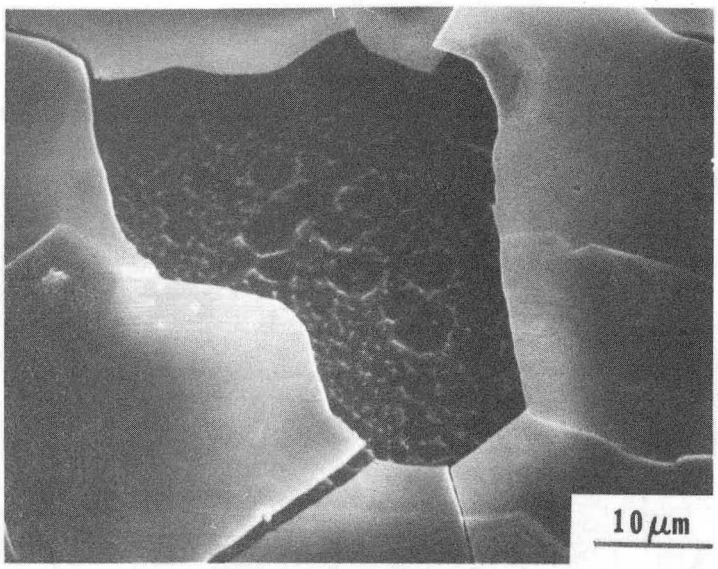

a

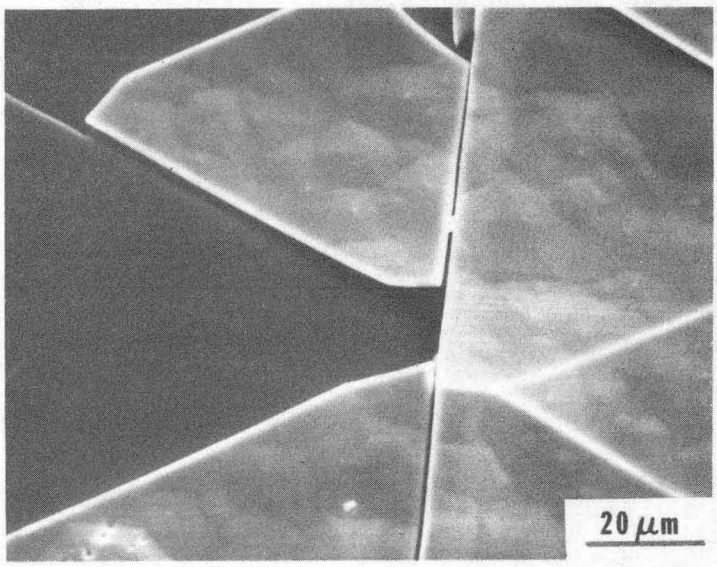

b

XBB 790 13602

Fig. 3.22

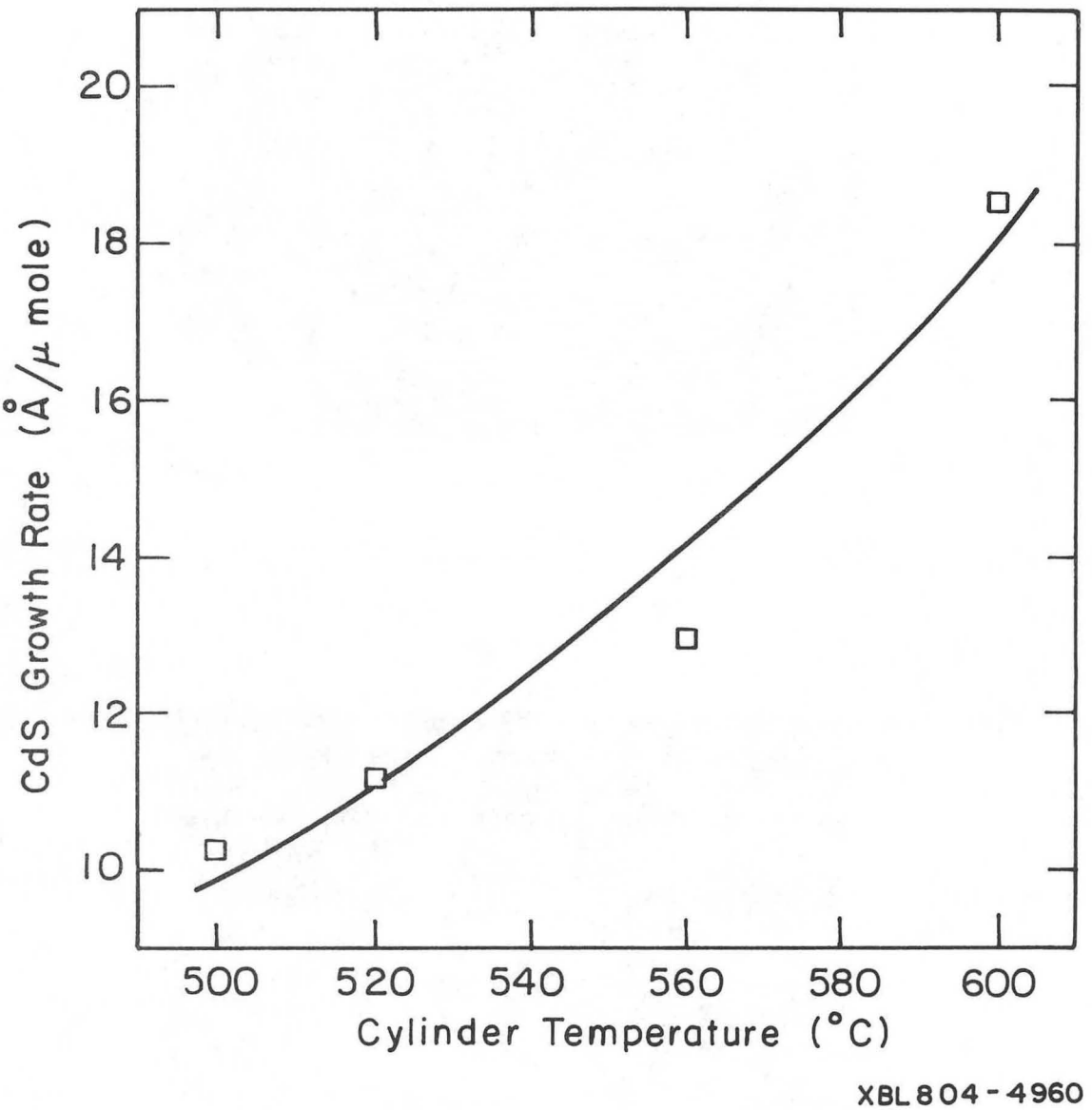
20
18
16
14
12
10
CdS Growth Rate (Å/μ mole)
500
520
540
560
580
600
Cylinder Temperature (°C)
XBL 804-4960

Fig. 3.23

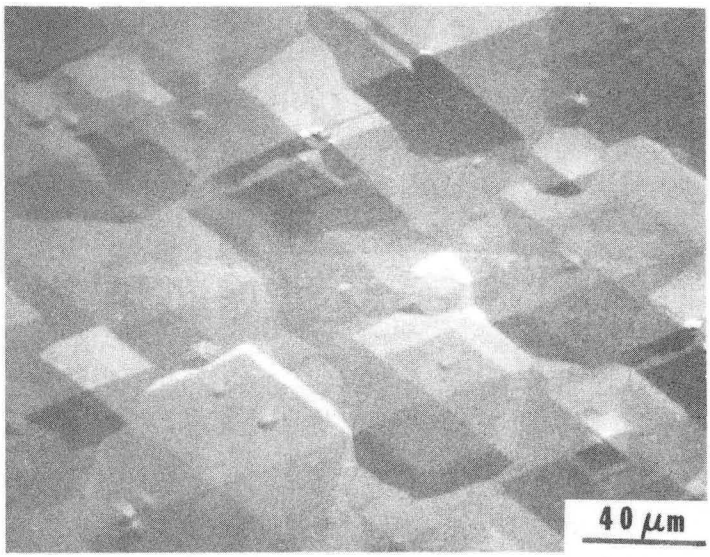

a

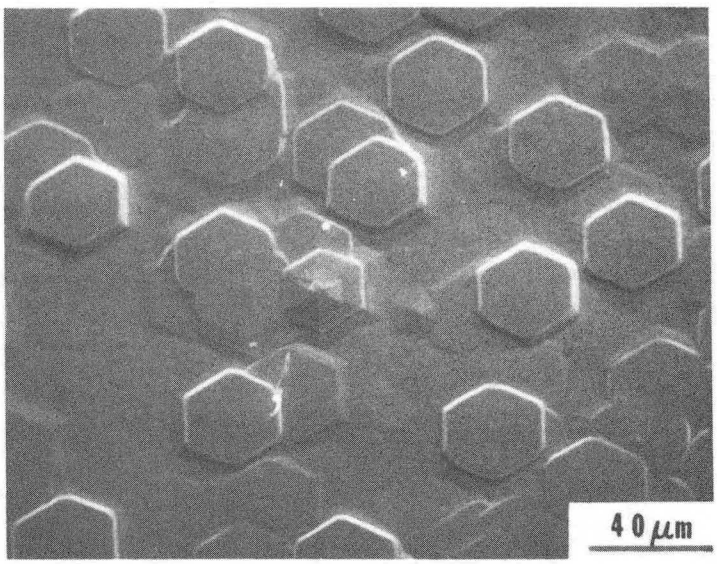

b

XBB 790 13603

Fig. 3.24

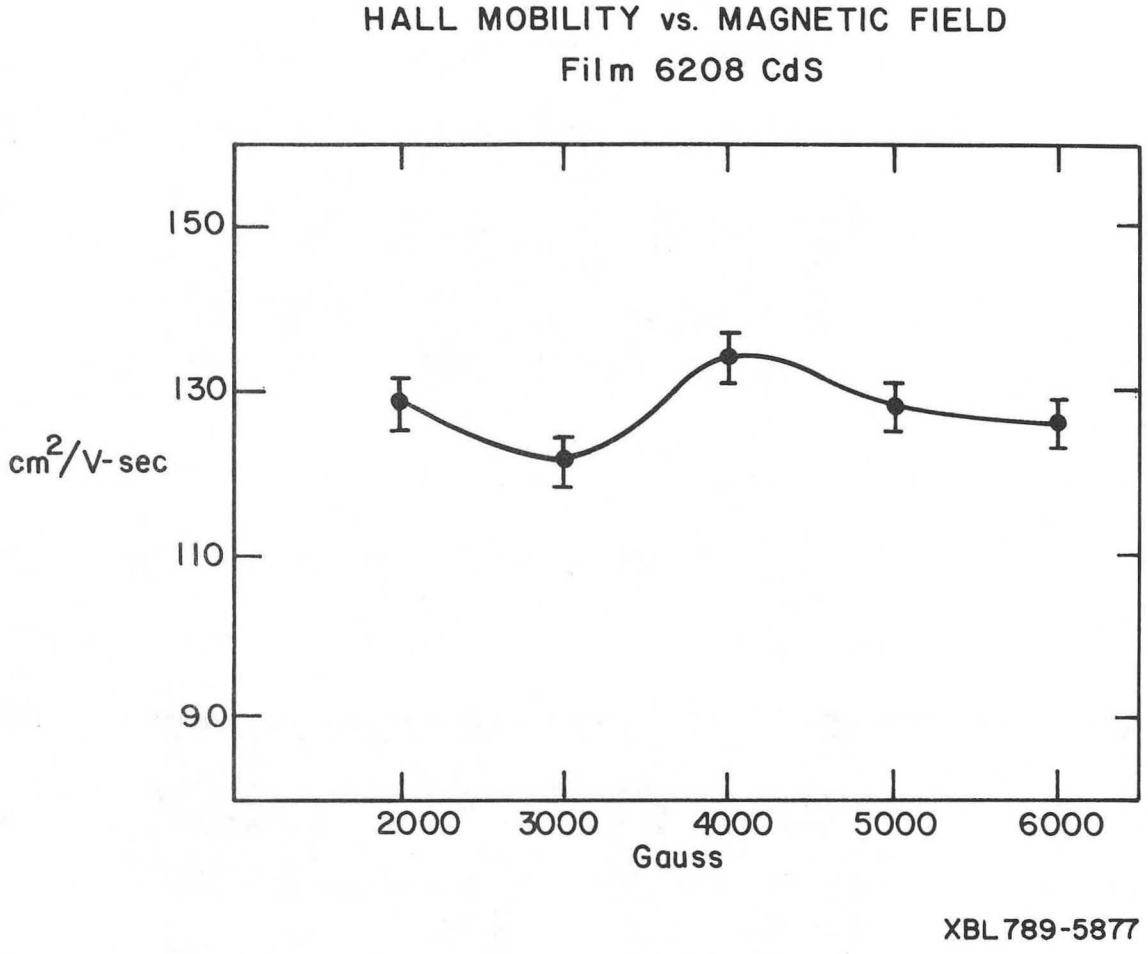
HALL MOBILITY vs. MAGNETIC FIELD
Film 6208 CdS
150
130
110
90
cm²/V-sec
2000
3000
4000
5000
6000
Gauss
XBL789-5877

Fig. 4.1

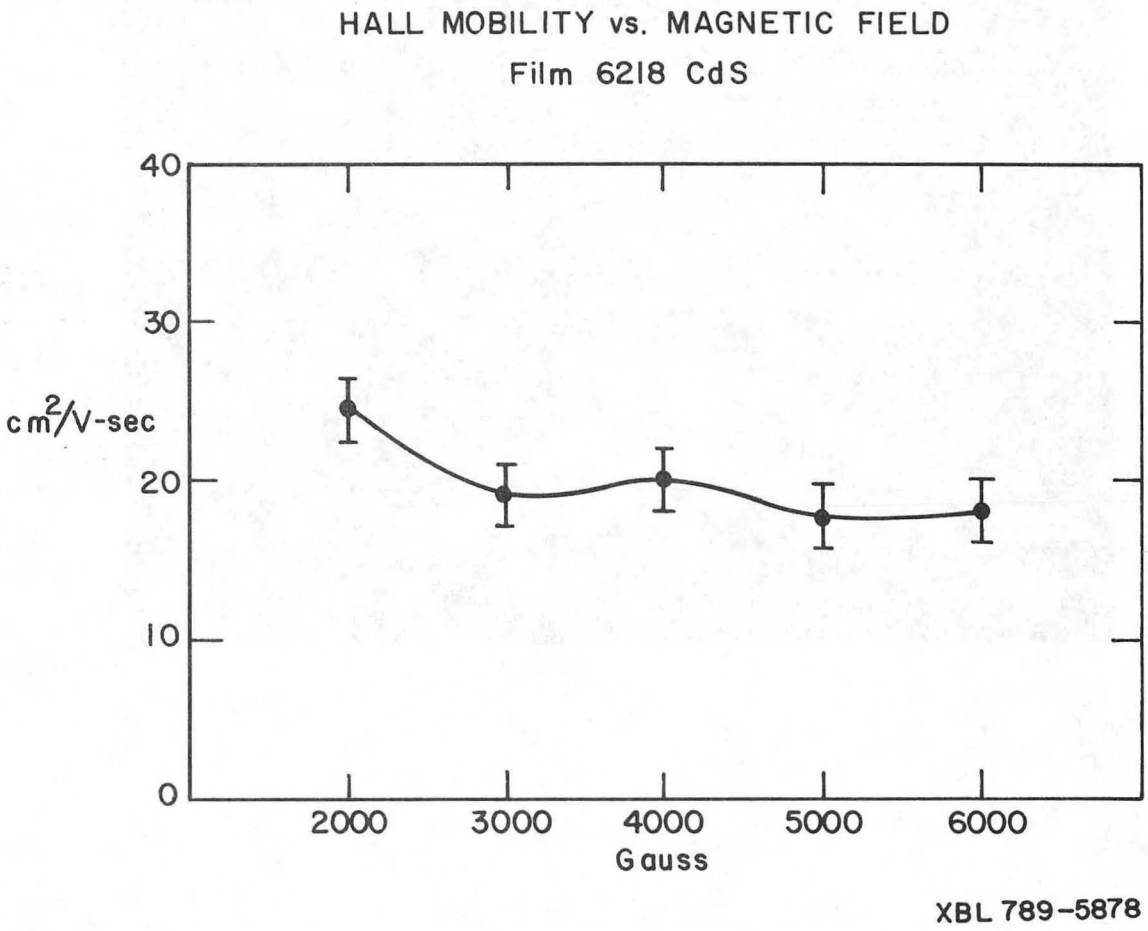
HALL MOBILITY vs. MAGNETIC FIELD
Film 6218 CdS
40
30
20
10
0
cm²/V-sec
2000
3000
4000
5000
6000
Gauss
XBL 789-5878

Fig. 4.2

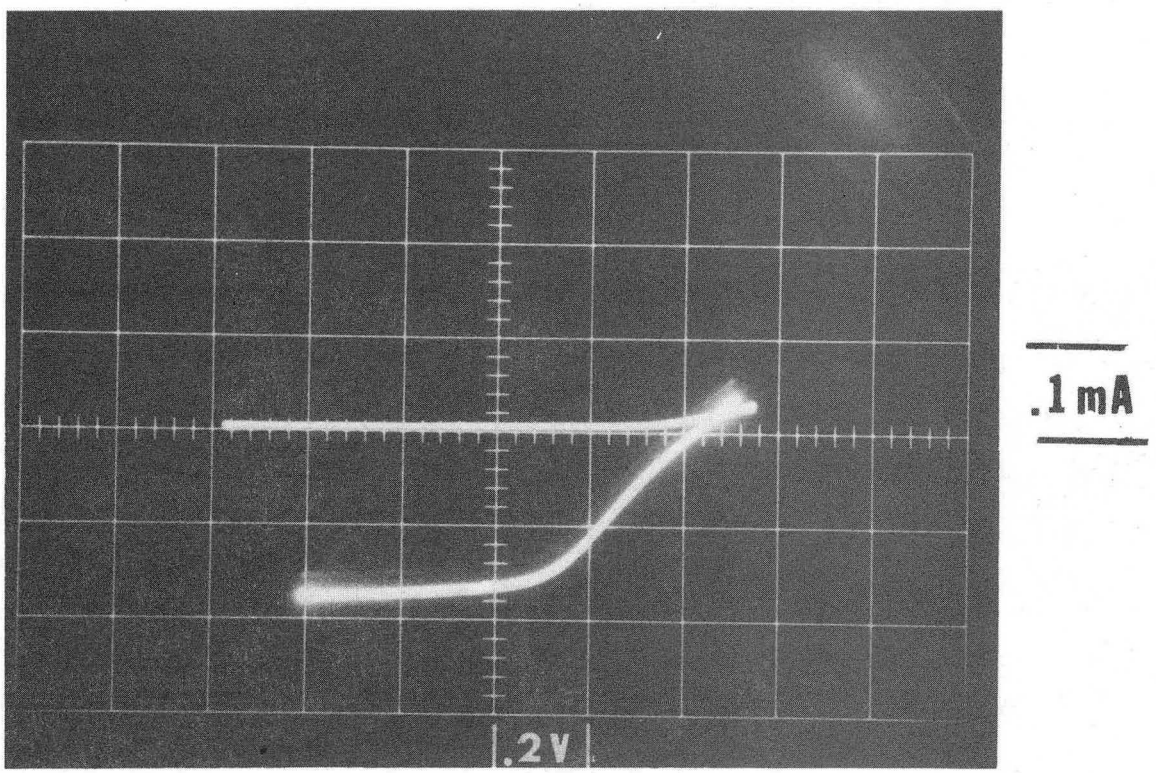

Cu_xS- $(Cd_{.97}Zn_{.03})S$ Single Crystal Cell

Cu_xS Sputtered by LLL

Under Tungsten Lamp Illumination

V_{oc}=.42V, J_{sc}=2mA/cm^2

XBB 784 4300

Fig. 4.3

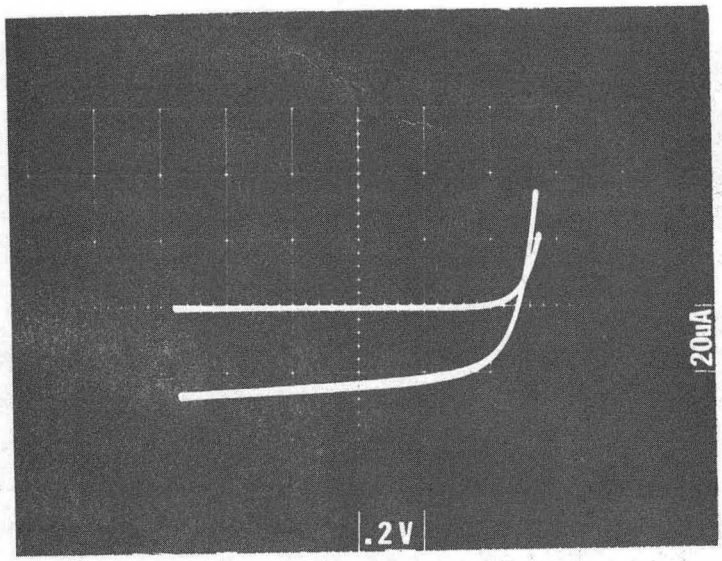

a

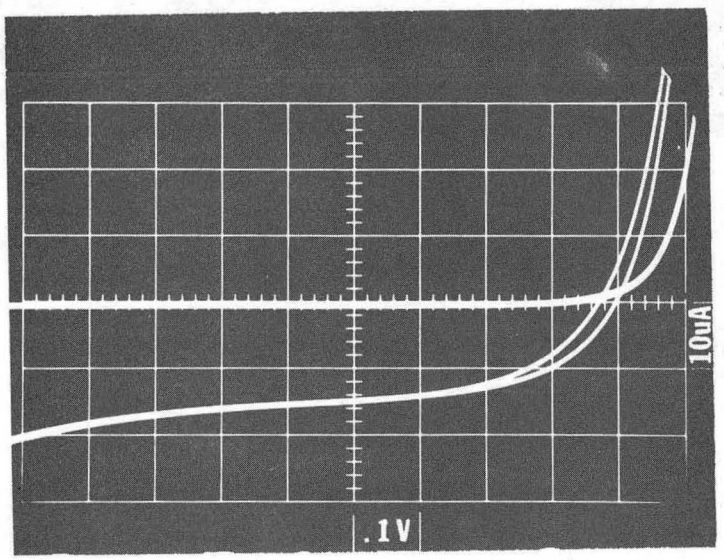

b

XBB 777 6683

Fig. 4.4

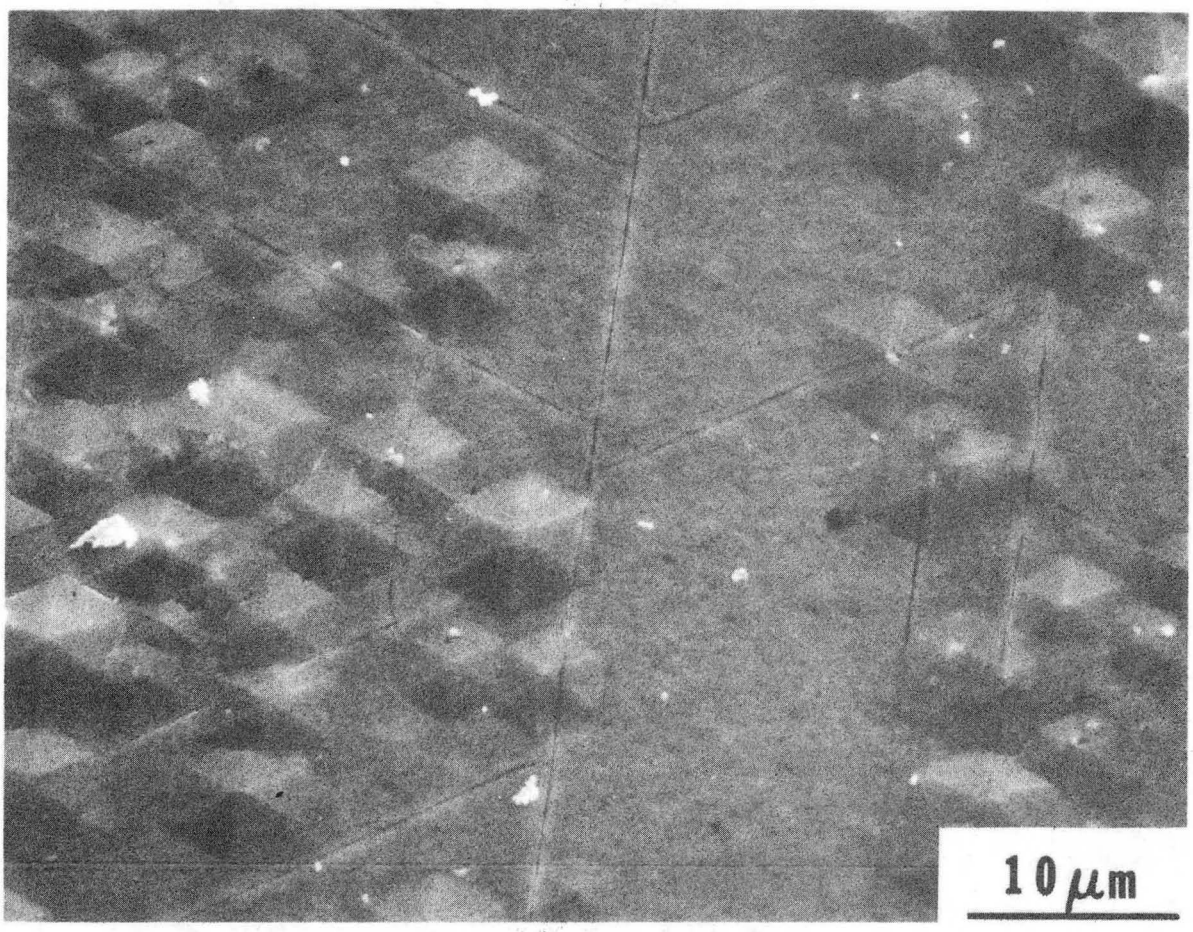

XBB 790 13124

Fig. 4.5

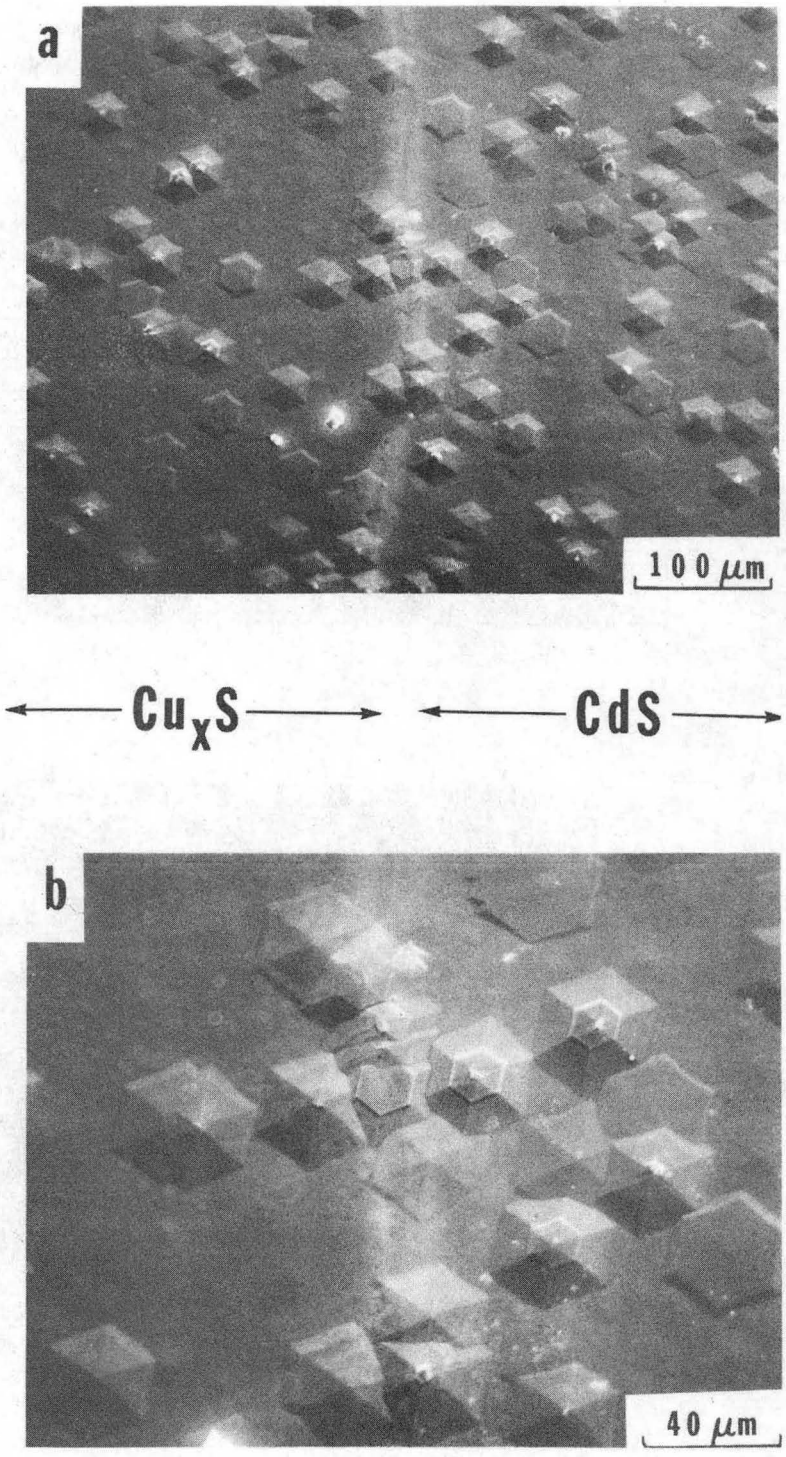

XBB 790 15812

Fig. 4.6

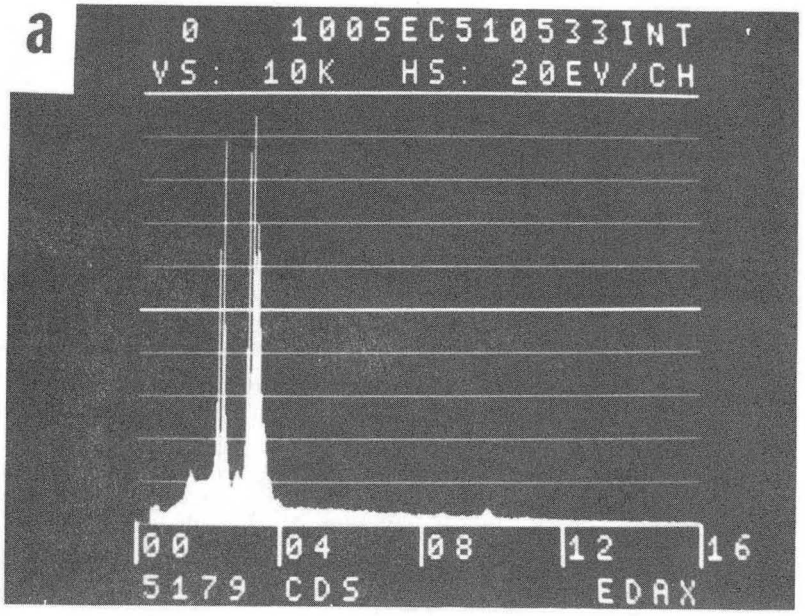

XBB 790 15814

Fig. 4.7

a. 8249A

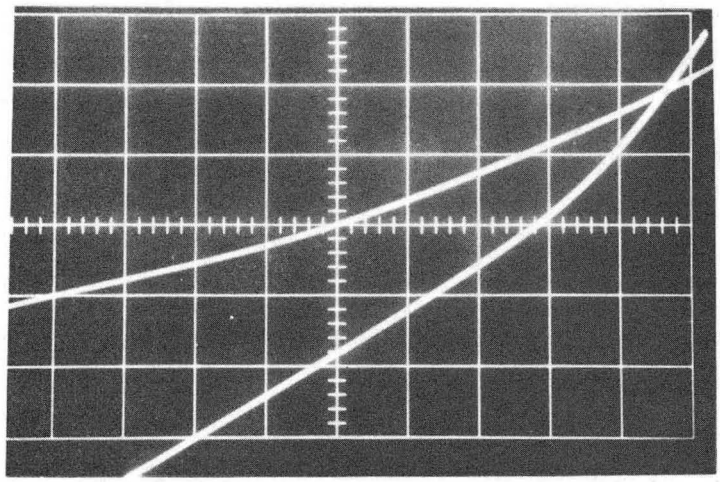

b. 5179A

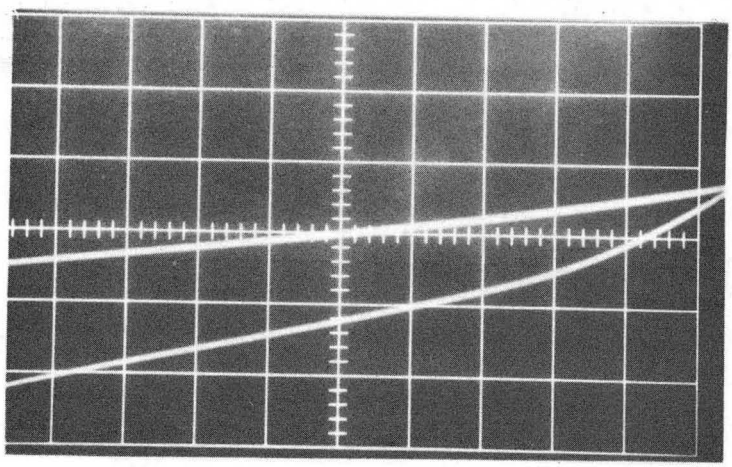

XBB 790 15813

Fig. 4.8

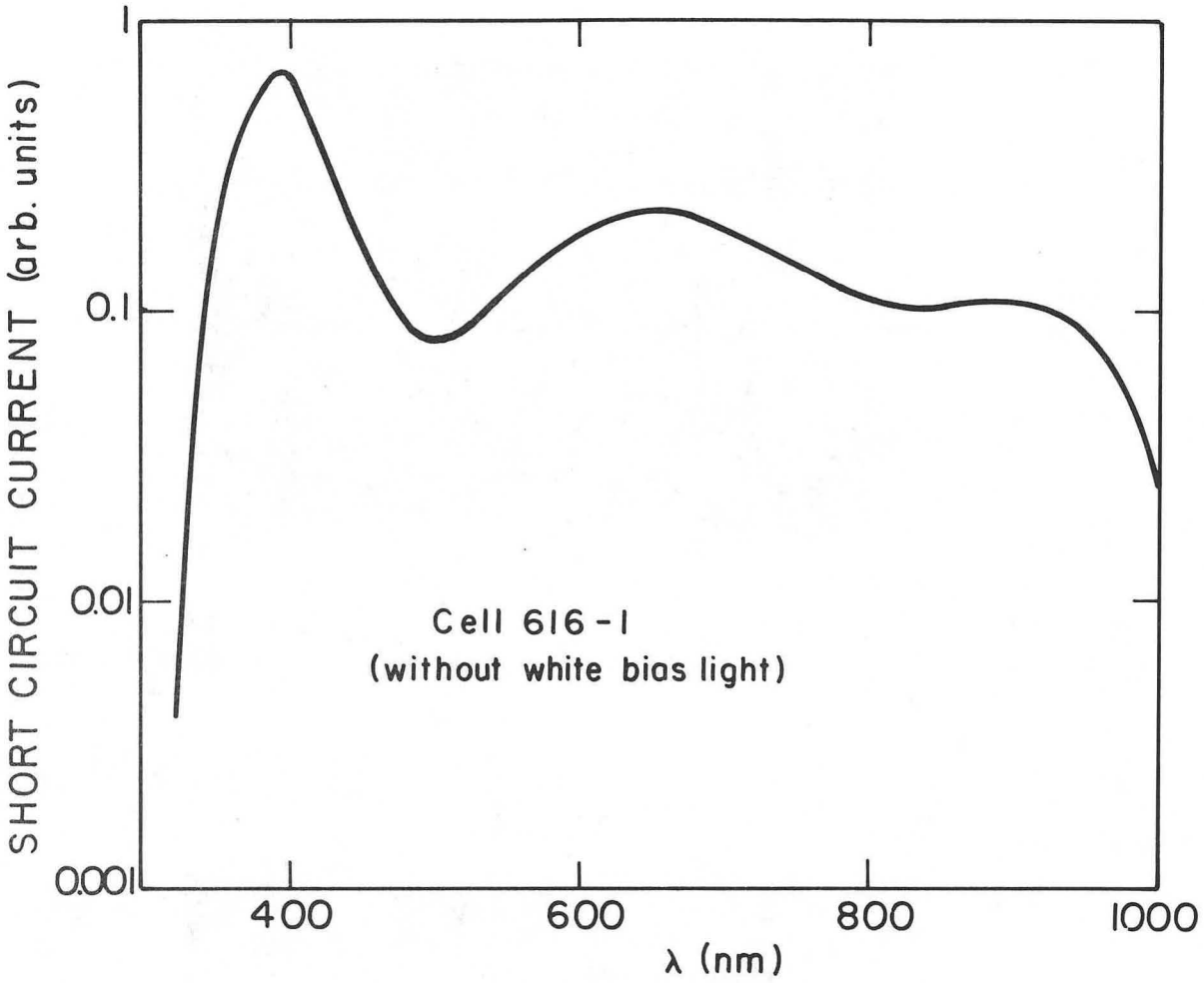
SHORT CIRCUIT CURRENT (arb. units)
1
0.1
0.01
0.001
400
600
800
1000
λ (nm)
Cell 616-1
(without white bias light)
XBL 777-5844

Fig. 4.9

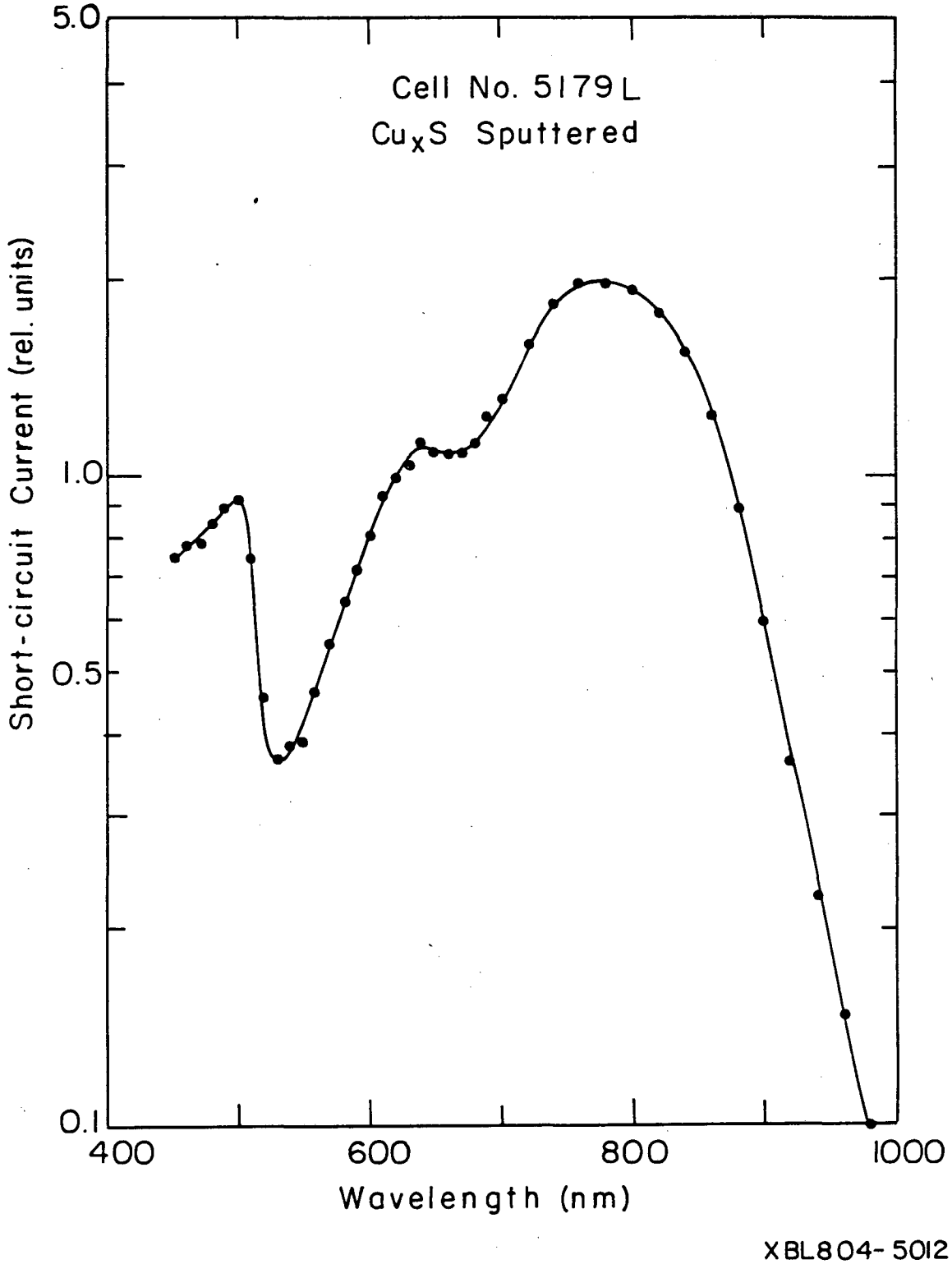
Cell No. 5179L
Cu_xS Sputtered
Short-circuit Current (rel. units)
5.0
1.0
0.5
0.1
400
600
800
1000
Wavelength (nm)
XBL804-5012

Fig. 4.10

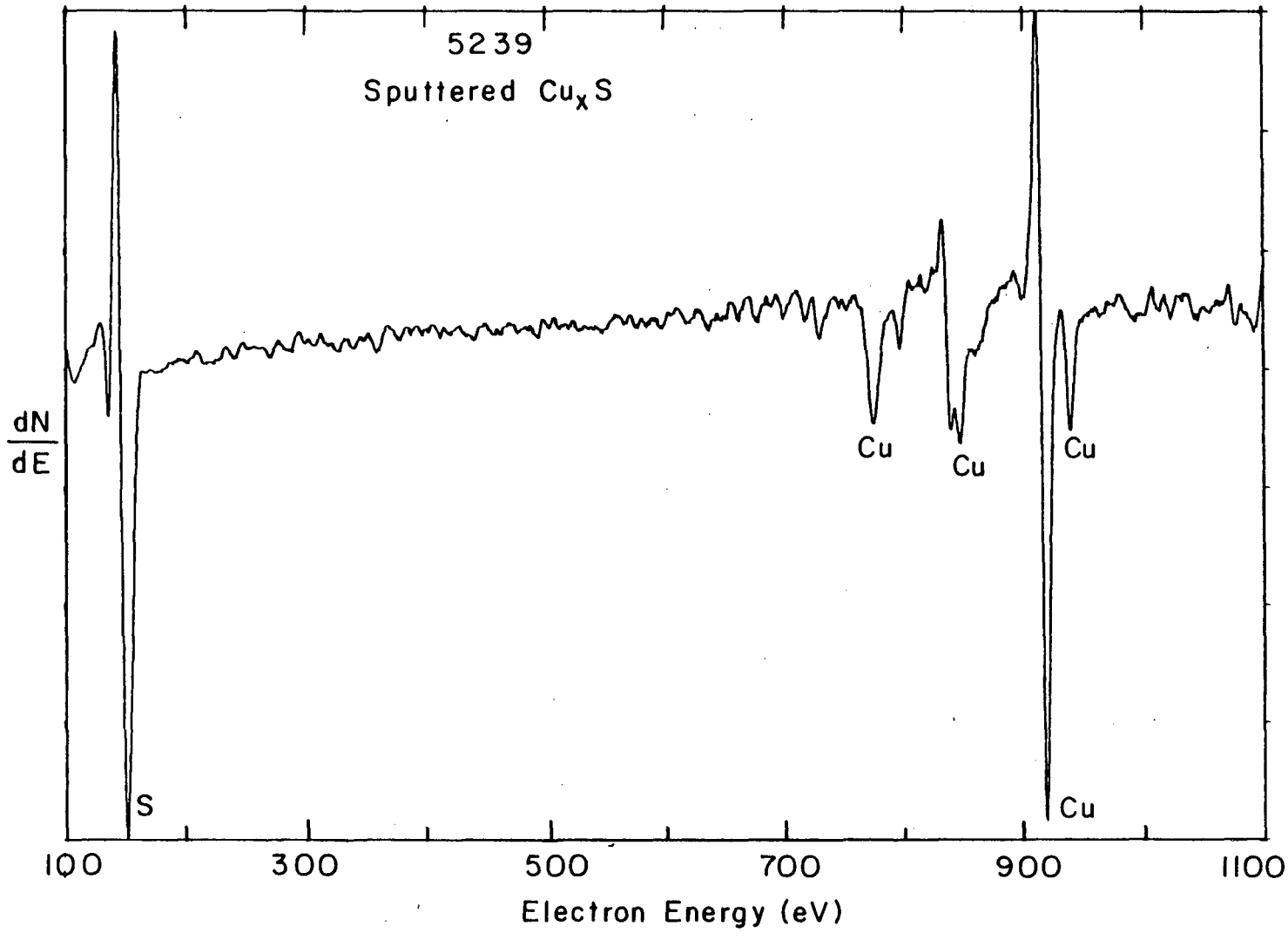

XBL 804-4990

Fig. 5.1

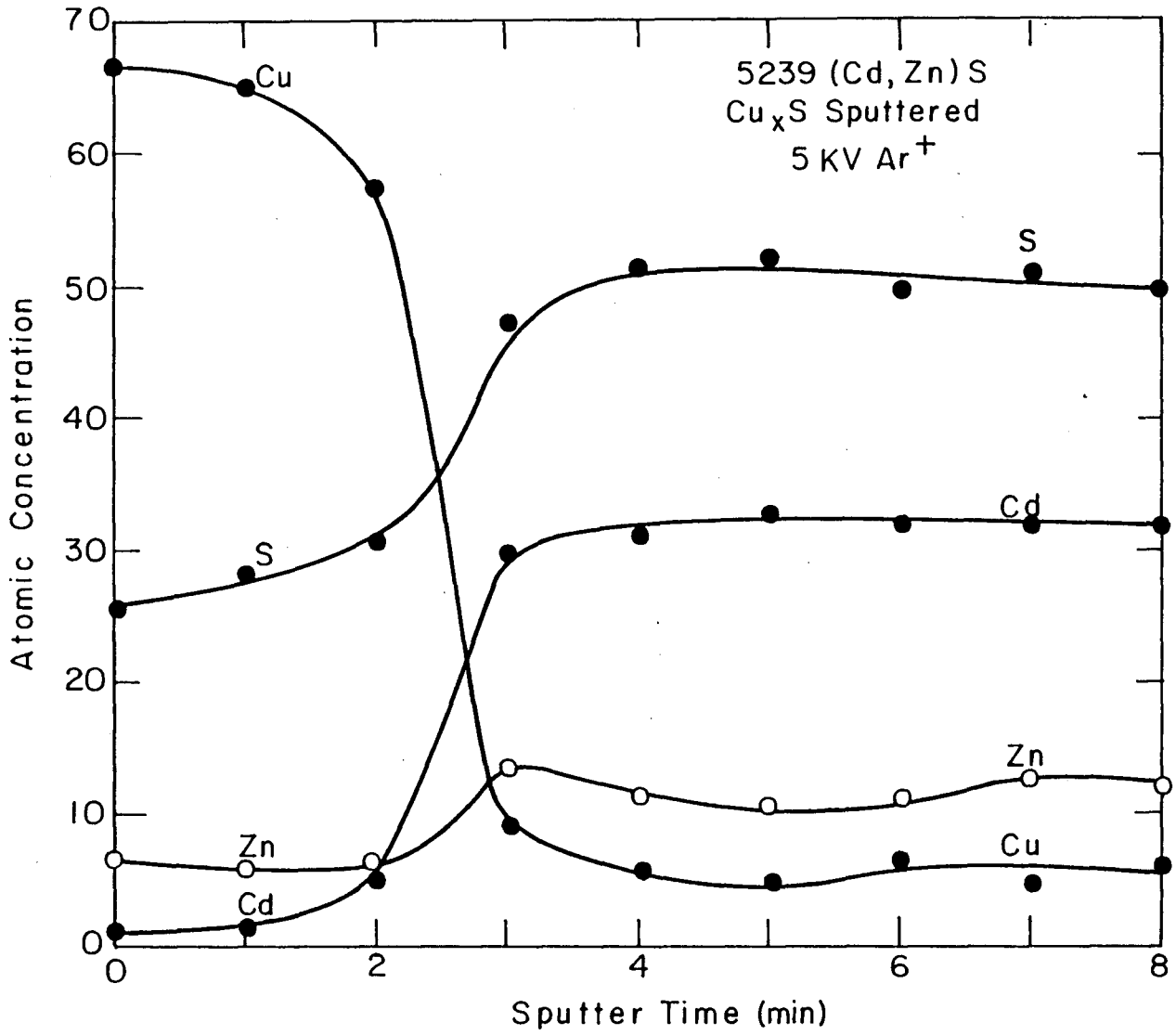

Fig. 5.2

XBL 804-4989

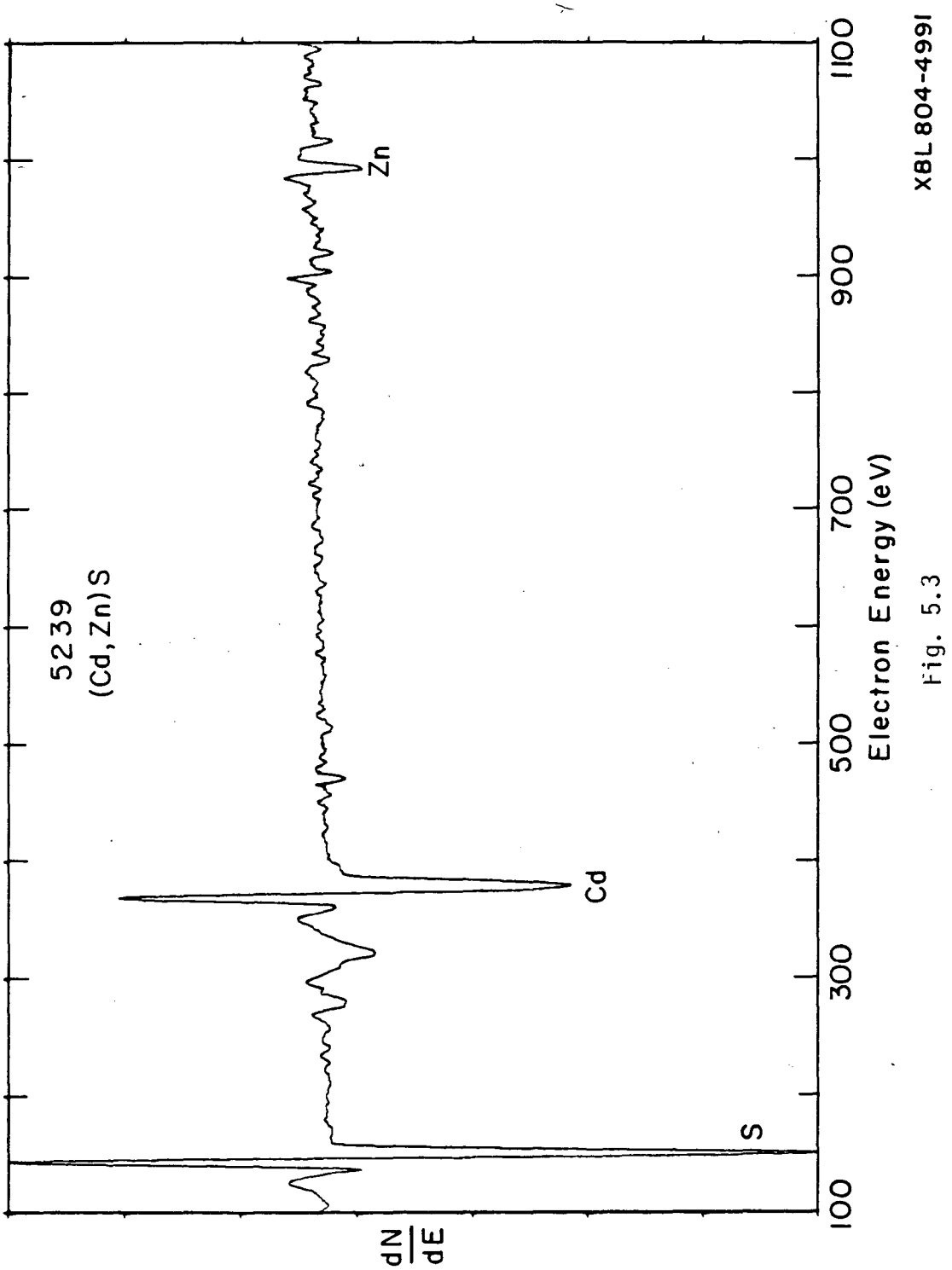
5239
(Cd,Zn)S
Zn
Cd
S
dN/dE
100
300
500
700
900
1100
Electron Energy (eV)
XBL804-4991

Fig. 5.3

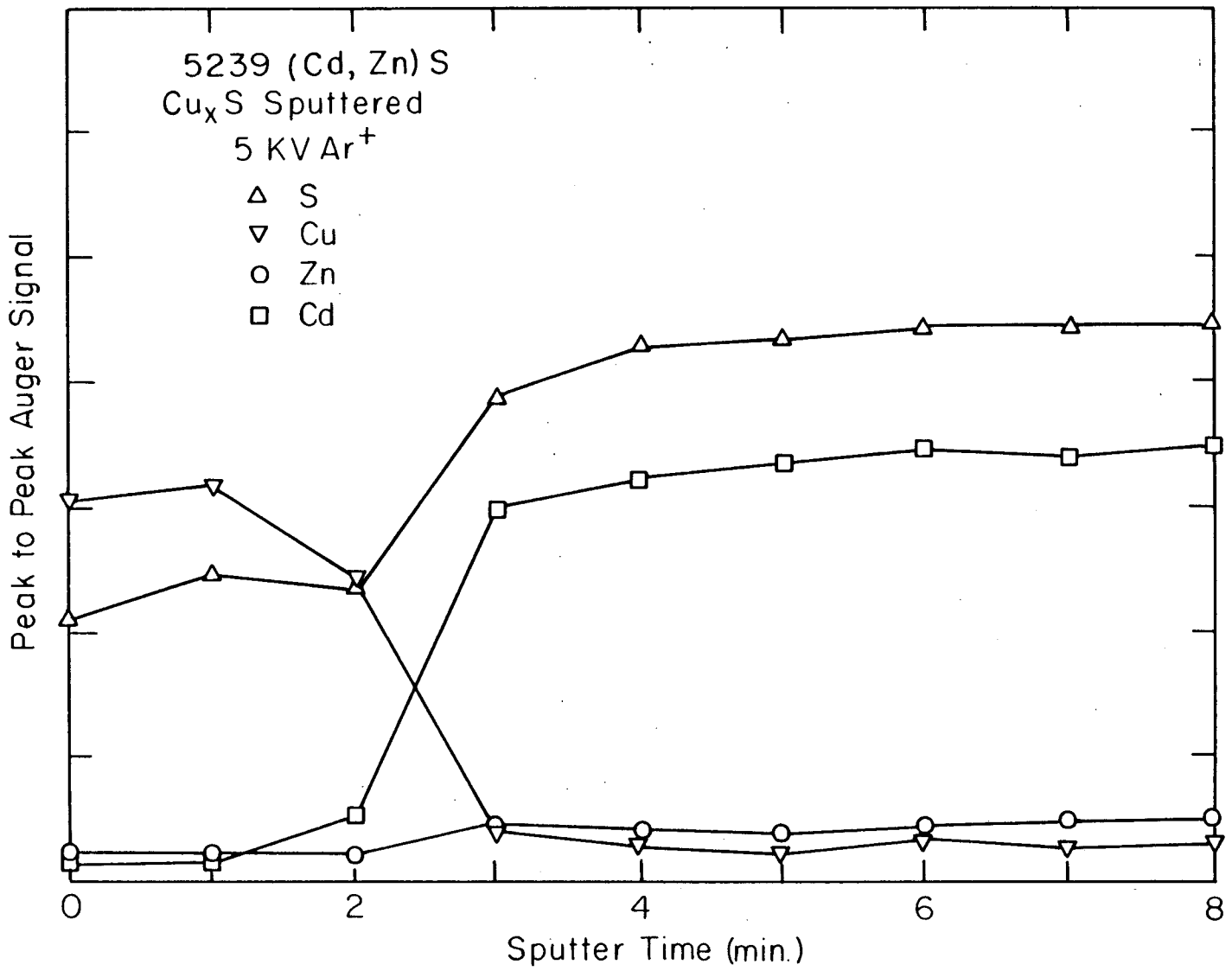

Fig. 5.4

XBL 805-5229

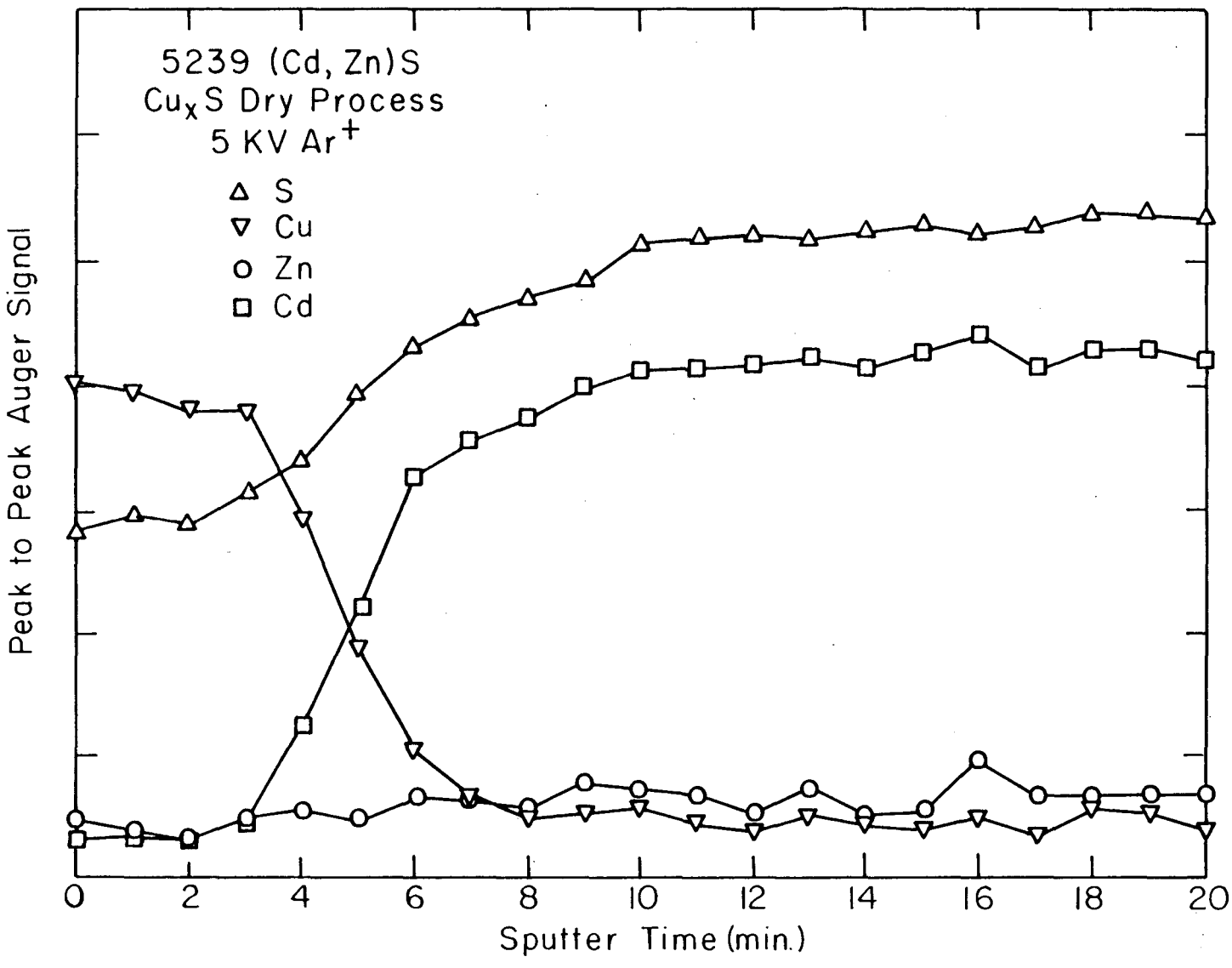

Fig. 5.5

XBL 805-5228

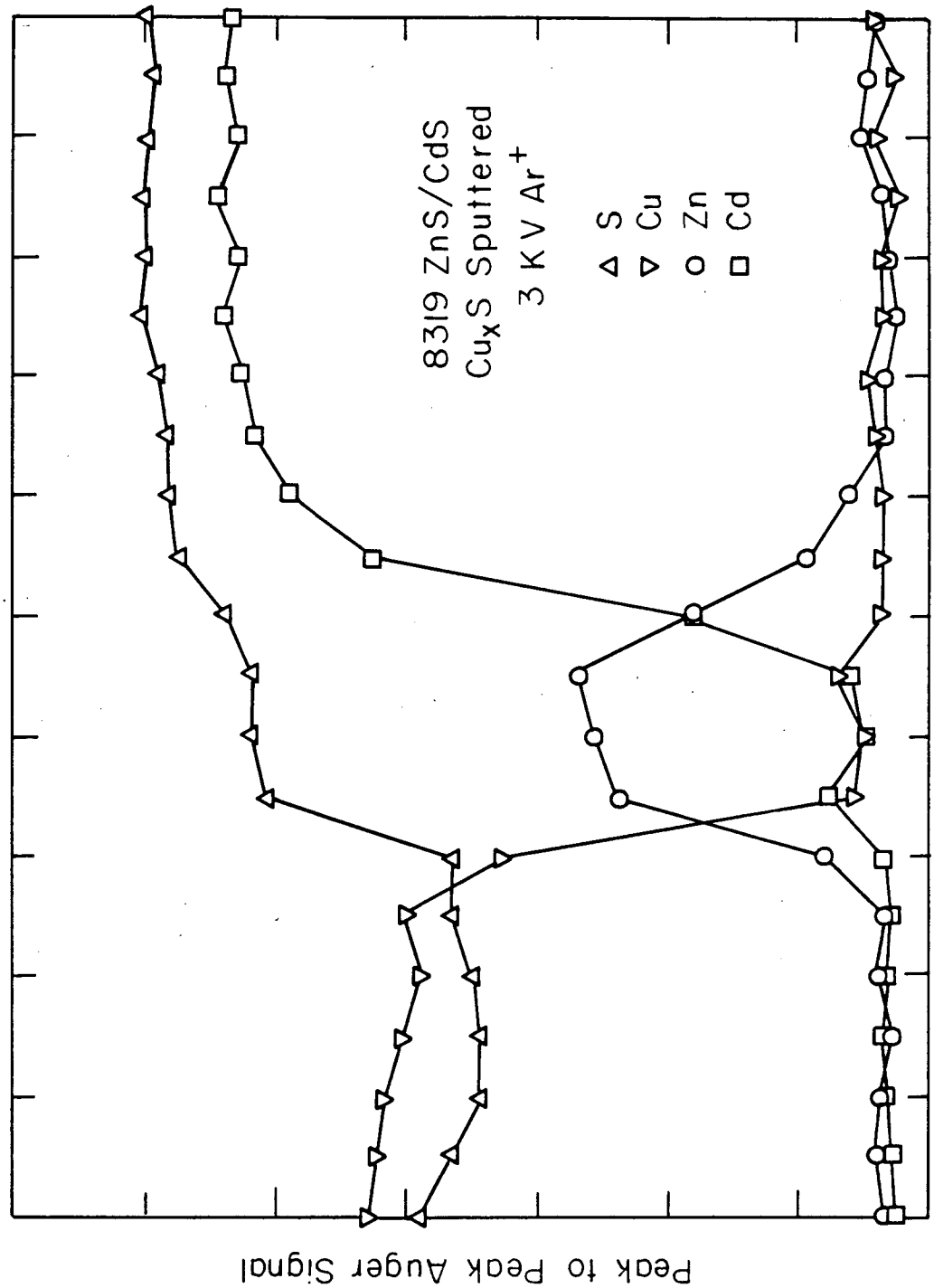

XBL 805-5227

Fig. 5.6

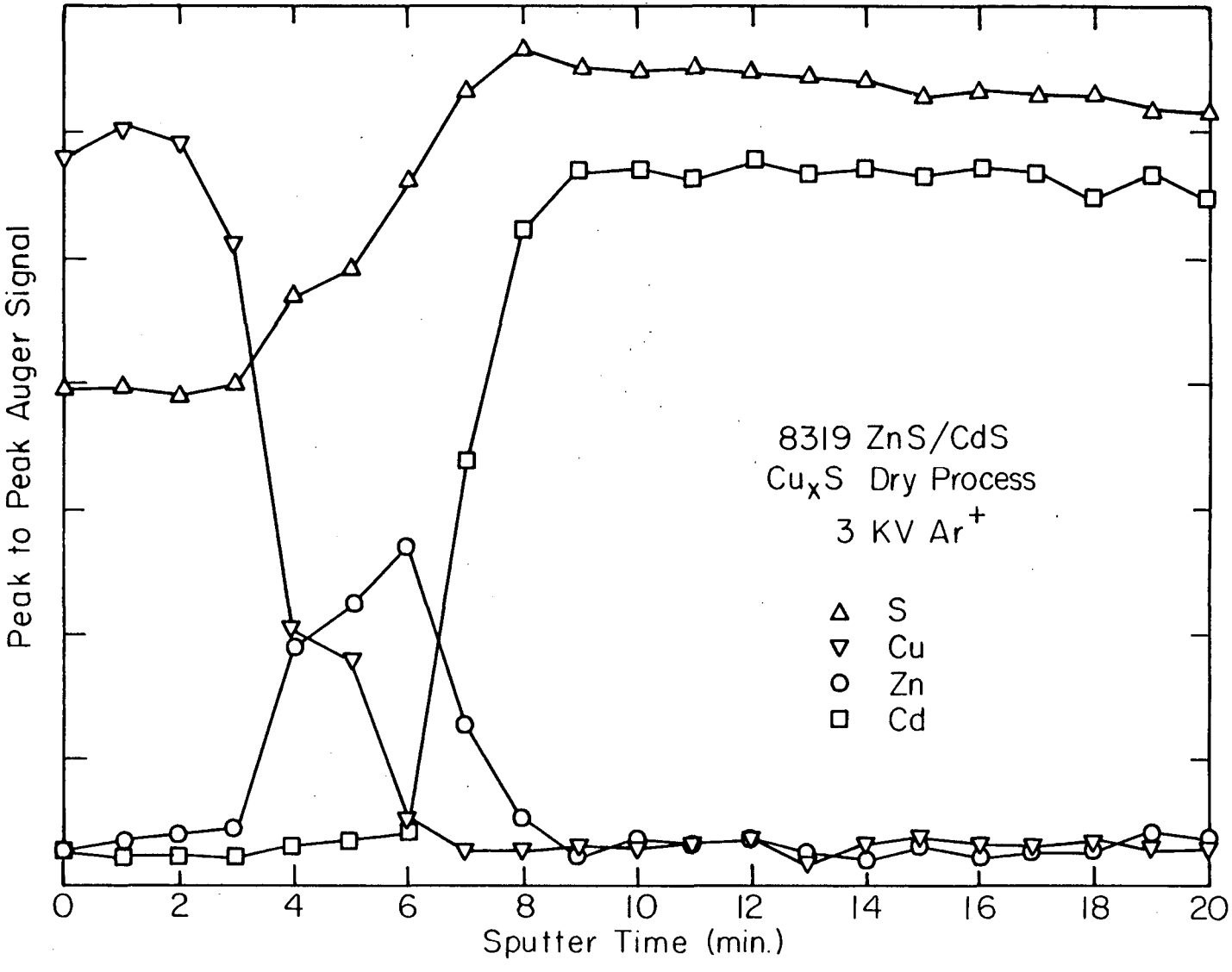

Fig. 5.7

XBL805-5226

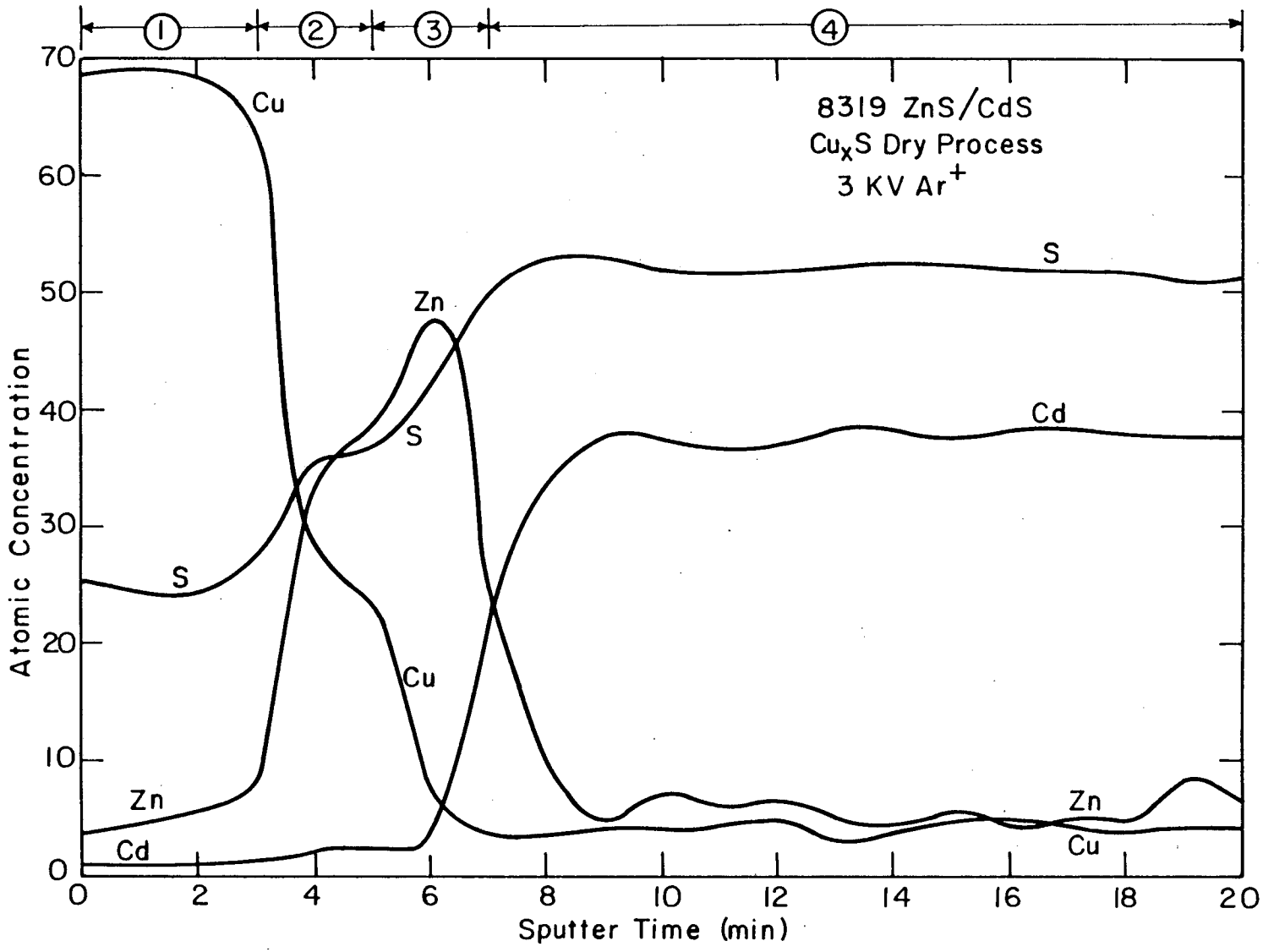

XBL804-4986

Fig. 5.8

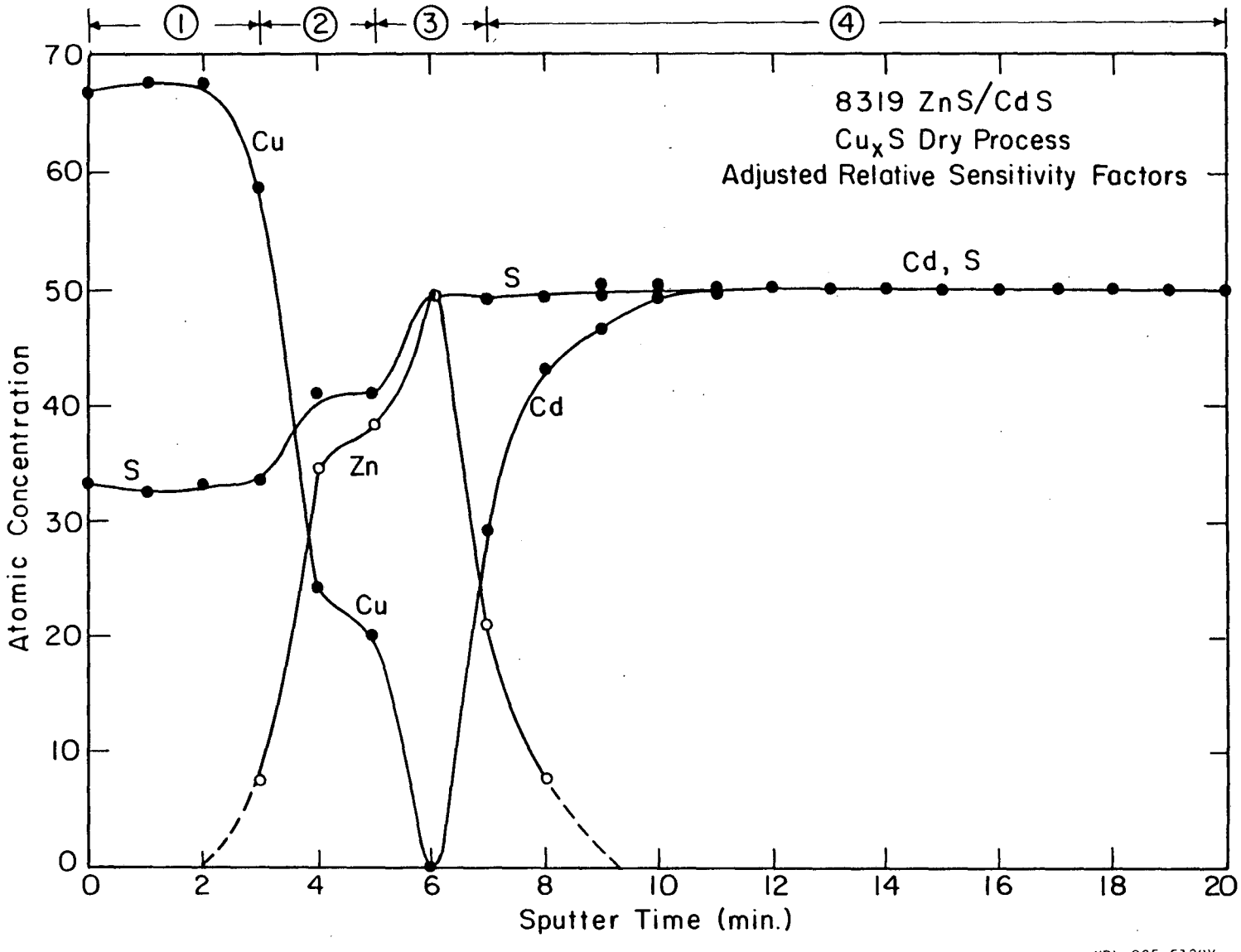

XBL 805-5138Y

Fig. 5.9

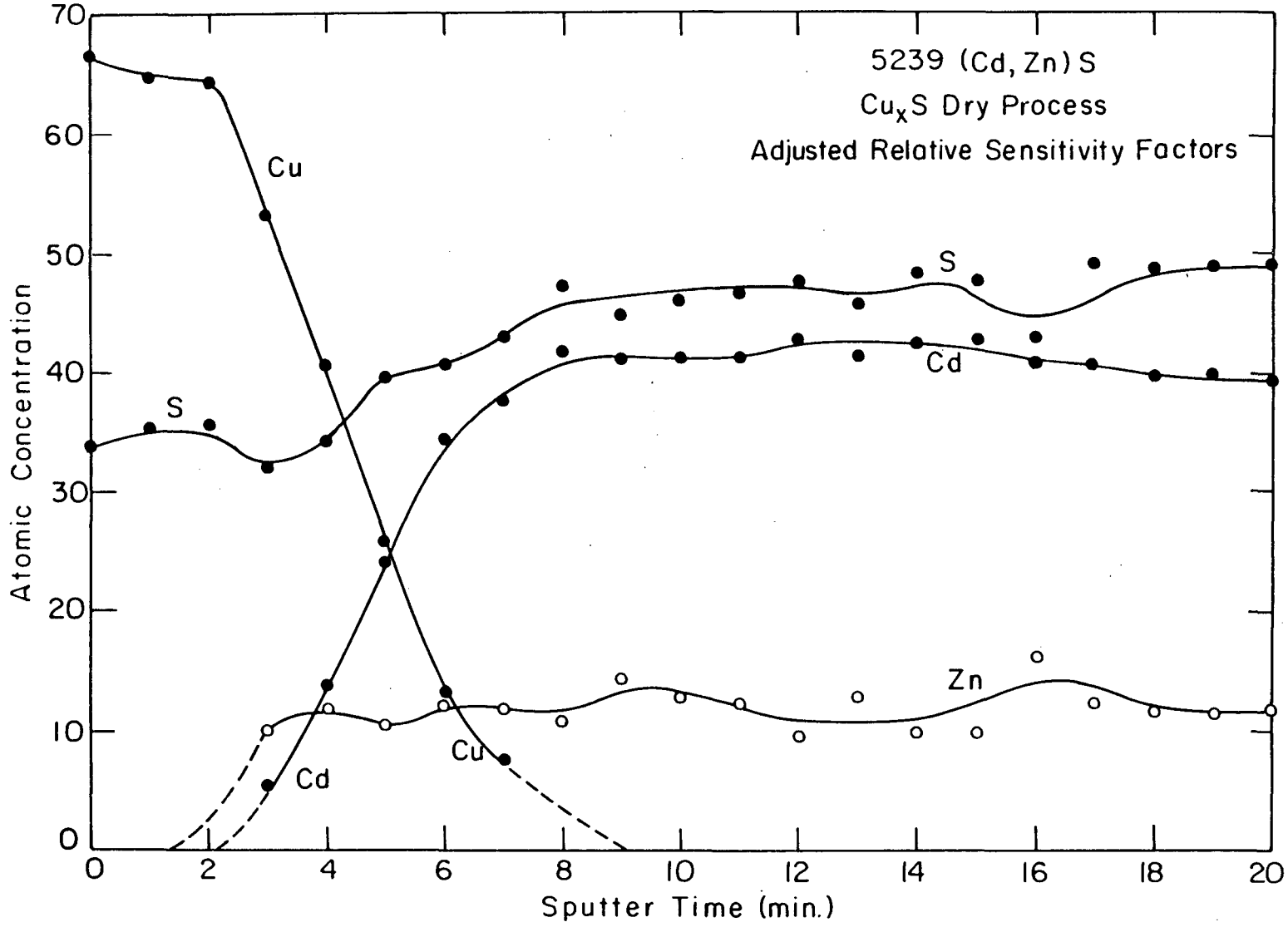

Fig. 5.10

XBL805-5139

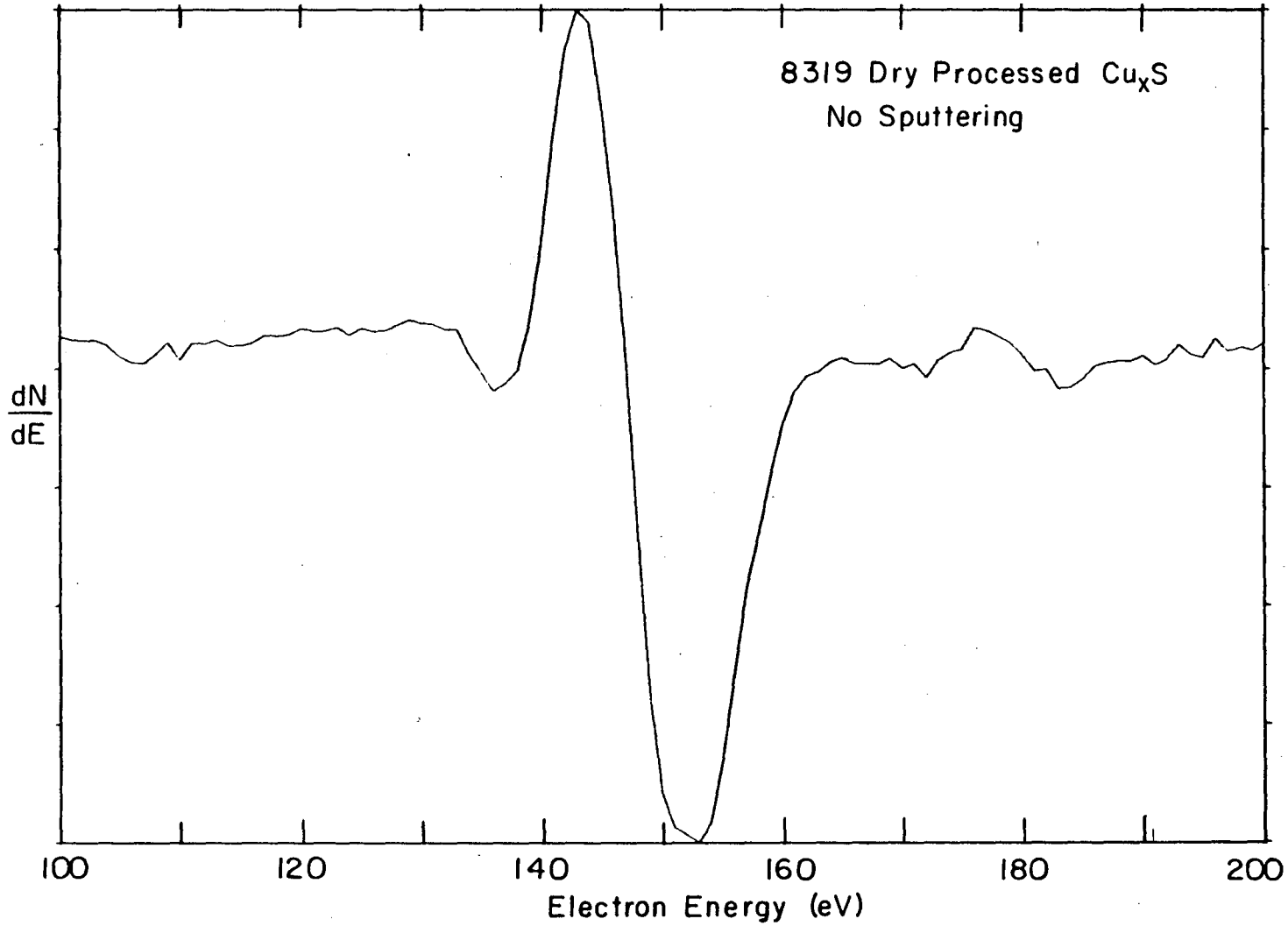

Fig. 5.11

XBL804-4992

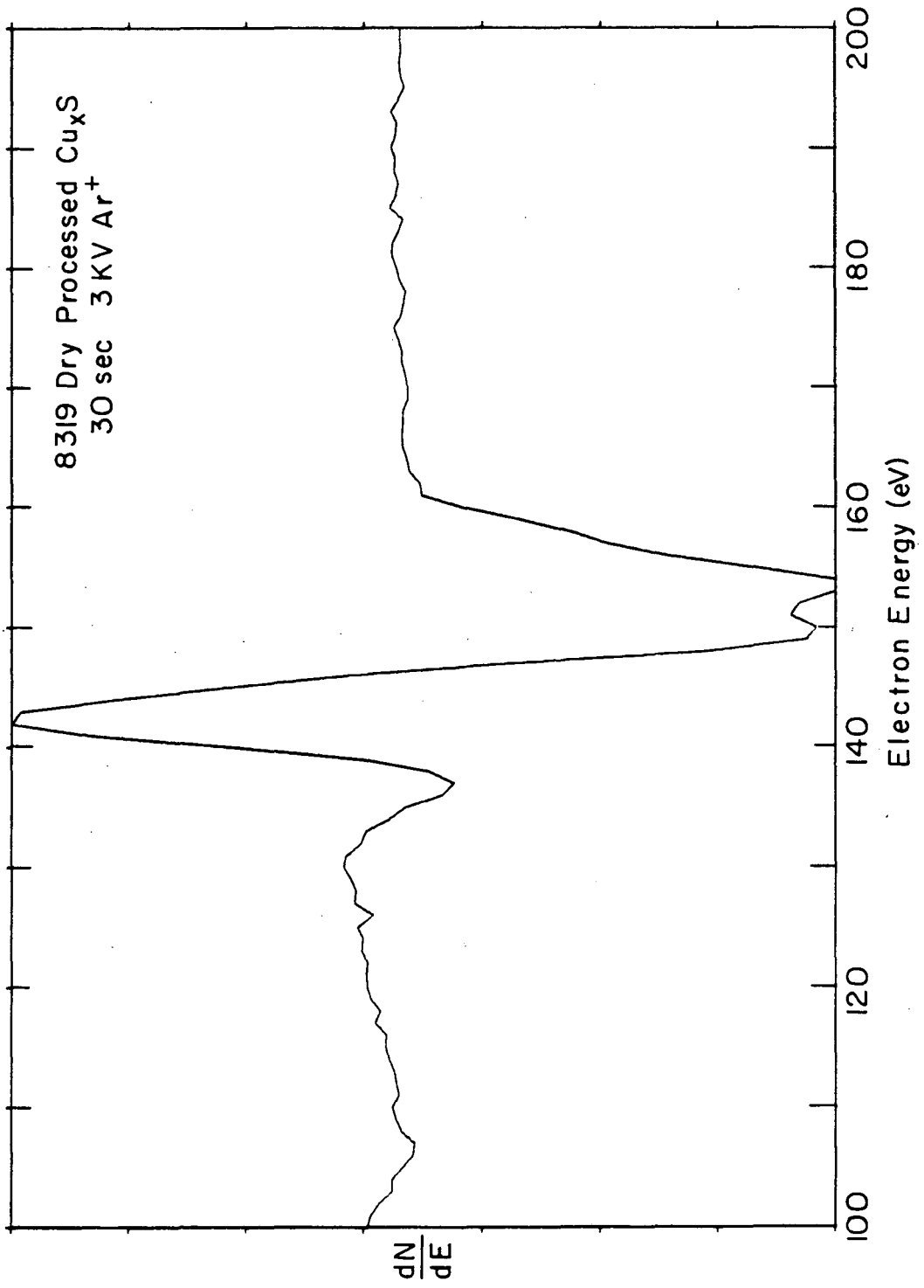

XBL804-4993

Fig. 5.12

This report was done with support from the Department of Energy. Any conclusions or opinions expressed in this report represent solely those of the author(s) and not necessarily those of The Regents of the University of California, the Lawrence Berkeley Laboratory or the Department of Energy.

Reference to a company or product name does not imply approval or recommendation of the product by the University of California or the U.S. Department of Energy to the exclusion of others that may be suitable.

TECHNICAL INFORMATION DEPARTMENT
LAWRENCE BERKELEY LABORATORY
UNIVERSITY OF CALIFORNIA
BERKELEY, CALIFORNIA 94720